Tension and Compression Behaviour of Masonry Walls with Shear Connectors

by

Danny Jose Romero

A thesis submitted in partial fulfillment of the requirements for the degree of

Master of Science
in
STRUCTURAL ENGINEERING

Department of Civil and Environmental Engineering
University of Alberta

ABSTRACT

Masonry connectors are used in wythe wall systems to either transfer lateral loads or increase composite behaviour. As future energy code requirements are updated, insulation is increasing which increases the cavity within walls which affects a connector's behaviour. Due to a lack of masonry research, North American design standards use an empirical design approach based on concrete capacity assumptions for all masonry connectors. Using one approach for all connectors creates overly conservative results for design because connectors with different geometries and material properties behave differently. This study aims to improve the understanding of connector behaviour within a double wythe wall specimen by testing four common connector types which are Z-tie and rectangular ties found in past construction and plated connectors in two different orientations found in modern construction. A novel inclined connector is also tested. 62 connectors are tested under tension and compression loading within a self-reacting testing frame with LVDTs and load cells used to measure the data. The connectors are in miniature double wythe wall specimens comprised of a concrete masonry unit, insulation, cavity, and veneer wythe of either clay or concrete. Another separate thesis program has tested the connectors in shear which discusses the composite behaviour. This study will investigate peak loads, displacements, and failure modes which will be verified to existing equations from previous research. Under tension loading, all tie connectors experienced a type of embedment breakout failure and the plated connectors experienced either breakout or pull-out failure. The utilization of an embedment veneer tie increases the effective concrete breakout area if a higher embedment tension capacity is required. Under compression, most specimens experienced elastic Euler buckling and were compared to the expected Euler buckling load with an effective length of 0.7. The recorded average

peak load under tension and compression for all connectors is greater than the P_{ult} minimum value of 1000 N used for ties in the CSA A370:14 standard.

PREFACE

I was responsible for the manuscript composition and the experiments performed. Douglas Tomlinson is the supervisor author and was involved in the concepts discussed and manuscript composition. Some of the work conducted for this thesis forms part of a research collaboration led by Professor Douglas Tomlinson and Professor Carlos Cruz-Noguez at the University of Alberta. The experimental tests referred to in Chapter 3 and 4 were performed by myself with assistance from department technicians (Greg Miller, Cam West) and an undergraduate summer research student (Amn Khaliqdina). The literature review in Chapter 2 and the discussion and analysis in Chapter 3 and 4 are my original work.

Elements of Chapter 3 were published as conference proceedings: Romero, D. and Tomlinson, D. (2023) “Tensile Response of Traditional and Contemporary Connectors in Masonry Cavity Walls with Thick Insulation.” Canadian Society for Civil Engineering Annual Conference, Moncton, NB, Canada.

DEDICATION

First and foremost, this is dedicated to my father, mother, and grandmother. To my parents Jose Romero and Esther Romero, who without their guidance throughout my life and sacrifices I would've never entered post-secondary education. Their values of hard work and putting in effort for everything you do has molded me throughout my post secondary education and engineering career. To my grandmother Nelly Romero, te amo mucho. "There are no goodbyes for us. Wherever you are, you will always be in my heart (Gandhi)."

To my close friends who've encouraged me throughout my program, Ashvin Ghurburrun, David Luong and Pailin Ismael. Thanks for being there during times of uncertainty as I was doing my thesis. Without you, I doubt this would've been completed.

My fellow classmates (now working professionals) Amy Huynh, Benedict Egbon, Alon Alonso Rivers, Rafael Gonzalez, Sergio Arevalo, thank you for helping me out during my times of need. I really appreciate the efforts you put in. If there's ever anything you'd like to ask, feel free to reach out.

A NUESTRO HIJO Danny: Como pasó el tiempo, parece que fue ayer cuando tu pequeño cuerpo de bebé, descansaba en el regazo de mamá. Dias, semanas, meses, años, pasaron raudos como queriendo escabullirse en el tiempo. Te vimos pegado a tus libros y computadoras, con un montón de números y ecuaciones que te absorbían, nosotros no entendíamos ni sabíamos nada; cuánta impotencia el no poder ayudarte. Solo pedíamos a Dios que te iluminara. Te acompañamos desde el inicio de tus estudios, volaste rápido por tu constancia y perseverancia. Ya te graduaste y mira el amplio futuro para con tu carrera de ingeniero. Danny seguramente en tu caminar por el largo sendero de la vida, nesecitaras de algún consejo y ahí estaremos incondicionalmente. Recuerda el major consejero para cualquier situación es y será Nuestro Bendito Redentor. La vida pone retos, los cuales sabrás sortearlos con esfuerzo y dedicación. Todo la familia, tu papá y mamá; nos sentimos grandemente agradecidos y bendecidos por Nuestro Padre Celestial; sabiendo que entregamos un professional útil a la sociedad. Gracias hijo por darnos esta alegria, seguros estamos, que en tu. "Ma Nelly" se deslizan por sus mejillas lagrimas de felicidad… alegría… Danny deseamos de todo corazón éxitos en tu carrera. Te amamos hijo, tus padres. Jose y Esther Romero. Te dedicamos de la Biblia. Josué 1: 9 mira que te mando que te esfuerces y seas valiente; no temas ni desmayes, porque Jehová tu Dios estará contigo en dondequiera que vayas

ACKNOWLEDGEMENTS

This thesis would not have been completed with the help and support from many people. First, I would like acknowledge my research supervisor Dr. Douglas Tomlinson who without his help, this thesis would not have been possible. I learned a wide breadth of both masonry knowledge and structural engineering in general. His patience during this thesis has helped me overcome certain challenges that were presented during the duration of this thesis program.

To Greg Miller and Cam West who supported my experimental work ensuring the 'intent' was possible. When I first embarked on this journey I was unaware of the practicality of some concepts I had in mind and without them these experiments would not have been possible. To Amn Khaliqdina, whose infectious energy and assistance allowed the experimental testing go smooth.

Louis St. Laurent, Justin German, Jordin and Scorpio Masonry for donating their time, laydown yard and efforts to my thesis specimens that were constructed in their yard. Without their input in construction, these would not have been constructed properly.

To Monica Guzman and Bennet Banting of the Canadian Masonry Centre, and Professor Carlos Cruz-Noguez MCAA Endowed Chair in Masonry Systems, thank you for giving me the opportunity to further masonry research and for answering my questions when published codes or research literature was not enough. Mike Lafontaine of Old Castle and Georgina Kostiuk of Brock White for donating the Expocrete brick material and standard stretchers, and Denis Charbonneau for the mortar and grout. Work in this project was funded through the Natural Science and Engineering Research Council (Canada) Collaborative Research and Development program grant 528050-18 "Resilient Concrete Masonry Walls to meet the needs for the Next Generation of Low-rise Structures".

Thank you all for helping me in this journey and upon finishing this I am ready to embark on another chapter of my life.

TABLE OF CONTENTS

LIST OF TABLES

LIST OF FIGURES

1. INTRODUCTION

1.1 Background

Building science is being incorporated more into Canadian building codes driven by a push by the federal government to reduce carbon emissions related to buildings. The Government of Canada plans to reach its emissions target of 40% below 2005 levels by 2030 and net-zero emissions by 2050. One way to reduce carbon emissions in buildings is to minimize space heating which is the primary energy use in the residential, commercial, and institutional sectors as shown in Figure 1.1.

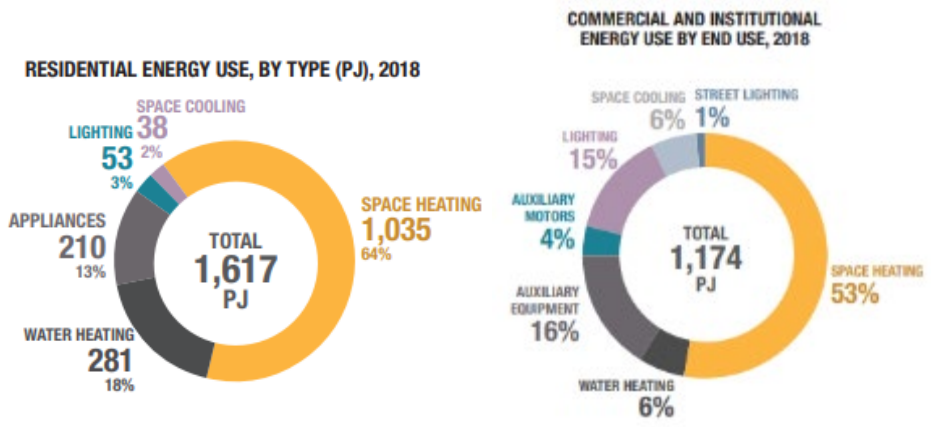

Figure 1.1: Energy use by type for Canadian industries illustrating how much energy is used for space heating (Natural Resources of Canada, 2020)

Masonry is a common building material in residential, low rise institutional/commercial buildings, and in historical buildings because of its longevity and aesthetics. Current structures that use masonry often have a masonry exterior veneer brick layer (referred to as a wythe) with connectors that connect the veneer to a structural backing. Modern masonry wall construction has insulation between the exterior wythe and structural backing. The intent of the insulation is to provide a sealed building envelope to limit heat and moisture transfer. Figure 1.2 shows common masonry veneer details commonly found in Canadian construction.

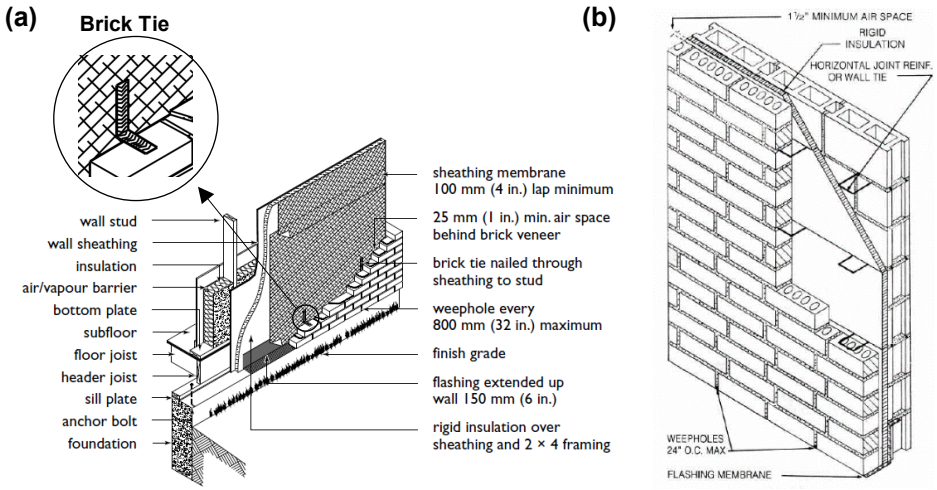

Figure 1.2: (a) Masonry veneer support cross section (Burrows & Canada Mortgage and Housing Corporation, 2013) (b) typical cavity wall with insulation (Satko, 2007)

The effect of insulation must be considered when evaluating how to minimize space heating for energy efficiency. Amirzadeh et al. (2018) assessed thermal insulation for masonry walls in historic multifamily buildings and found that the colder the climate, the larger the energy cost savings would be on a dollar per square metre basis for insulation like expanded polystyrene (EPS) insulation. The payback period also reduces greatly for EPS insulation when shifting from 75 to 150 mm as shown in Figure 1.3. 'R-value' is a means of quantifying thermal resistance of different materials and assemblies. Larger R-values means that a material or assembly has low thermal conductivity and reduced heat flow through the assembly. Insulation like EPS has very low thermal conductivity (i.e., leads to large R-values) and is typically used in walls because of this reason.

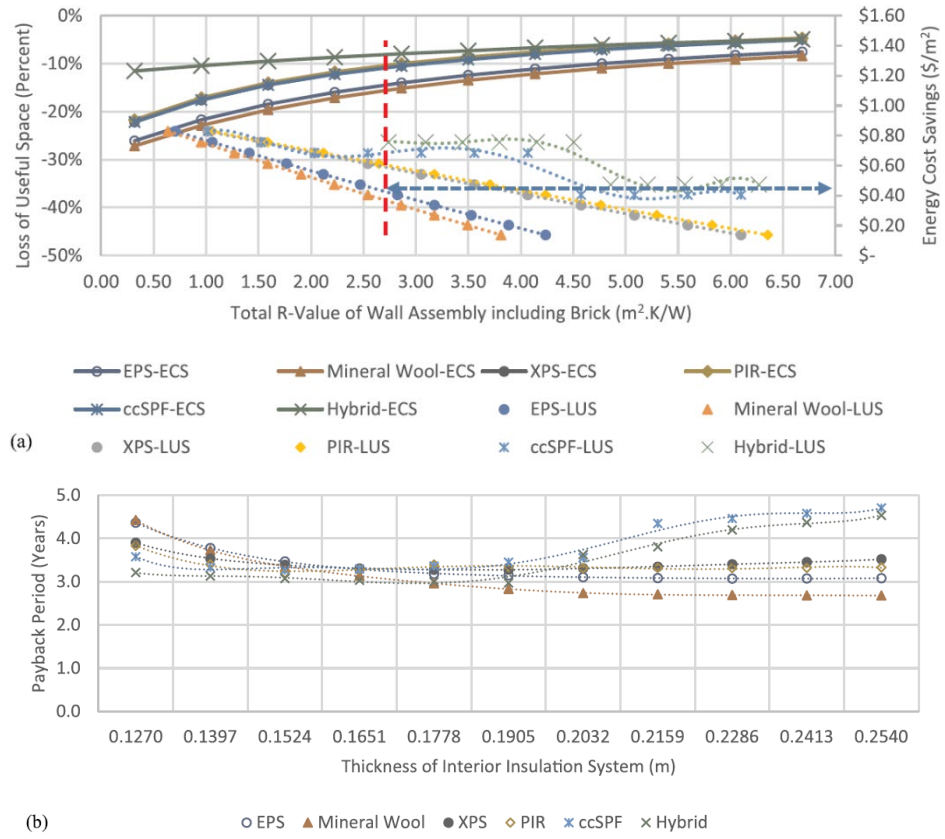

Figure 1.3: (a) Modelled energy cost savings and loss of useful space from the installation of interior insulation for Duluth and (b) payback period (Amirzadeh et al. 2018)

Another way to increase thermal resistance of building envelopes is by minimizing thermal bridges. Thermal bridges are locations in the wall where heat can pass through insulation penetrations made by high thermal conductivity materials. In masonry cavity walls, thermal bridges occur through metallic connectors between wythes and shelf angles. Shelf angles are not addressed in this thesis but can be significant thermal bridges (Ismaiel et al. 2022).

Figure 1.4 shows various traditional masonry wall cross sections and R-Values of the overall wall system which shows that the thicker the insulation, the larger the R-Value (thermal resistance) is present (Satko, 2007).

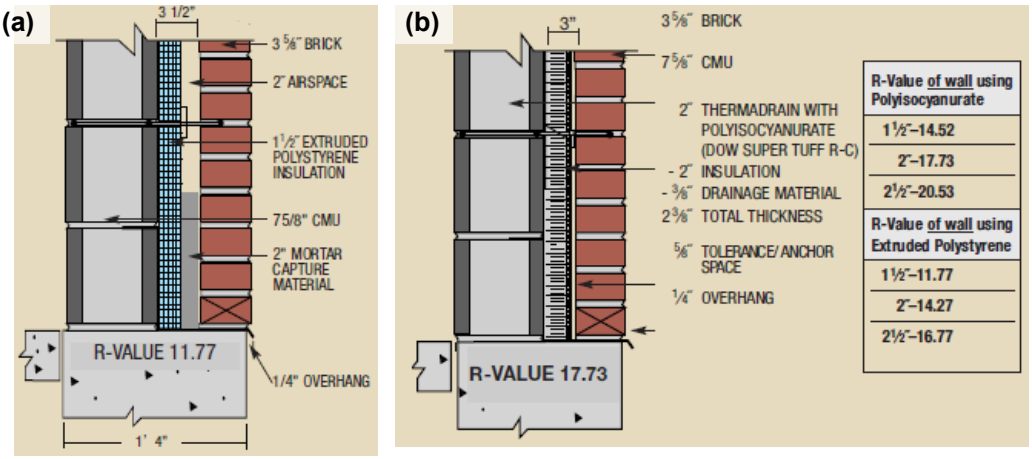

Figure 1.4: 1980's traditional cavity wall, cavity wall R-Values of (a) 38.1 mm (1.5 inches) EPS insulation, (b) 50.8 mm (2.0 inches) insulation (Satko, 2007). All measurements are in inches. R-values given in US units ($ft^2°Fh/BTU$).

Carson Dunlop, a prominent Canadian home inspection authority, stated that the two types of brick houses are brick veneer and solid masonry further adding that brick houses built in the last 30 years have been brick veneer construction however a solid masonry wall can, "if properly maintained, provide hundreds of years of service" (Dunlop, 2014). Modern masonry has become thinner compared to historical masonry though structural design limits and rain penetration are challenges to address with thinner walls. A potential solution for rain penetration was to seal the wall with stucco, paint, and/or other sealants but these require frequent maintenance which makes it unpopular in North America (Drysdale et al., 2005). An alternative approach is to build masonry walls with two layers. These double wythe walls comprise an outer masonry wythe connected to but separated by an air space or cavity from an inner wall (Drysdale et al., 2005).

A typical masonry double wythe wall consists of an exterior brick wythe, followed by an air cavity, insulation and finally an interior concrete masonry unit (CMU) layer. Whether or not the exterior wythe takes part in composite action (i.e. performs structural resistance to the overall system) is determined by the connectors used and structural detailing described later. The purpose of the air cavity is to mitigate rain penetration by providing a path for water to escape in combination with flashings. Figure 1.2 (b) illustrates a typical cavity wall with insulation.

Structural failure in unreinforced masonry buildings under lateral load is primarily caused by poor tie connections and strength (Muhit et al., 2022) which has been observed in walls of damaged buildings (Arslan et al., 2021). Associated out of plane failure was due to weak connections between wythes which is related to the failure of the wall tie connections (Arslan et al., 2021). Ties

transfer out of plane lateral loads from the exterior veneer to the back-up and, depending on their design, allow in-plane movement to accommodate differential movement. Proper tie design is essential to the structural performance of the overall wall (Muhit et al., 2022). If the two wythes are not properly connected, the out of plane strength may be considerably smaller than an equivalent solid wall with the same thickness (Arslan et al., 2021). Common ties used in past masonry veneer construction are Z-ties and rectangular ties (Figure 1.2 (b)) embedded into mortar joints in both the CMU and brick veneers. Brick ties shown in Figure 1.2(a) are commonly used in stud frame wall construction by placing the bottom leg of the tie within a brick's horizontal mortar joint and nailing it through the sheathing to the stud. The brick tie concept of using flat plates instead of cylindrical rods used in rectangular ties is prevalent in modern construction ties.

Similar to concrete wall composite behaviour, masonry double wythe walls are fully composite when complete shear transfer occurs (wythes act as a unit), non-composite when zero shear transfer occurs (wythes act independently), and partially composite when the wall behaviour is between those two extreme limits (Tomlinson, 2015). By having two separate layers, the level of composite action between both the interior wythe and exterior wythe is based on the intent of the structural design. Through the use and number of connectors, walls can act as one or act as two separate elements. Composite behaviour is briefly discussed later but the focus of this thesis is on connectors loaded under tension and compression.

Hatzinikolas et al. (1979) tested various ties in tension and compression to determine failure loads with the frame shown in Figure 1.5 and proposed design equations. Since then, others like Arslan et al. (2021), have evaluated connectors and included additional design considerations and failure modes. There is limited connector testing with thick cavity widths which will be discussed more in Chapter 2. To achieve larger R-Values due to an increase of insulation, thicker cavity widths are required and connectors for these systems need testing.

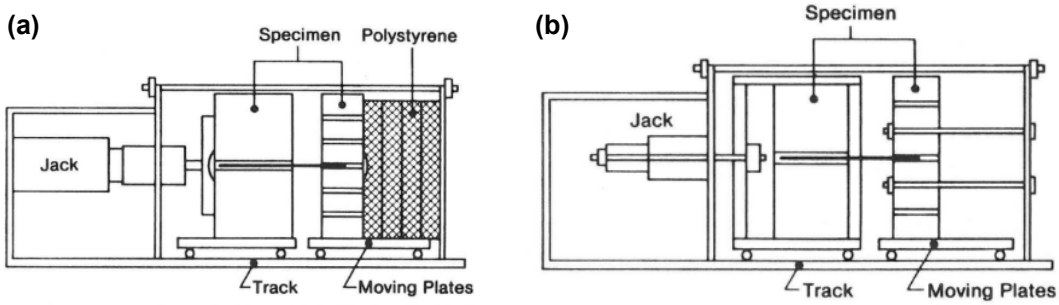

Figure 1.5: Representation of testing system for (a) compression,(b) tension (Hatzinikolas et al., 1979)

Researchers on reinforced concrete walls have proposed methods of measuring composite action though masonry is further behind. Understanding this behaviour will allow designers to verify existing masonry design methods for multi-wythe wall systems and the wall connectors being used. There is limited understanding effects that different connectors have on composite behaviour in masonry. Masonry connectors are mostly proprietary and designed/tested in house by companies or are a simplistic prescriptive design that satisfies Canadian standard requirements of CSA A370:14 and S304-14. Due to connectors being tested in house by companies, available knowledge for composite behaviour of whole wall systems is low resulting in limited understanding of connector behaviour.

Limited information on connector behaviour can be further divided into knowledge gaps on how connectors behave in tension, compression and shear. Shear behaviour is most critical for composite action. However, if tension and compression response are not well understood then axial response may cause premature failure regardless of shear response.

1.2 Research Objective

The objective of this thesis is to evaluate the axial behaviour of masonry wythe connectors that represent typical connectors in practice as well as a novel inclined connector. The tested wall components have thicker than conventional insulation to reflect 2022 National Canadian Energy Code Requirements. This thesis presents the first phase of a larger research program with future work evaluating shear loading and thermal gradients at the connector and full-scale wall levels. The following items were completed to achieve this thesis's objective:

- **Item 1:** Complete a literature review on masonry wall connectors under axial loads and research done on these connectors. Shear and overall composite wall design are also discussed to present larger contexts.
- **Item 2:** Design and procure a loading frame to evaluate double wythe masonry wall/tie systems under axial loads.
- **Item 3:** Construct and test the tensile resistance of 31 double wythe wall specimens including masonry wythes, cavity, and connectors. Five connector types and two exterior wythe types (clay brick, concrete brick) are investigated. Cavities include an insulation layer (152 mm) that is thicker than typical wall systems (75 mm). Testing evaluates capacity, general response, and failure modes of connectors under tension.

Item 4: Construct and test the compression resistance of 31 double wythe wall specimens including masonry wythes, cavity, and connectors. Test specimens and details are identical to those from Item 3. Testing evaluates the capacity, general response, and failure modes of connectors under compression.

Item 5: Analyze results from Items 3 and 4. This will assist in the development of constitutive relationships for tension and compression for future research that can be combined with shear behaviour and overall wall system behaviour. Failure mechanisms, peak loads, stiffness, and post-peak response will be evaluated and compared to existing design provisions.

1.3 Thesis Scope

This study focuses on the tensile and compressive response of four steel connectors in 62 masonry double wythe wall specimens obtained through physical testing. Connector behaviour is the scope of this work. Full wall behaviour, for instance determining optimum tie wall spacings or tie load distributions, is not considered but encouraged for future research and practice. All specimens were constructed with 190 mm thick concrete masonry unit (CMU) backup wythes and either concrete brick or clay brick as a veneer wythe. Insulation consists of 152 mm thick EPS. Connector behaviour is investigated for four connectors with configurations used in practice and a novel inclined connector. The total wall thickness for all specimens was 476 mm. Data collected includes loads and deformations. Test data was compared to previous expressions from literature, and first principle concepts such as Euler buckling capacity. Finite element analysis (FEA) is beyond the scope of this thesis though the literature review will present some research that used FEA for similar systems.

1.4 Thesis Organization

This experimental program was divided into two phases: the fabrication phase of the 62 specimens and testing frame followed by the testing phase. The testing phase was divided into two sub-phases that correspond to tension and compression loading respectively. Results are analyzed and discussed based on assessed failure modes and response. The thesis contents are:

Chapter 1: Introduction to the research objective, scope, and structure.

Chapter 2: A literature review on masonry walls and masonry connectors with a focus on the axial response of connectors. Previous testing on walls with connectors is included. Shear connectors, reinforced concrete wall systems, and overall composite

behaviour are briefly discussed to provide overall context. ***Item 1*** is addressed in this Chapter.

Chapter 3: Results and discussion from experimental work on evaluating structural behaviour of wall specimens with connectors under tension. ***Item 3*** and part of ***Item 2 and 5*** are addressed in this Chapter.

Chapter 4: Results and discussion from experimental work on evaluating structural behaviour of wall specimens with connectors under compression. ***Item 4*** and part of ***Item 2 and 5*** are addressed in this Chapter.

Chapter 5: Thesis summary, conclusions, and recommendations.

References

Appendix A: The auxiliary testing results is provided for the mortar, grout, concrete masonry unit, rebar and connector properties.

Appendix B: Loading rates of each specimen.

Appendix C: Photos taken before, during and after testing of failure modes. This includes experimental frame removal photos.

2. LITERATURE REVIEW

The literature review provides an overview of masonry wall design under tension and compression with a focus on masonry connectors and the CSA S304.1-14 standard. Research on composite wall behaviour and shear behaviour is discussed to show the next steps in understanding multi-wythe masonry wall behaviour when considering connector properties and geometries.

2.1 Current Challenges and Limitations in Masonry Education and Research

There is a lack of masonry research compared to other building materials such as steel, reinforced concrete and wood. This lack of advancement may be due to post secondary institutions not giving the same attention to masonry as other materials. Shrive and Sturgeon (2001) reported on a post secondary survey that masonry is last in receiving attention compared to concrete, steel, wood and asphalt while noting that masonry receives less than 3% the attention that concrete does. There has been increased focus on masonry research from the Canadian Concrete Masonry Producers Association (CCMPA) and the Canada Masonry Design Centre (CMDC) which aim to establish Canada as a world leader in masonry research. They indicate that research takes a while for its impact to be felt by industry due to the slow process of developing codes and standards. However, when an industry lags in research, markets once thought untouchable disappear (Banting 2016).

Another potential cause for the lack of masonry advancement is difficulty in achieving accurate information due to the variability from masonry's individual components. Masonry is not homogenous and consists of various materials (e.g., bricks, blocks, grout) and mortar joints (Lourenço et al. 2007). In addition to the large number of possible combinations generated by the geometry, nature, and arrangement of units as well as characteristics of mortars, this level of complexity creates large scatter in experimental data (Lourenço et al. 2007). Limited resources have been allocated to the study of the mechanical behaviour of masonry which includes non-destructive in-situ testing, laboratory testing, and development of reliable numerical tools (Lourenço 2002).

2.2 Exterior Masonry Wall Types and Design Evolution

2.2.1 Ancient Masonry Wall Construction

In structural design, the fundamental challenges are how to span vertically and how to span horizontally. A few structural elements used to solve these challenges are walls, columns, beams, lintels and arches. The simplest method of masonry construction in early history was to stack

masonry units on each other. However, this method creates uneven bearing area and lack of vertical alignment not to mention the lack of a lateral force resisting system. Pyramid construction in Ancient Egypt attempted to solve these issues; this approach is now known as bearing design. Early masonry wall construction was limited by stability issues. The traditional solution was to rely on extremely large bearing areas resulting in an excess of material as evidenced by ancient Mesopotamian walls with five metre thicknesses. An alternative option was to use a large base that tapered as height increased. This satisfied loading and stability constraints though the material use was inefficient and the functionality of these structures is limited. Ancient walls used significantly less material than pyramids but were still thick compared to modern walls. This bearing design approach was more recently used in the 1890 Monadnock building in Chicago with 1.8 m thick masonry walls at the base (Drysdale et. al. 2005) and 100 mm masonry wall thickness changes for every storey to handle increasing self-weight.

A common ancient construction method used by the Romans was an exterior face finished by a mason while the interior face and infill material was placed by labourers (Drysdale et. al. 2005). The Roman method is illustrated in Figure 2.1 which has similar concepts used to this day in residential wood frame construction in the sense that the outer wythe is carefully crafted with smaller masonry units while the interior wythe is there for load bearing. Figure 2.1(b) is an early example of how composite behaviour was introduced using header courses to bond the inner and outer wythe as one unit in comparison to Figure 1.2 which is a more modern wall system. These ancient methods utilized what we know as cavity and composite walls today but were still reliant on bearing design.

Connectors provide more stability to double wythe walls by bonding the inner and outer wythe which provides greater resistance to lateral loading. The common bearing design approach described earlier of using a higher wall thickness does provide greater stability but when minimizing thermal heat loss a thicker wall is reliant on its own thermal properties whereas a cavity wall has an insulation layer which has better thermal properties. A cavity wall with a connector mechanism also uses less material and is less labour intensive when compared to thicker walls constructed in past construction such as the Ancient Mesopotamian walls with five metre thickness and the more recent Monadnock building with 1.8 m thick masonry walls in Chicago.

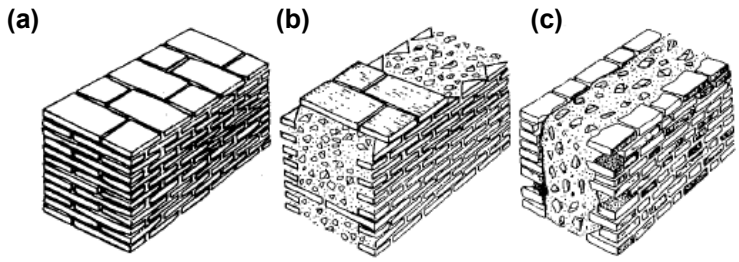

Figure 2.1: Roman masonry walls from Drysdale et. al. (2005) (a) bonded brick wall, (b) brick faced wall with header courses,(c) brick faced wall

The similarity of the concepts of utilizing a 'connector' to unite wythes in cavity walls has not changed dramatically from ancient times to now. The use of metal ties in brick masonry dates to loadbearing walls in the 1850's and historically the size, spacing, and type of ties has been empirical (Brick Industry Association 2003). CMU's were adopted in the early 1900's when the first block producing machine was patented to mass produce units (Alberta Masonry Council 2023). Another major advancement was placing reinforcement in masonry units due to traditional masonry's poor response in seismic events. The use of reinforcement started in the late 1930's in the United States (Tobriner 1984) with Canadian masonry standards now restricting unreinforced masonry usage due to their poor lateral load resistance. (Laird et. al. 2005).

Current masonry wall design practices use a mixture of empirical methods, masonry specific 'rules of thumb', and design philosophies borrowed from reinforced concrete. Recent Canadian masonry research is investigating masonry wall behaviour with a focus on the modernization of design standards (Cruz-Noguez 2020) for slender masonry walls (Mariscal 2022), increasing accuracy of shear strength predictions for masonry walls (Izquierdo et al. 2023), improving thermal resistance of masonry exterior walls (Ismaiel et al. 2022), and creating mechanical and probabilistic models for masonry walls (Metwally et al. 2022).

2.2.2 Masonry Wall Types

Walls are classified as flexural walls or shear walls based on the applied loading and design intent. Flexural walls are designed to resist axial load due to load transfer from other building elements such as floors or roof in addition to out-of-plane lateral loads that are usually from either seismic or wind. Shear walls are designed to resist mainly in-plane shear loads due to earthquake or wind loads as well as likely non-negligible axial loads. The focus of this thesis is on flexural walls so the literature review will focus on this application. The common failure modes checked for flexural

walls are flexural failure, out-of-plane shear failure, and sliding shear failure while serviceability is checked with deflections.

There are many different types of flexural walls for different purposes though exterior walls are the focus of this thesis. An exterior wall encloses the building above grade, resists wind acting perpendicular to the wall plane (out-of-plane forces), prevents water entry into the building, and provides a thermal barrier. Exterior wall design involves considering the three failure modes previously discussed as well as an air cavity used for moisture and vapour flow to meet drainage or thermal considerations. These two considerations are greater challenges in masonry compared to concrete since masonry walls have more joints that allow for more penetration.

2.2.3 Composite Wall Design Approach: Cavity and Veneer Wall

The most common masonry walls that cover the range of maximum composite behaviour to a minimum are cavity walls and veneer walls respectively. Cavity walls are designed to achieve composite behaviour using connectors that transfer large shear forces so that load sharing occurs between both wythes. Veneer walls are designed to minimize load sharing by only connecting the structural inner wythe to the overall gravity load resisting system, in this case an interior structural wythe. The inside portion of the veneer is connected to the structural wythe at the top and bottom to avoid carrying any vertical load beyond self weight. Ties are placed along the wall height in the veneer joints to transfer lateral wind or seismic loads to the structural backing. Although ties are only meant to transfer lateral loads, a small amount of shear transfer is expected but negligible compared to larger connectors used specifically to transfer shear in cavity walls.

Cavity walls are a multi-wythe wall with masonry used primarily as the structural wythe and connectors installed in the mortar joints to promote composite behaviour. Building envelope challenges are addressed by putting insulation between wythes in addition to a vapour barrier. Transformed moments of inertia, elastic section moduli and effective areas are used for composite wall design with the same design principles as non-composite walls. Figure 1.2(b) shows an accepted rectangular tie wall system used in past construction while Figure 2.2 shows a more modern masonry wall system that uses plated connectors.

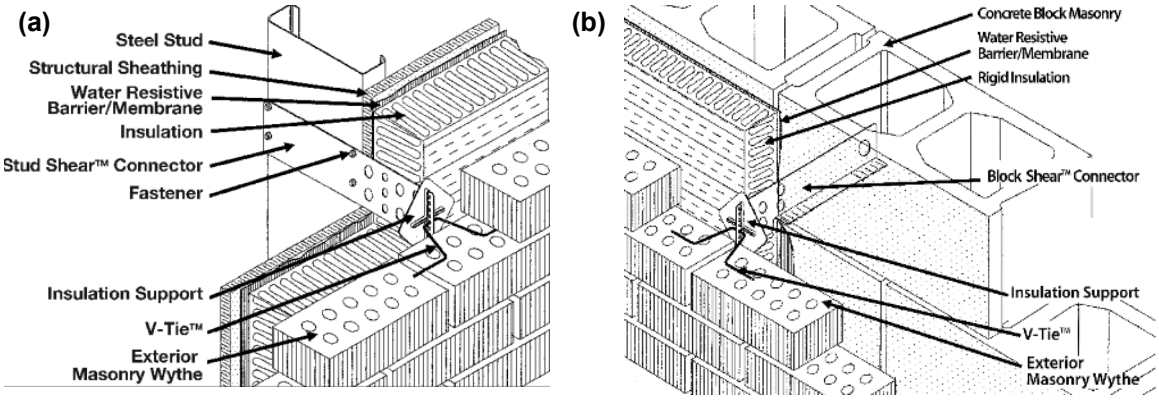

Figure 2.2: Shear connector illustrations on different structural backings for (a) stud shear connector for composite action (b) block shear connector illustration from FERO technical notes (FERO Corporation 2014)

Cavity walls were first built in North America late in the 19th century with insulation later becoming common around the 1970's (Satko 2007). A driver for the more accepted usage of insulation in buildings was the Arab oil embargo in the mid 1970's causing a shortage of energy thus a push for larger R-values due to new energy codes and various insulations were used and explored (Satko 2007). Though increasing insulation thickness reduces heat flow through the wall system, it is unknown how this affects connector behaviour or if this will be negligible.

Under compression, insulation will provide resistance similar to the confining effect of ties in reinforced concrete columns however the increase of required connector length to accommodate the insulation thickness increase may offset this effect and affect the peak load. There is minimal research for how much additional transverse compression resistance is provided by the insulation itself however there is research from non-masonry wall systems that sheathing does contribute to increased stability under compression loading applied to the top of the wall longitudinally. The stability of light gauge steel walls in compression with plasterboards was researched by Lawson et al. (2020) concluding that the lateral restraint provided by the plasterboard is equivalent to an effective length reduction factor of 0.7 in the minor axis direction. Precast sandwich wall panels with GFRP connections under compression load were tested with insulation ranging from 160 mm to 350 mm by Carstens and Pahn (2022) concluding that as insulation increases between 250 and 350 mm, the Euler equation calculates the resistance very well and under long term compression loading, there is an increased influence of temperature and humidity on the failure load (Carstens and Pahn, 2022). Sandwich composite walls with truss connectors were tested in compression and fire simultaneously with one conclusion stating that when the axial compression ratio was reduced from 0.5 to 0.3, the deformation of the wall was changed from compression-predominant to

expansion predominant deformation (Du et al. 2022). The axial compression ratio is calculated by Equation 2.1 where n is the axial compression ratio, N is the axial pressure, $f_{ck}$is the axial compressive strength of the concrete obtained from the test, f_y is the yield strength of the steel obtained based on the test, $A_c$is the concrete area of the wall section, $A_s$is the total area of steel plates of the wall section, 1.25 is a partial coefficient of axial pressure generated by the representative value of gravity load, and 1.4 and 1.1 are the material partial coefficients of concrete and steel, respectively (Du et al. 2022).

$$n = \frac{1.25N}{\frac{f_{ck}}{1.4}A_c + \frac{f_y}{1.1}A_s} \quad \text{(Eq. 2.1)}$$

Previous research indicates that the provision of sheet steel as sheathing has been found to improve the in-plane shear capacity of light gauge steel-framed walls (Dias et al. 2019).

The main differences veneer walls have compared to cavity walls are (Hatzinikolas et. al. 2005):

- The outer wythe is non-load bearing
- The structural backing is not always masonry but can be wood, concrete, or steel
- Composite action is not intended

In practical applications, masonry walls cannot be fully composite due to the uneconomical amount of connectors required which in turn will introduce many thermal bridge and thermal bowing challenges. Thermal bowing creates unwanted deflections, stresses on the wall/connection and gaps in structures on their corners (Arevalo 2019) as investigated in precast concrete insulated wall panels which are similar in concept to double wythe masonry walls. Among the largest thermal bridging sources in masonry walls are traditional steel veneer ties and steel shelf angles (Roppel et al. 2021, CCMP 2013, Ismaiel et al. 2022).

Transformed moments of inertia, elastic section moduli, and effective areas are used for composite wall design with the same design principles of capacity for non-composite wall design. For design, shear that should be transferred is calculated with first principles by dividing the maximum applied moment on the wall by the moment arm and the amount of connectors required is determined by the connector's shear flow capacity which is usually provided by manufacturers. Typical design veers on the conservative side when adding shear connectors for

composite behaviour especially for walls close to large openings to further promote load sharing due to the load path of the lintel's tributary area.

Cavity walls are referenced in Clause 6.7.1 of S304.14 which states that for lateral load effects, the cavity wall stiffness shall be taken as the sum of the stiffnesses of the two wythes acting non-compositely. Ties act as struts and force the two wythes into similar curvatures but it is assumed that no shear is transferred across the cavity.

$$M_o = \frac{E_o I_o}{E_o I_o + E_i I_i} M_t \quad \text{(Eq. 2.2)}$$

$$w_o = \frac{E_o I_o}{E_o I_o + E_i I_i} w_t \quad \text{(Eq. 2.3)}$$

$$M_i = \frac{E_i I_i}{E_o I_o + E_i I_i} M_t \quad \text{(Eq. 2.4)}$$

$$w_i = \frac{E_i I_i}{E_o I_o + E_i I_i} w_t \quad \text{(Eq. 2.5)}$$

Equations 2.2 to 2.5 represent the load sharing between wythes where E is the modulus of elasticity of each wythe, I is the moment of inertia, M is the maximum bending moment, M_t is the total bending moment acting on the wall, w is the lateral load applied to the wythe, and w_t is the total lateral load acting on the wall. The equation subscripts i, o, and t represent the interior wythe, outer wythe, and total applied load respectively. These expressions assumes rigid connectors that achieve composite behaviour and is derived from assuming equal mid-height deflections at both the interior and exterior wythe.

The design of a veneer wall for the inner wythe is similar to how flexural walls are designed with the added check of determining if the backing is flexible or stiff followed by checking the tie resistance to transfer the lateral load to the inner wythe.

S304-14 states in Clause 9.1.4.2 that the structural backing system is flexible if it is 2.5 times less than the uncracked veneer stiffness. For cavity walls, research found that the load resisted by a tie depends on the flexural stiffness, EI, of the structural backing relative to that of the veneer, tie spacing, and connector axial stiffness (Brown and Elling 1979, Hatzinikolas et al. 2005). The elastic modulus for both wythes is based on the empirical equation $E = 850 f'_m$ with each wythe

likely having different f'_m due to different material properties (e.g., brick, CMU). The moment of inertia can be calculated for each wythe from first principles and transformed section analysis though design tables are typically used for brick and CMU cross-sectional properties. If reinforcement is present, the structural backup stiffness is based on the cracked moment of inertia. If a flexible structural backing is present, each tie needs to be designed for 40% of the tributary lateral load on a vertical line of ties but not less than double the tributary lateral load on the tie (Hatzinikolas et al. 2005). This requirement of 40% distribution of loads amongst ties comes from Brown and Elling (1979) who conducted theoretical analyses of masonry cavity walls connected at discrete intervals by linear springs and concluded that the lateral load distribution between wythes depends on the end boundary conditions, number and spacing of wall ties, and the relative flexural stiffness of the wythes. Ties near the ends of the wall carry more axial force compared to the interior ties and in some cases can carry as much as 25% of the total lateral force on a strip of wall (Brown and Elling 1979). Figure 2.3 shows the lateral loads on double wythes and ties using equilibrium based on distributions from previous research.

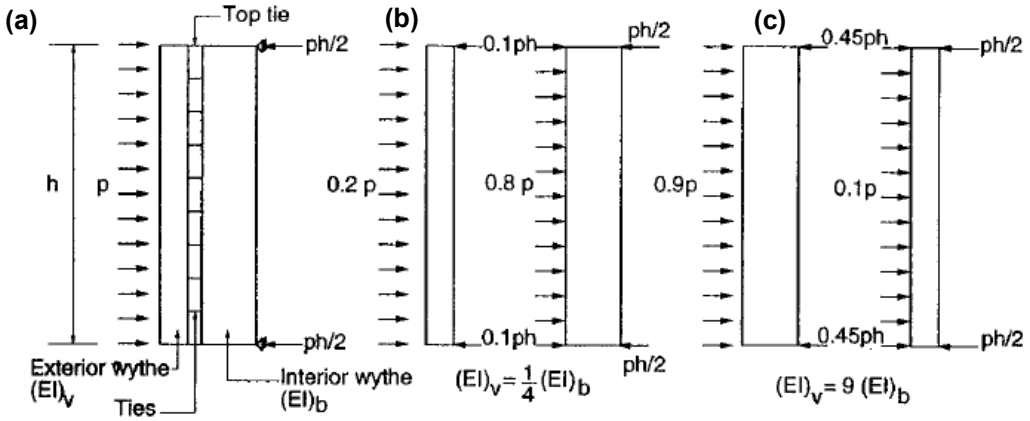

Figure 2.3: (a) Lateral load distribution in two-wythe walls, (b) load distribution for rigid backing, and (c) load distribution for flexible backing (Drysdale et al. 2005)

A common load distribution for cavity walls that occur in reality are cases which involve positive wind pressure and negative wind pressure. When designing cavity walls for ventilation considerations, there are three common types of cavity walls which are unventilated, pressure-equalized, and ventilated shown in Figure 2.4. Unventilated cavity walls were commonly used until the late 1900s where newer designs such as the pressure-equalized cavity wall and the ventilated cavity wall have emerged to reduce the positive force of wind-driven rain against the veneer and for moisture management (Ismaiel et al., 2022). Figure 2.4 (b) shows a realistic load

distribution within the air cavity applied to the brick veneer wythe undergoing either tension or compression due to the presence of wind loads. There is a weep hole at the veneer's base allowing air to enter the cavity which can either reduce the amount of net pressure due to wind driven rain or create a suction force within the air cavity shown.

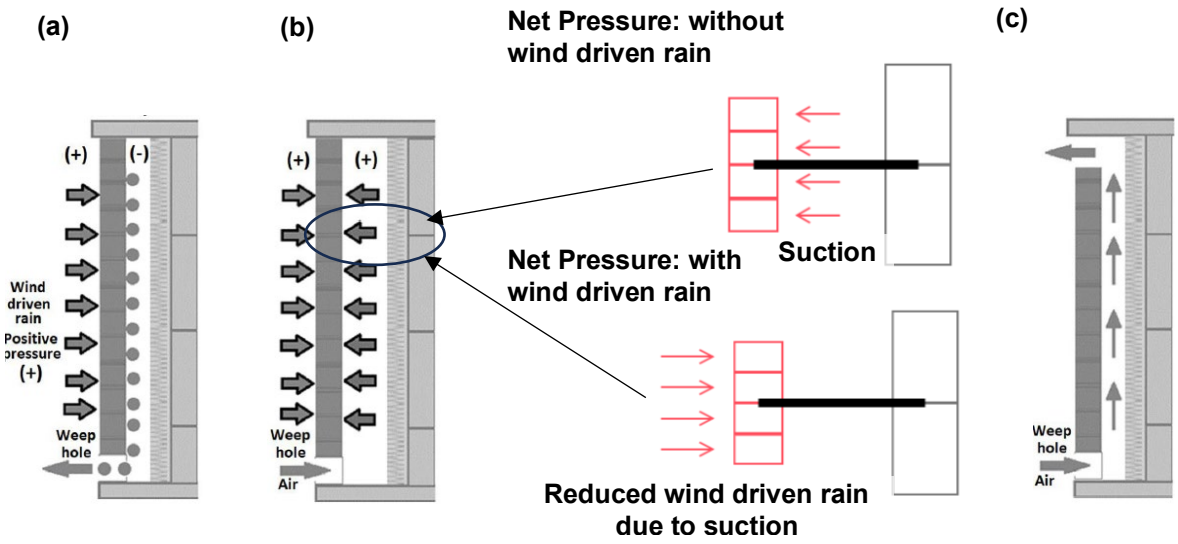

Figure 2.4: Common cavity wall types (a) unventilated cavity wall, (b) pressure-equalized cavity wall, (c) ventilated cavity wall from Ismaiel et al. (2022)

McGinley and Hamoush (2008) investigated the behaviour of full-scale wood stud backed clay masonry veneer walls with corrugated steel ties of different gauges under quasi-static out-of-plane loading. They determined that the brick veneer, once cracked, rotates around the cracked mortar joint and spans between the ties (McGinley and Hamoush 2008). Wood studs then transfer lateral loads to the supports at the top and bottom of the wall (McGinley and Hamoush 2008). The typical failure mechanism for the veneer system is pull-out of the nails from the stud backup but when this connection was strengthened, the failure mode switched to veneer bed joint pull-out (McGinley and Hamoush 2008).

Reneckis et al. (2004) investigated full-scale out-of-plane performance of brick veneer walls on wood frame construction with corrugated sheet metal ties. They concluded that ties anchored at or near stiff regions of the wood frame backup (floor or roof/ceiling framing) were more heavily loaded than ties near more flexible regions (halfway up the wall panel), where the wood frame backup could deflect together with the veneer (Reneckis et al. 2004).

Figure 2.5 shows various connectors used in industry. The main connectors used in North America and accepted as prescriptive solutions are Z-ties and rectangular tie connectors. L-ties are

more common in the Netherlands and are similar to Z ties. Corrugated sheet metal ties are more common in low-rise residential construction due to the ability to nail or screw the structural backing end to wooden studs commonly used as framing in North American residential construction.

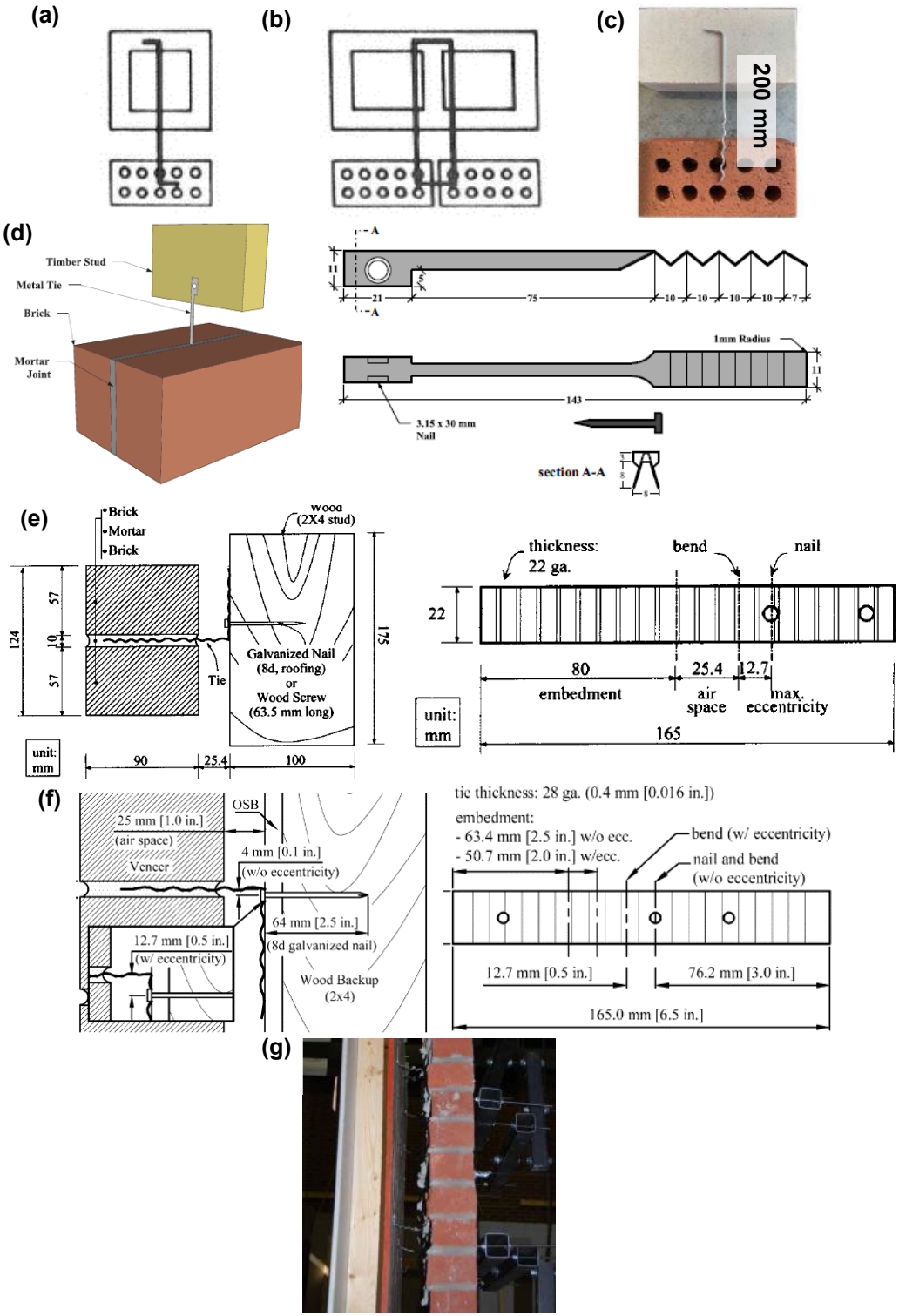

Figure 2.5: Different connectors used in industry (a) Z-tie (Hatzinikolas et al. 1979), (b) rectangular tie (Hatzinikolas et al. 1979), (c) L tie (Arslan et al. 2021), (d) Side-fixed veneer tie (Muhit et al. 2022), (e) corrugated metal tie (Choi and LaFave 2004), (f) corrugated sheet tmetal tie (Reneckis et al. 2004), (g) corrugated metal strip tie (McGinley and Hamoush 2008). All measurements are in mm.

2.3 Masonry Connectors under Axial Loading

There are various connectors available though the majority are proprietary with a combination of empirical and prescriptive design methods being used. Equation 2.6 represents the design capacity of a connector from A370:14.

$$R_{co} = F_{co}P_{ult} \quad \text{(Eq. 2.6)}$$

R_{co} is the resistance of a connector, P_{ult} is the strength of the connector with a minimum value of 1000 N for ties required by the standard, and F_{co} is an empirical resistance factor. The resistance factor is 0.9 for connector material failure and 0.6 for connector buckling, wythe material embedment or fastener failure. The origin of 1000 N as a minimum allowable resistance is unclear and appears to be a legacy provision from older versions of the standard that were based on working stress.

A search for masonry tie literature load data was done to report peak loads and compare with the results presented in Chapters 3 and 4. These past studies were selected due to a masonry tie connector being either tested in tension, compression or both within a two wythe system. Four studies were found conducted by Hatzinikolas et al. (1979), Choi and LaFave (2004), Arslan et al. (2021), and Muhit et al. (2022). Table 2.1- 2.3 summarize tension peak loads of Z ties and rectangular ties from Hatzinikolas et al. (1979), L-ties from Arslan et al. (2021), and metal ties from both Choi and LaFave (2004) with Muhit et al. (2022) respectively. Table 2.4- 2.7 summarize compression peak loads of Z ties and rectangular ties from Hatzinikolas et al (1979), L-ties from Arslan et al. (2021) and metal ties from Choi and LaFave (2004) with Muhit et al. (2022) respectively.

Table 2.1: Experimental tension peak loads for ties tested in previous research done by Hatzinikolas et al. (1979)

Connector Type	Z-Tie-1 (Type H)	Z-Tie-2 (Type H)	Z-Tie-3 (Type H)	Rectangular Tie-1 (Type G)
Peak Load, kN	1.4	0.6	0.8	2.3
Displacement, mm	--	--	--	--
Initial stiffness, kN/mm	--	--	--	--
Cavity width, mm	50	50	100	150
Mortar strength, MPa	7.7	6.5	6.5	6.8
Failure mode	CMU embedment	Brick embedment	Brick embedment	Brick embedment
Structural wythe	CMU	CMU	CMU	Clay Brick
Structural wythe embedment depth, mm	175	175	175	175
Veneer wythe	Clay Brick	Clay Brick	Clay Brick	Clay Brick
Veneer embedment depth, mm	45	45	45	50
Tie cross section, mm	3.66 mm rod	4.76 mm rod	4.76 mm rod	3.66 mm rod

Table 2.2: Experimental tension peak loads for L-ties tested in previous research done by Arslan et al. (2021)

Connector Type	L Tie-1 (Type CS70)	L Tie-2 (Type CB50)	L Tie-3 (Type CS50)	L Tie-4 (Type CS70-15D)
Peak Load, kN	2.4	3.4/4.2	1.9	2.5
Displacement, mm	--	--	--	--
Initial stiffness, kN/mm	--	--	--	--
Cavity width, mm	80	80	80	80
Mortar strength, MPa	5.7	5.7	5.7	5.7
Failure mode	Tie pull-out	Tie pull-out/ Tie fracture	Tie pull-out	Tie pull-out
Structural wythe	Test clamp	Test clamp	Test clamp	Test clamp
Structural wythe embedment depth, mm	Test clamp	Test clamp	Test clamp	Test clamp
Veneer wythe	Calcium Silicate Brick	Clay Brick	Calcium Silicate Brick	Calcium Silicate Brick
Veneer embedment depth, mm	70	50	50	70
Tie cross section, mm	3.6 mm rod	3.6 mm rod	3.6 mm rod	3.6 mm rod

Table 2.3: Experimental tension peak loads for corrugated sheet metal ties tested in previous research done by Muhit et al. (2022) and Choi and LaFave (2004)

Connector Type	Side-fixed sheet metal tie	Corrugated metal tie-1 (NSTE22)	Corrugated metal tie-2 (SSTE22)	Corrugated metal tie-3 (NSTE28)	Corrugated metal tie-4 (SSTE16)
Study	Muhit et al. (2022)	Choi and LaFave (2004)	Choi and LaFave (2004)	Choi and LaFave (2004)	Choi and LaFave (2004)
Peak Load, kN	1.3	0.7	1.8	0.6	1.7
Displacement, mm	7.4	--	--	--	--
Initial stiffness, kN/mm	0.5	0.15	0.11	0.03	0.31
Cavity width, mm	50	25.4	25.4	25.4	25.4
Mortar strength, MPa	10-15	5.2	5.2	5.2	5.2
Failure mode	Nail pull-out	Tie pull-out	Tie pull-out	Tie hole yielding/ tie pull-out	Tie pull-out
Structural wythe	Machine graded pine timber stud	Wood – 2×4 stud	Wood – 2×4 stud	Wood – 2×4 stud	Wood – 2×4 stud
Structural wythe to connector interface	Nail to stud	Galvanized nail to stud	Wooden screw to stud	Galvanized nail to stud	Wooden screw to stud
Veneer wythe	Clay brick	Clay brick	Clay brick	Clay brick	Clay brick
Veneer embedment depth, mm	50	80	80	80	80
Tie cross section, mm	0.9 × 6	0.8 × 22	0.8 × 22	0.4 × 22	1.6 × 22

Table 2.4: Experimental compression peak loads for Z ties tested in previous research from Hatzinikolas et al. (1979)

Connector Type	Z-Tie-1 (Type H)	Z-Tie-2 (Type H)	Z-Tie-3 (Type H)	Z-Tie-4 (Type H)	Z-Tie-5 (Type H)
Peak Load, kN	2.2	2.0	2.0	0.9	1.0
Displacement, mm	--	--	--	--	--
Initial stiffness, kN/mm	--	--	--	--	--
Cavity width, mm	50	50	100	50	100
Mortar strength, MPa	11	11	11	7.7	7.7
Failure mode	Embedment in CMU	Embedment in CMU	Embedment in CMU	Embedment in CMU	Embedment in CMU
Structural wythe	Clay brick	CMU	CMU	CMU	CMU
Structural wythe embedment depth, mm	125	175	175	175	175
Veneer wythe	Clay Brick	Clay Brick	Clay Brick	Clay Brick	Clay Brick
Veneer embedment depth, mm	50	50	50	50	50
Tie cross section, mm	3.66 mm rod	3.66 mm rod	3.66 mm rod	3.66 mm rod	3.66 mm rod

Table 2.5: Experimental compression peak loads for rectangular ties tested in previous research from Hatzinikolas et al. (1979)

Connector Type	RectangularTie-1 (Type G)	Rectangular Tie-2 (Type G)	Rectangular Tie-3 (Type G)
Peak Load, kN	4.4	3.2	4.4
Displacement, mm	--	--	--
Initial stiffness, kN/mm	--	--	--
Cavity width, mm	100	100	150
Mortar strength, MPa	11.0	7.5	14.8
Failure mode	Embedment failure in brick	Embedment failure in brick	Embedment failure in brick
Structural wythe	CMU	CMU	Clay Brick
Structural wythe embedment depth, mm	175	175	125
Veneer wythe	Clay Brick	Clay Brick	Clay Brick
Veneer embedment depth, mm	50	50	50
Tie cross section, mm	3.66 mm rod	3.66 mm rod	3.66 mm rod

Table 2.6: Experimental compression peak load for L-ties tested in previous research done by Arslan et al. (2021)

Connector Type	L Tie-1 (Type CS70)	L Tie-2 (Type CB50)	L Tie-3 (Type CS50)	L Tie-4 (Type CS70-15D)
Peak Load, kN	1.5 / 1.8	1.8	1.8	1.4
Displacement, mm	--	--	--	--
Initial stiffness, kN/mm	--	--	--	--
Cavity width, mm	80	80	80	80
Mortar strength, MPa	5.7	5.7	5.7	5.7
Failure mode	Piercing/ Buckling	Buckling	Buckling	Buckling
Structural wythe	Test clamp	Test clamp	Test clamp	Test clamp
Structural wythe embedment depth, mm	Test clamp	Test clamp	Test clamp	Test clamp
Veneer wythe	Calcium Silicate Brick	Clay Brick	Calcium Silicate Brick	Calcium Silicate Brick
Veneer embedment depth, mm	70	50	50	70
Tie cross section, mm	3.6 mm rod	3.6 mm rod	3.6 mm rod	3.6 mm rod

Table 2.7: Experimental compression peak loads for corrugated sheet metal ties tested in previous research done by Muhit et al. (2022) and Choi and LaFave (2004)

Connector Type	Side-fixed sheet metal tie	Corrugated metal tie-1 (NSCO22)	Corrugated metal tie-2 (SSCO22)	Corrugated metal tie-3 (NSCO28)	Corrugated metal tie-4 (SSCO16)
Study	Muhit et al. (2022)	Choi and LaFave (2004)	Choi and LaFave (2004)	Choi and LaFave (2004)	Choi and LaFave (2004)
Peak Load, kN	1.0 kN	0.55	0.60	0.18	3.4
Displacement, mm	3.1	--	--	--	--
Initial stiffness, kN/mm	0.7	0.15	0.13	0.12	0.86
Cavity width, mm	50	25.4	25.4	25.4	25.4
Mortar strength, MPa	10-15	5.2 (	5.2	5.2	5.2
Failure mode	Buckling	Buckling	Buckling	Buckling	Buckling
Structural wythe	Machine graded pine timber stud	Wood – 2x4 stud	Wood – 2x4 stud	Wood – 2x4 stud	Wood – 2x4 stud
Structural wythe embedment depth, mm	43	Galvanized nail to stud	Wooden screw to stud	Galvanized nail to stud	Wooden screw to stud
Veneer wythe	Clay brick	Clay brick	Clay brick	Clay brick	Clay brick
Veneer embedment depth, mm	50	80	80	80	80
Tie cross section, mm	0.9 × 6	0.8 × 22	0.8 × 22	0.4 × 22	1.6 × 22

2.3.1 Masonry Connectors under Tension

Hatzinikolas et. al. (1980), proposed Equation 2.7 to determine the capacity ties in a push or pull-out action based on conditions shown in Figure 2.6. Hatzinikolas et al. (1979) tested 11 masonry cavity wall specimens in tension and 35 in compression with eight commercially available ties shown in Figure 2.6(b). Of those 46 specimens, 12 are relevant in this thesis (rectangular ties and Z-ties, discussed more in Chapters 3 and 4). Average failure loads were compared to proposed equations which compared favourably with test results (Hatzinikolas et al. 1979). Hatzinikolas et al. (1979) concluded there is a complex interaction between tie shape, mortar strength, cavity width, and workmanship. The ability of ties to transfer load to back-ups is a function of cavity width as it relates to tie buckling, the connection of the tie to masonry as it relates to the bond strength between mortar and the masonry unit and bond between mortar and the tie, and workmanship as it relates to the position of the tie within the wall system and alignment of the tie within the cavity (Hatzinikolas et al.1979).

$$P_{ult} = 6Kd^2\left(0.15\sqrt{f_m} + vf_c\right) + \mu 2\pi rl \qquad \text{(Eq. 2.7)}$$

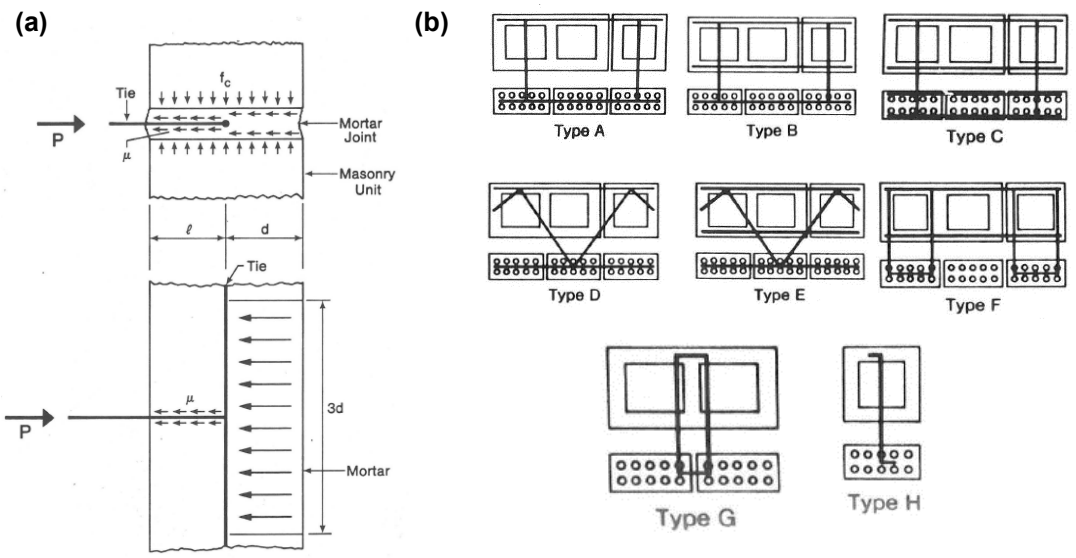

Figure 2.6: (a) Forces resisting push-out force for masonry ties with horizontal rods, (b) connector types tested from Hatzinikolas et al. (1979)

In Equation 2.7, K is a constant related to the tie diameter (1.0 for a 3.66 mm rod and 1.25 for a 4.76 mm rod), d is the distance from the horizontal rod to the face of the mortar joint, f_m is the compressive strength of mortar, f_c is the compressive stress due to vertical load at the level

considered, v is the coefficient of friction, μ is the bond strength between the rod and mortar, l is the embedment length, and r is the tie diameter. Hatzinikolas et al. (1979) used a coefficient of friction of 0.75 and an empirical bond strength shown in Equation 2.8.

$$\mu = 0.15\sqrt{f_m} \quad \text{(Eq. 2.8)}$$

For Z-ties and rectangular ties, $3d$ can be replaced by ¼ of the horizontal length of the tie limited to a maximum of 50 mm and the total horizontal length limited with a maximum of $3d$ respectively (Hatzinikolas et al. 1979).

Arslan et al. (2021) tested 202 cavity wall specimens under tension or compression with each specimen having their wythes connected by an L-shaped metal tie. The goal of their research was to develop a mechanical model to predict the failure mode and capacity of metal tie connections in masonry cavity walls under axial force and validating against their previous tests on masonry ties (Arslan et al. 2021). Arslan et al. (2021) concluded that mortar with larger strength, reduced cavity width, longer embedment depth, and brick material moderately influenced failure mode and tie capacity. Figure 2.7 shows the L-shaped tie with a zigzag-end embedded in calcium silicate brick masonry and the hooked-end embedded in perforated clay brick masonry. Potential failure modes that wall ties exhibit under tension are tie failure (fracture), cone break-out failure, and pull-out failure (Arslan et al. 2021) with pull-out being most common for connectors in tension (Table 2.2).

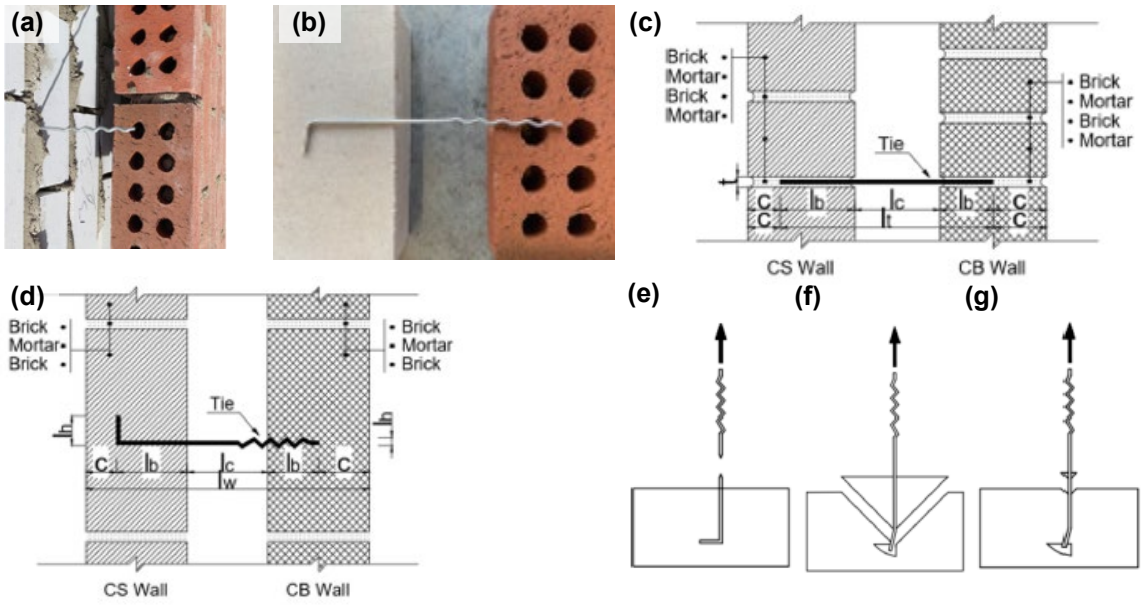

Figure 2.7: (a)Tie embedded in calcium silicate brick,(b) cavity wall tie,(c) cavity wall side view,(d) cavity wall plan view, (e) tie failure mode, (f) cone break out failure mode, (g) pull-out failure mode from Arslan et al. (2021)

Equation 2.9 was used for L-Shaped ties to determine tie capacity. A_s is the cross-sectional tie area and f_u is the tensile strength of the tie. Tie failure represents the upper limit of tensile capacity of the tie system (Arslan et al. 2021). Equation 2.10 predicts masonry cone breakout failure capacity which is similar in concept to concrete cone breakout with an assumed 45° breakout angle. The first term in Equation 2.10 defines tensile breakout of the mortar and remaining terms are related to the friction coefficient and shear strength of mortar (Arslan et al. 2021). Equation 2.11 predicts pull-out failure of the tie through the clay brick characterised by tie straightening by a combination of local crushing of mortar and the yielding of the tie, followed by extensive slip (Arslan et al. 2021).

$$N = A_s f_u \qquad \text{(Eq. 2.9)}$$

$$N = 0.332 A_{pt}\sqrt{f_m} + 2\left(\mu f_p + f_{v0}\right)A_w \qquad \text{(Eq. 2.10)}$$

$$N = 1.5 f_m l_h d + \propto \sqrt{f_m}\pi(l_h + l_b)d + \frac{12EI\emptyset}{l_c d^3} \qquad \text{(Eq. 2.11)}$$

Muhit et al. (2022) tested 25 specimens with masonry exterior veneers and timber stud back up walls in tension. The failure mode was ductile nail pull-out from the timber stud for all specimens. No pull-out of the tie from the mortar joint or tie hole yielding was observed (Muhit et al. 2022). Figure 2.8 shows a representation of their test specimen with a side-fixed veneer tie. Brick veneer and timber stud systems are typical of residential construction in North America, Australia, and New Zealand. An interesting observation during buckling was that each tie started to bend at a 90 degree angle at 20-30 mm from the nail tie timber connection (Muhit et al, 2022).

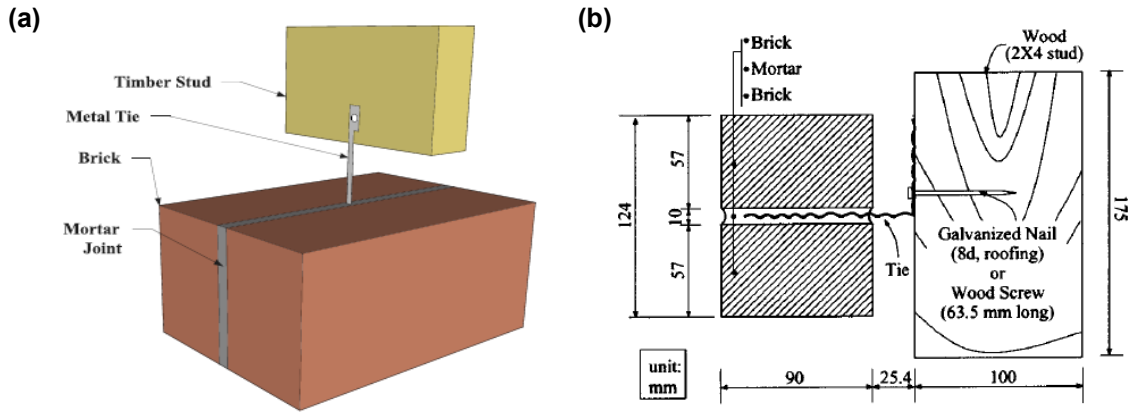

Figure 2.8: (a) Brick-tie-timber subassembly specimen with side fixed veneer tie from Muhit et. al. (2021), (b) testing system for corrugated metal ties from Choi and LaFave (2004)

Choi and LaFave (2004) tested 160 specimens to investigate corrugated metal ties for brick veneer walls of which 40 specimens underwent tension and 24 specimens underwent compression. The remaining 96 specimens of Choi and LaFave (2004) were tested in either shear, cyclic tension/compression or with an eccentricity which is not in the scope of this literature review. Specimens consisted of a brick-tie-wood assembly similar to Muhit et al. (2022) with a corrugated sheet metal tie used to connect wythes (Figure 2.8(b)). The metal ties had thicknesses of 1.6 mm (16 gauge), 0.8 mm (22 gauge), and 0.4 mm (28 gauge) fastened by either a screw or a nail to the wood stud. Choi and LaFave (2004) concluded that tension specimens with 0.4 mm thick ties failed at the tie due to low tie thickness and for 1.6 mm thick ties, failures tended to occur at mortar joints (i.e., tie pull-out). 0.8 mm thick ties failed at different locations depending on other parameters (Choi and LaFave 2004). The 1.6 mm thick ties had five times the strength and more than six times the stiffness of 0.8 mm thick ties under compression but 0.8 mm thick ties had similar tensile strength as to 0.4 mm thick ties (Choi and LaFave 2004). The reason why tie thickness did not affect tensile strength is because the tensile failure mode was tie pull-out which is more affected

by embedment length and mortar strength. Choi and LaFave (2004) also compared nail versus screw fasteners to the wood, effect of initial offset displacement, cyclic loading, eccentricity, and embedment length.

2.3.2 Masonry Connectors under Compression

The Z- and rectangular ties tested in compression by Hatzinikolas et al. (1979) were all governed by mortar in block failure modes and however the ladder type ties were governed by buckling. Figure 2.9 shows as the cavity width increases for ladder type ties under compression, the failure load capacity greatly decreases which can be attributed to elastic buckling failure.

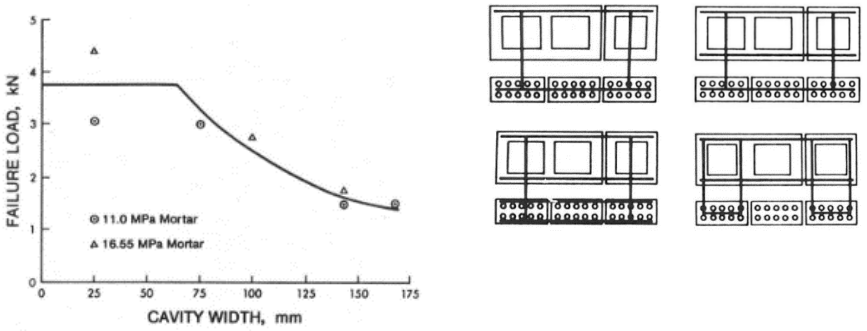

Figure 2.9: Effect of cavity width on tie compression capacity for ladder type ties from Hatzinikolas et al. (1979)

Arslan et al. (2021) investigated multiple potential failure modes for ties under compression: buckling, punching and piercing are illustrated in Figure 2.10 respectively. Table 2.6 shows the common failure mode under compression loading for Arslan's experimental program is buckling.

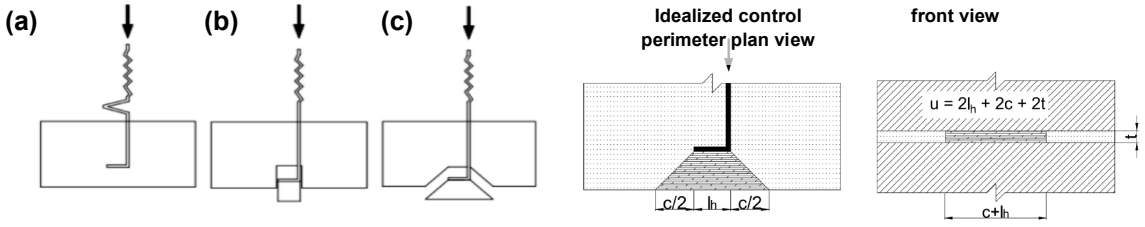

Figure 2.10: Possible compression failure modes of a) buckling failure, b) piercing failure c) punching failure from Arslan et al. (2021)

Equation 2.12 uses the critical Euler buckling load in the first term while the second term accounts for initial deformation (Arslan et al. 2021) illustrated in Figure 2.10(a). Equation 2.13 represents piercing failure (bearing failure) illustrated in Figure 2.10(b) . f_t is the tensile strength of the mortar, A_1 is the area of the loaded end which is under either the hooked end or zigzag end, and A_2 is the piercing area of mortar under the loaded end. Equation 2.14 represents the punching

failure based on the ACI empirical relationship for concrete punching failure (Arslan et al. 2021) where u represents an idealized control perimeter at a distance c from the end of the tie shown in Figure 2.10 (c).

$$N = \frac{\pi^2 EI}{K^2 l_c^2} - \frac{12EI}{l_c d^3} \quad \text{(Eq. 2.12)}$$

$$N = A_1\left(f_m + 12.5 f_t\left(\sqrt{\frac{A_2}{A_1}} - 1\right)\right) \quad \text{(Eq. 2.13)}$$

$$N = 0.332\sqrt{f_m}uc \quad \text{(Eq. 2.14)}$$

Muhit et al. (2022) tested 25 specimens in compression and 23 failed by tie buckling and the two remaining specimens failed by a combination of tie buckling and pull-out of the nail from timber. Choi and LaFave (2004) tested 24 specimens in compression with no initial displacement with the fastener being either a nail or screw and the ties between 0.4 and 1.6 mm thickness. The primary failure mode was buckling.

Figure 2.11: Primary failure mode in compression from Muhit et al. (2022)

2.4 Shear Behaviour

A masonry double wythe wall can be designed for either high or low composite action. When out-of-plane lateral load is applied to a wall, transverse shear stress acts on the member and due to the

complementary property of shear, a corresponding longitudinal shear stress also acts. A system with zero shear stiffness is non-composite and slip along the member, largest at the ends, occurs. A system perfectly bonded together (i.e., infinite shear stiffness) will have no slip as shown in Figure 2.12 (a). Systems with responses between these extremes are partially composite and analysis of these systems is particularly complex. Ensuring whether stiff or flexible connectors, the primary influence on composite action, are required for a wall to transfer load is up to the design engineer.

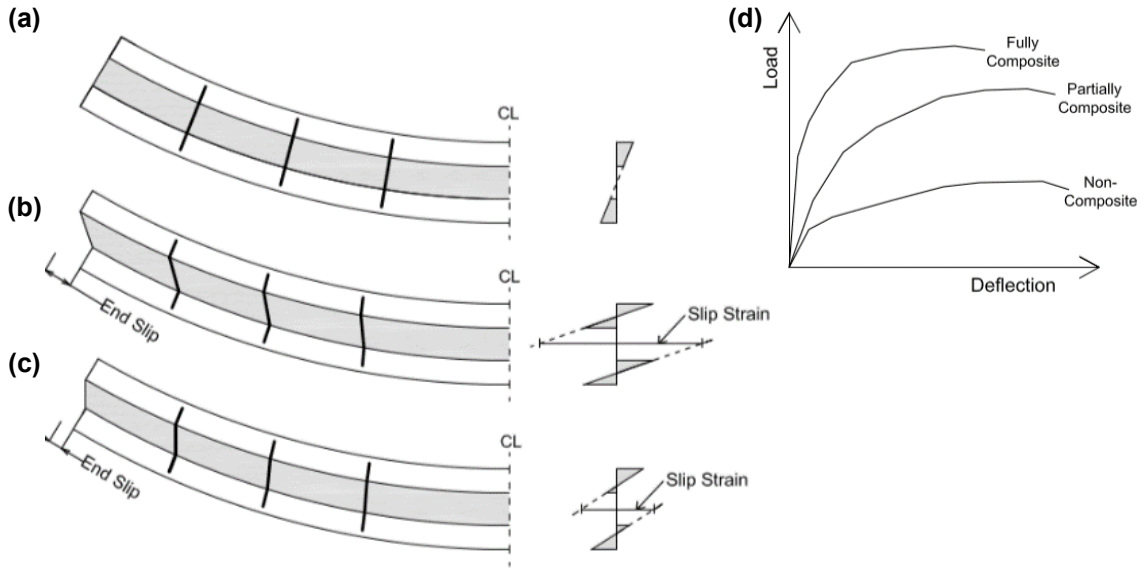

Figure 2.12: Panel showing deflected shape and strain profiles from Tomlinson (2015) for (a) fully composite, (b) non-composite, and (c) partially composite walls. In (d), sample load-deflection relationships for the three panel profiles are also shown.

The shear response of connectors has not been well studied in masonry but has been a major focus in research on insulated concrete wall panels. Arevalo (2019) tested stiff precast concrete sandwich panel connectors resulting in a wall with high levels of composite action. Goudarzi (2016) investigated connectors on out-of-plane flexural behaviour of precast insulated concrete panels and stated that truss-type connectors have larger shear strength, stiffness, and energy absorption per unit length compared to pin, grid, and ladder connectors (Bush and Stine 1994, Einea et al. 1994, Naito et al. 2012). However, Goudarzi (2016) also stated that although truss connectors have sufficient strength and stiffness to induce composite flexural behaviour in precast sandwich panels, compressive web members of truss connectors are prone to buckling, after which the interlayer shear forces are only carried by tensile web members. Due to buckling of the compressive web

members, the full plastic shear capacity of truss connectors is not mobilized; i.e. not all members of the truss connectors reach their plastic capacity which is an inefficient use of material (Goudarzi 2016).

O'Hegarty et al. (2019) tested and modeled double wythe insulated concrete walls under shear with various thicknesses shown in Figure 2.13 and concluded that all their panels had composite behaviour of less than 5% which could be due to the bond between insulation and concrete and the low stiffness of the connectors. O'Hegarty et al. (2019) based the degree of composite action on measured deflection during the linear elastic behaviour to determine the experimental moment of inertia which is an earlier method developed by Pessiki and Mlynarcyzyk (2003).

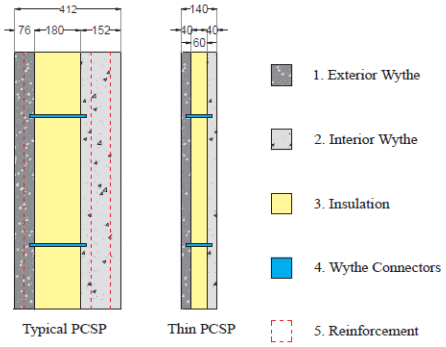

Figure 2.13: Thick and thin test specimens from O'Hegarty et al. (2019)

2.5 Gaps in Literature Review

There is a lack of understanding and testing on masonry connectors in the literature. Specifically, there are limitations with connectors tested under tension, compression, and shear loading. Existing research on masonry wall connectors focuses on simplistic metal ties but not on modern masonry connectors such as plated connectors or any type of inclined connector which may provide large degrees of composite action. There are models proposed by recent researchers but these models have not been well verified by others. These models are also only applicable to brick veneer wythes and whether the veneer material type such as selecting concrete bricks is a factor that affects the wall behaviour has not been researched for masonry wall systems with connectors. The connector design capacity from A370.14 prescribes a conservative tie resistance factor F_{co} of 0.6 and conservative connector ultimate strength P_{ult} value of a minimum of 1000 N for ties regardless of the type of connector used. These conservative connector design values are used due to a lack of understanding how different types of connectors behave in wall systems. Chapters 3

and 4 seek to address some of these gaps by investigating different connectors under tension and compression through testing and comparison to existing models from research.

3. EXPERIMENTAL INVESTIGATION OF DOUBLE WYTHE MASONRY WALL WITH DIFFERENT CONNECTORS UNDER TENSION

3.1 Introduction

Cavity walls are vulnerable to out-of-plane failure when connections between wythes are weak (Arslan, 2021; Brown and Elling, 1979; Mcginley and Hamoush, 2008; Reneckis et. al., 2004) therefore masonry connector behaviour needs to be understood. The continued development of masonry design standards and cladding failures that occurred since the 1960s brought focus to connector design and though many of these failures are associated with precast concrete or stone facing units, they are applicable to masonry cladding (Drysdale et. al., 1994).

Typical double wythe wall systems are made of an interior load-bearing wythe followed by insulation layer, air cavity, and finally an exterior wythe that can be load bearing or non-load bearing depending on the intent of the design. Wythes are connected by masonry connectors that transfer force between them without excessive relative movement (Drysdale et. al., 1994). The wall tie connections must support the veneer and transfer lateral load from the veneer to the back up wall through both tension and compression.

The expected load distribution for ties in a wall is given in CSA S304-14 by requiring ties to resist a conservative value of 40% of the tributary lateral load on a vertical line of ties but not less than double the tributary lateral load which is in agreement with research that indicates larger tie loads at the top and bottom of walls (Brown and Elling, 1979; Mcginley and Hamoush, 2008; Reneckis et. al., 2004). Tie load distribution in a full wall is beyond the scope of this thesis but is important to mention since this chapter shows the axial capacity individual ties can support under tension and relevant to assessing tie capacity at the top and bottom of a wall.

Individual connector behaviours are required to understand the behaviour of a full wall. Some research programs with connector data use a wood stud structural backing (Muhit et. al., 2022; Choi and LaFave, 2004) while others use a CMU structural backing (Hatzinikolas et al., 1979; Arslan et. al., 2021). A key difference when comparing previous research (see Section 2.3) is that cavity width is not the same for all of them.

To investigate the tension behaviour of masonry cavity walls with four different connectors, a test frame inspired by Hatzinikolas et al. (1979) was fabricated to apply tension to an individual connector embedded in masonry wythes. The tested connectors are longer than typical connectors

used in industry since these tests account for expected increases in insulation thickness from future energy codes. Peak loads and deformations are compared to previous research where applicable.

3.2 Experimental Program

Thirty one specimens were tested in tension. There were four different tested connectors (Z-tie, rectangular tie, plated connector, inclined connector) with a general overview of them shown in Figure 3.1. Tests included specimens with exterior veneers being either clay brick or concrete brick while all interior structural backings were CMUs. CMUs were used due to their popularity in North American construction. The CMUs are typical of structural wall systems with nominal 200 mm width while the brick veneer is 100 mm in width. A clay brick veneer is the most common choice driven by architects due to aesthetics when selecting a veneer for the structural backing. A concrete brick veneer was selected to have a comparison point to architects who may prefer a concrete veneer. Beyond aesthetics, durability which is often linked to compressive strength can be compared between concrete and clay brick due to different compressive strength properties ranging around 20 MPa and 20 to 145 MPa respectively (Drysdale et al., 2005).

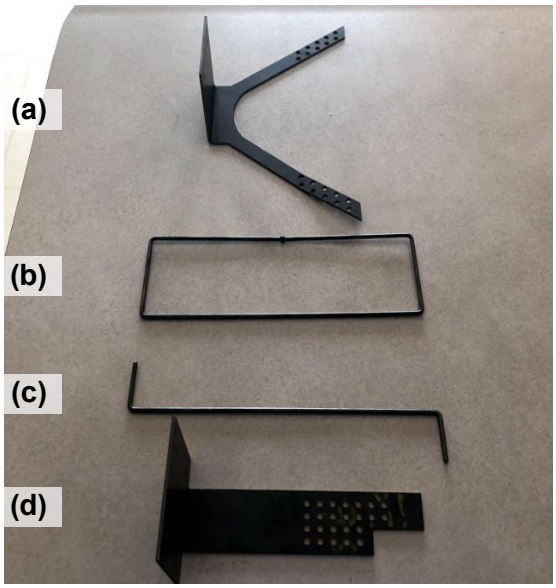

Figure 3.1: Connectors tested in this research program (a) inclined connector, (b) rectangular connector, (c) Z-tie connector, and (d) plated connector

The reason why different connectors were tested is because the selected connectors cover a range of connectors used in past and modern construction. This is done to assess connector behaviours for most types used in industry because there is limited to no available information due to many connectors in use being proprietary. The Z-tie and rectangular ties reflect past construction, plated

connectors reflect modern construction, and the inclined connectors are a novel concept described more later.

Insulation in this program will be 150 mm to reflect alternative options for future building energy code requirements. Residential construction often uses ~150 mm thick fibreglass batt insulation which is less efficient than the EPS used in these tests (i.e., 150 mm of EPS has a larger R-value than 150 mm of fibreglass batt insulation). That said, the insulation thickness increase will not affect tensile behaviour of the connectors. The air cavity in each specimen is 25 mm thick to provide proper air/vapour flow to the building envelope and represents current construction practice.

The total wall thickness of each specimen is 481 mm which is representative of the expected wall thickness in practice. The other dimensions (height and width) were minimized to satisfy lab space constraints and specimen weight while still being large enough to be representative of a full wall (for instance, permitting potential breakout cones to form without edge effects or restraints). Figure 3.2 shows a specimen's individual components which are the wythes, insulation and cavity.

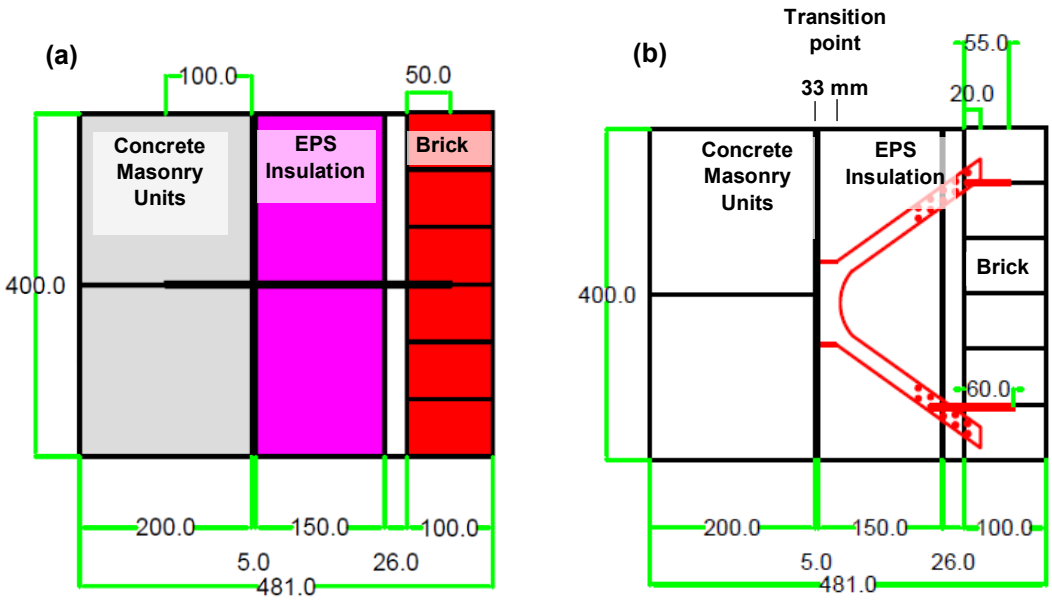

Figure 3.2: Specimen side view illustrations (a) typical connectors (b) inclined connector. All dimensions in mm.

3.2.1 Connector Description – Z-ties

Z-tie connectors were selected because these are commonly used in masonry walls and tested by Hatzinikolas et. al (1979) to determine connector capacity in tension and compression. Arslan et

al. (2021) tested L-shaped ties which are similar to these Z-ties and serves as further comparison. The Z-tie has a steel grade of 380W, typical of the CSA G40.21 standard, and classified as weldable plain steel. The connector has a nominal diameter of 4.8 mm and nominal cross-sectional area of 18 mm^2. Ties were embedded 50 mm into the brick veneer and 100 mm into the CMU backing. These are representative of practice where connectors are embedded to half the wythe thickness with the other half used as cover. The main anchorage mechanism for the Z-tie connectors are embedment and hooks at both ends within the mortar joints as shown in Figure 3.3.

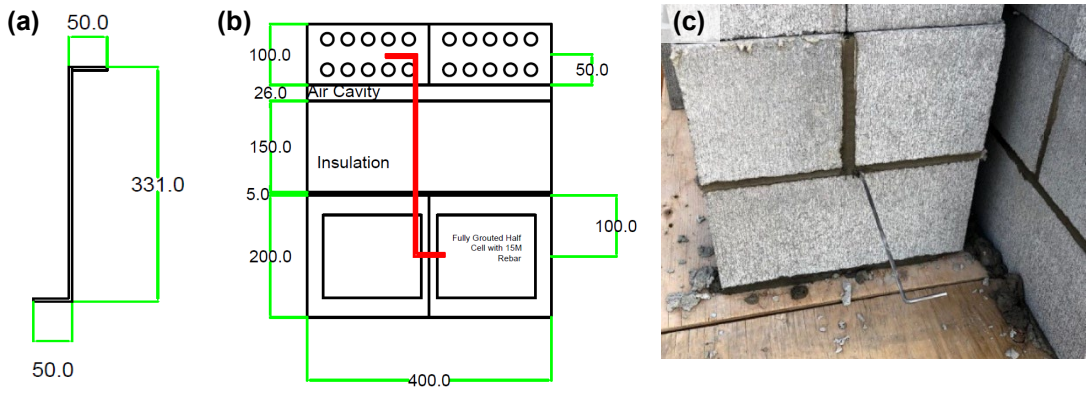

Figure 3.3: Z –tie connector illustrations (a) Z-tie, (b) wall cross-section with Z-tie, (c) wall specimen without brick veneer. All dimensions in mm.

3.2.2 Connector Description – Rectangular Ties

Rectangular tie connectors, shown in Figure 3.4, were selected because, like Z-ties, they were part of Hatzinikolas et al. (1979) test program. The rectangular tie steel grade and nominal diameter is the same as the Z-tie. The total nominal connector area was 36 mm^2 since two legs cross the cavity between the two wythes. The embedment depth for the rectangular tie into the exterior wythe is 25 mm shown in Figure 3.4 (b). The embedment depth was meant to be 50 mm to match construction practice but the rectangular ties were not constructed per the original drawings due to a miscommunication with the masonry trade during construction.

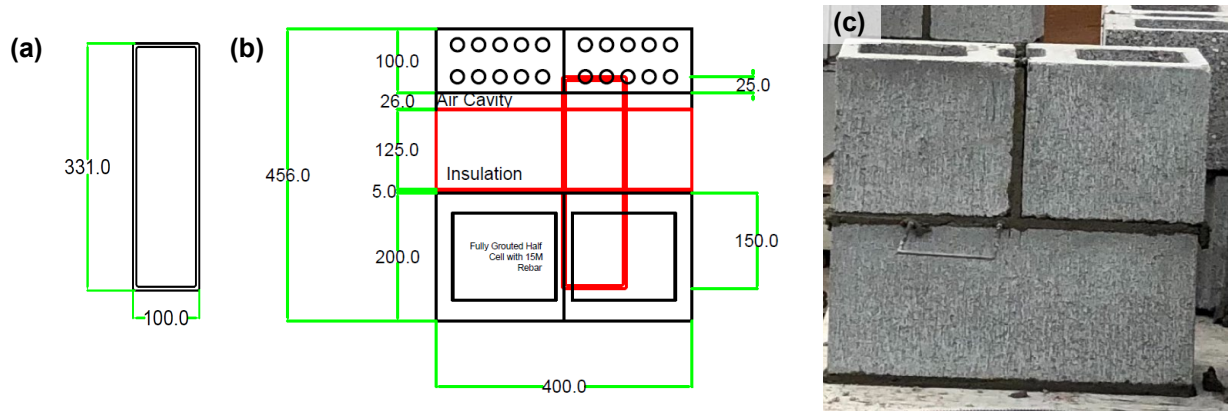

Figure 3.4: Rectangular tie connector illustrations (a) rectangular tie, (b) wall cross-section with rectangular tie, (c) wall specimen without brick veneer. All dimensions in mm.

3.2.3 Connector Description – Plated Connector – Lying Orientation

Plated connectors were chosen to assist in composite behaviour due to their expected shear transferring capabilities and this configuration is similar to masonry connectors on the market. This plated connector with a lying down orientation is most similar to the brick tie used in stud frame wall construction (Figure 1.2(a)). General dimensions of the plate connectors are provided in Figure 3.5. The nominal connector area and thickness is 150 mm^2 and 3.0 mm respectively. Cross section A1 with four holes and cross section B1 with two holes illustrated in Figure 3.5 is 90 mm^2 and 60 mm^2 respectively which also shows the location and amount of holes.

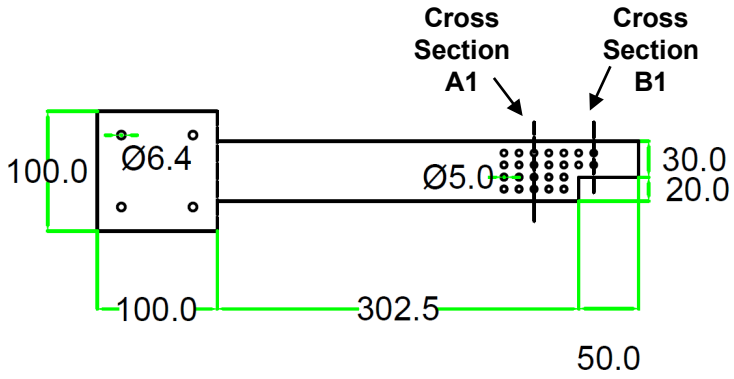

Figure 3.5: Plated connector reduced cross sectional areas due to connector openings. All dimensions in mm.

More details on the connectors and how they interact with masonry is given in Figure 3.6. The anchorage to the CMU for the plated connectors consists of commercial stainless steel Hex Tapcons with a 6.4 mm diameter and 69.9 mm length drilled into the CMU. These fasteners are typically used on concrete and masonry elements. Four fasteners were used for each specimen to prevent fastener failure per the Tapcon manufacturer's performance tables (Tapcon, 2013). The

specified tensile capacity for a 6.4 mm diameter Tapcon fastener with a minimum embedment of 44.5 mm is 9.0 kN in 13.8 MPa concrete. The intent of this research program is to focus on connector and veneer behaviour so the wall tie connection to the CMU was over designed with four Tapcon fasteners. Even considering prying and group effects, the total expected tension capacity for these four fasteners is larger than the expected tensile capacities of the connectors used in this program. This is evidenced by fastener failure not being observed in any tests.

For the veneer wythe, the anchorage mechanism is through a 50 mm embedment of the plated connector into the horizontal mortar joint shown in Figure 3.6(b). The embedment veneer tie shown in Figure 3.6(a) was not used for the plated connector with a lying orientation due to the challenge in lining up with a vertical mortar joint in the brick veneer.

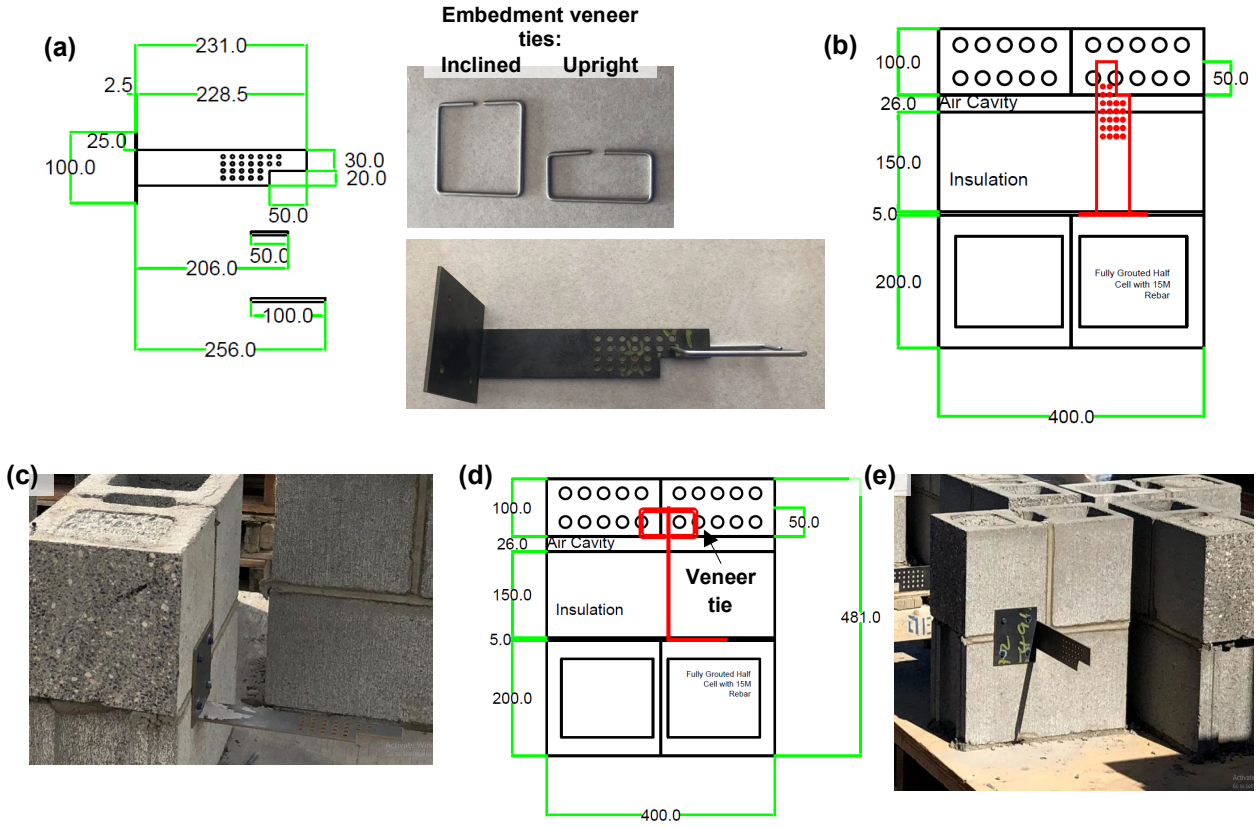

Figure 3.6: Plated connector illustrations (a) plated connector including embedment veneer ties, (b) wall cross-section with lying connector, (c) wall specimen without brick veneer, (d) wall cross-section with upright connector, (e) wall specimen without brick veneer . All dimensions in mm.

3.2.4 Connector Description – Plated Connector – Upright Orientation

This plated connector has the same properties as the previous connector described in section 3.2.3 with the main differences being that it was placed in an upright orientation and it had an

embedment veneer tie shown in Figure 3.6(d) and (e). The upright orientation had less mortar joint location challenges allowing proper veneer tie embedment compared to the lying down orientation. This allowed the connector to have an embedment veneer tie placed in a connector hole. 5 mm diameter holes were drilled into the connectors to facilitate multiple options of placement for the embedment veneer tie and improve anchorage to the veneer wythe.

3.2.5 Connector Description – Inclined Connector

The inclined connector, shown in Figure 3.7, is a novel system designed by myself not currently used in industry but intended to have a greater resistance than modern plated connectors under longitudinal shear due to truss action. To my knowledge there are no inclined masonry connectors existing in industry likely due to the challenges in anchorage at the veneer wythe due to multiple mortar joints. This challenge is mitigated by embedment veneer ties taken into account by myself during the design concept of this novel inclined connector system explained further below. This inclined connector may reduce the number of connectors required for a wall but will be assessed more in future studies. The potential for fewer thermal bridges is another advantage to using an inclined connector. Since the inclined connector has twice as many anchorage points due to the legs and embedment veneer ties, this is expected to increase capacity compared to the connectors previously discussed.

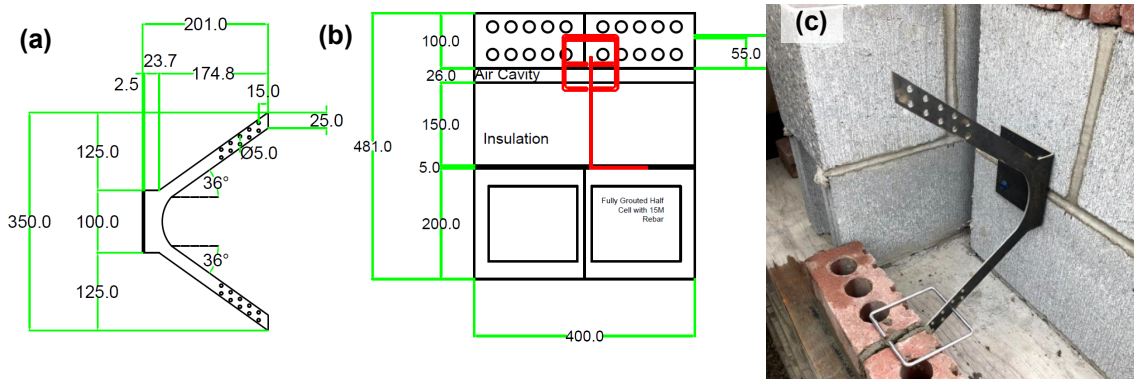

Figure 3.7: Inclined connector illustrations (a) inclined connector, (b) wall cross-section with upright connector, (c) wall specimen without brick veneer. All dimensions in mm.

Due to the challenge of a veneer tie lining up with a horizontal mortar joint multiple connector openings were drilled into the inclined connector's legs. The connector openings can also act to minimize thermal bridging. An inclination angle of 36° was selected so that both the top and bottom ends of the inclined connector meet a horizontal mortar joint for increased anchorage and

to ensure that holes line up with the veneer tie. Figure 3.2(b) and 3.7(c) shows the veneer ties located at the highest and lowest possible mortar joint. This concept of adjusting veneer ties at various heights was inspired by Dr. Hatzinikolas who developed a commercial masonry connector using this concept. The actual brick veneer embedment of these veneer ties for the inclined connector were 55 mm for the top horizontal mortar joint and 60 mm for the bottom horizontal mortar joint. Since the thickness of the plate is 3.0 mm, the cross-sectional area for the inclined connector with no holes is 75 mm^2. for each individual leg. Cross section C1 with two holes for each individual leg is illustrated in Figure 3.8 as 45 mm^2. Cross section C1 and D1 show the location of the embedment veneer tie in Figure 3.8.

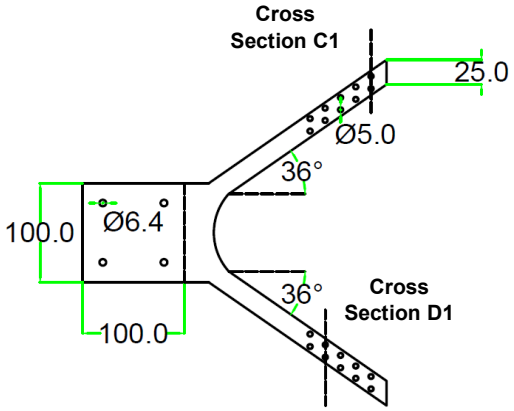

Figure 3.8: Inclined connector reduced cross sectional area due to connector openings. All dimensions in mm.

3.2.6 Tension Test Matrix

Table 3.1 shows the tension test matrix. Either the connector type was changed (described in Section 3.2.1 through Section 3.2.5) or the exterior veneer material was changed (described in Section 3.2).

Table 3.1: Tension test matrix

Test Identifier	Connector type	Connector Diameter / Thickness, mm	Nominal connector area, mm^2	Embedment in Brick Veneer, mm	Veneer brick material
T-Z.CN-1,2,3	Z-tie	4.8	18	50	Concrete
T-Z.CL-1,2,3	Z-tie	4.8	18	50	Clay
T-R.CN-1,2,3	Rectangular tie	4.8	36	25	Concrete
T-R.CL-1,2,3	Rectangular tie	4.8	36	25	Clay
T-PV.CN-1,2,3	Plated connector	3.0	150	50	Concrete
T-PV.CL-1,2,3	Plated connector	3.0	150	50	Clay
T-PH.CN-1,2,3	Plated connector	3.0	150	50	Concrete
T-PH.CL-1,2,3	Plated connector	3.0	150	50	Clay
T-IN.CN-2,3	Inclined connector	3.0	150	20	Concrete
T-IN.CL-1,2,3,4,5	Inclined connector	3.0	150	20	Clay

The first designation specifies C for Compression and T for Tension (for this chapter only T is considered). The second specifies R for a rectangular tie, Z for Z-tie, PH for plate connector placed lying down (H = horizontal), PV for plate connector placed upright (V = vertical) and IN for inclined connector. The third specifies CL for clay brick veneer and CN for concrete brick veneer. The final numbers specify the specimen ID number. Most specimens had three identical specimens to investigate variability with the T-IN.CN and T-IN.CL specimens having a different amount due to damage during transportation and extra material respectively. An example of this test identifier format is C-Z.CL-2 which represents a compression wall specimen with a Z-Tie connector of clay brick veneer and the second specimen of that type tested.

3.2.7 Materials

The specimens had core fill course grout, Type S portland lime and sand premixed mortar, and connector materials tested as part of an ancillary program. The plate connectors had a thickness of 3.0 mm consisting of mild steel and the wire connectors had a diameter of 4.8 mm. Findings are shown in Table 3.2 comparing the tested average yield value with the standard material specification listed by the supplier.

Table 3.2: Material properties

Material	Mean Tested Value, MPa	Standard Deviation of Tested Values, MPa	CoV	Specification Value, MPa	Relevant Standard
Grout	28.2	2.3	0.08	20.6	CSA A179
Mortar	16.9	4.9	0.29	12.5	CSA A179
Plated Connectors	234	5.5	--	--	CSAG40.21
Tie Connectors	569	8.5	--	--	--
Clay Brick	N/A	N/A	N/A	N/A	CSA A82
Concrete Brick	N/A	N/A	N/A	55	CSA A165.2
CMU	17.1	1.42	0.08	15	CSA A165.1

The brick units did not undergo auxiliary testing but it is noted that there is variability in their material properties. Due to the observed failure modes that the wall system underwent with tension and compression testing, mortar and connector properties were the main materials that governed failure. Further explanation into auxiliary testing protocol and commentary is provided in Appendix A.

3.2.8 Specimen Fabrication

A certified mason constructed all specimens with the assistance of myself. Elevated pallet platforms to contain four specimens each were set up before construction for a forklift to easily lift multiple specimens loading onto a transportation vehicle. I assisted the mason by carrying material,

placing the correct amount of masonry units onto each pallet, and placing the insulation in each specimen which included cutting of the insulation layer to the required specimen's size. Each specimen was constructed in three stages: the CMU/connector phase, cavity phase, and the veneer phase. Figure 3.9 illustrates the construction process. Starting with the CMU/connector phase shown in Figure 3.9(a), CMUs were stacked with mortar joints, grout filled, and vertical reinforcement placed in one cell by the mason. Grout mixes and mortar mixes were made by the certified mason and his equipment. I acquired grout cylinders and mortar cubes throughout different phases of construction for auxiliary testing to be performed later. Reinforcement was 10M and cut to match the height of the specimen. Reinforcement was placed by the mason at the midpoint of the CMU cell in only one cell which is typical in construction practice. Grout and mortar were given a minimum of 48 hours to cure to develop sufficient strength for the cavity phase. If the connector for that specimen was a tie, it was placed in the mortar joint at the same time as the joints were made by the mason. The cavity phase involved placement of the insulation through the connector done by myself. Typical insulation is available in 75 mm thicknesses so two insulation boards were glued together with a construction adhesive to ensure they bonded as a 150 mm thick insulation. The veneer phase in Figure 3.9(c) consisted of placing the brick veneer and mixing mortar done by the mason. The main difference in the construction specimen process with a masonry plate connector is that the connector was not placed until the grout cured for a minimum of 48 hours. Fastener holes were drilled in the CMU wythe by the mason. The plated connector was then fastened into the concrete masonry unit with four fasteners by the mason. Another minor difference is the placement of the embedment veneer ties during the veneer phase as the brick mortar joints were being placed.

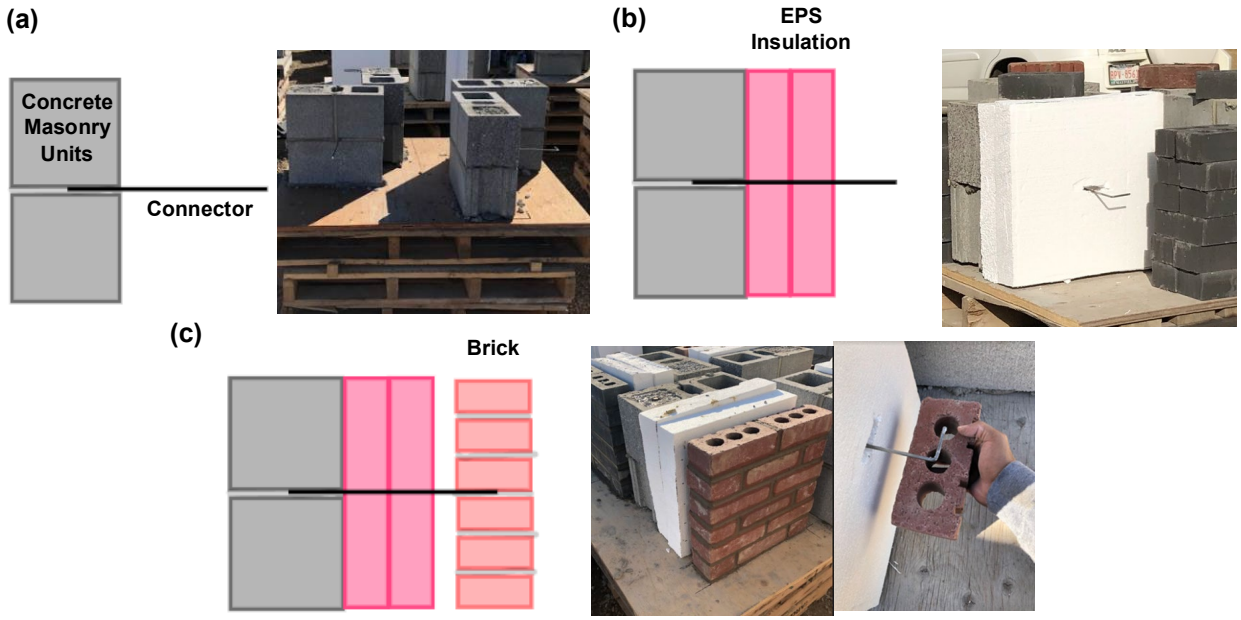

Figure 3.9: Specimen construction illustrations of tie connectors (a) CMU/connector phase, (b) cavity phase, (c) veneer phase

Specimens were constructed outside in a masonry company's yard. Specimens were covered in tarps at the end of each day to protect them from the elements by myself. When samples were tested, they all met or exceeded the listed fabricator's specified 28 day strength. Further comments and data on the auxiliary testing is provided in Appendix A. Lab access for testing was a challenge during the COVID-19 pandemic and specimens were left outside for months to experience the extreme temperature ranges (~+30°C to −30°C) of Edmonton, Alberta due to the specimens being constructed in July and stored outside until they were transported to an indoor facility in March.

3.2.9 Test Frame Design

The test frame was designed by myself and inspired by Hatzinikolas et. al. (1979) who presented a frame consisting of two plates sliding on metal tracks and a hydraulic jack for load application shown in Figure 1.5. S-Frame (Altair, 2021) was used by myself to analyze and design the test frame in this program. The primary sections used for the frame are HSS steel and threaded rods. A third party steel fabricator (Carry Steel) constructed the test frame and delivered it to the testing location.

The self reacting test frame was designed by myself to test specimens under tension or compression similar to the frame shown in Figure 1.5. Specimen clearances between wythes and specimen size were taken into consideration by myself when designing the frame for testing.

Section view A-A in Figure 3.10 (a) shows an 'X' layout made of steel HSS used to provide a surface for CMU wythe bearing under compression and to provide four location points for the threaded rods to hold the CMU wythe in place under tension shown in Figure 3.11(d). Customized platforms shown in Figure 3.12 were designed by myself to withstand and apply load to the various specimen configurations with a conservative capacity of 50 kN because the maximum expected loading for connector material failure modes was around 30 kN.

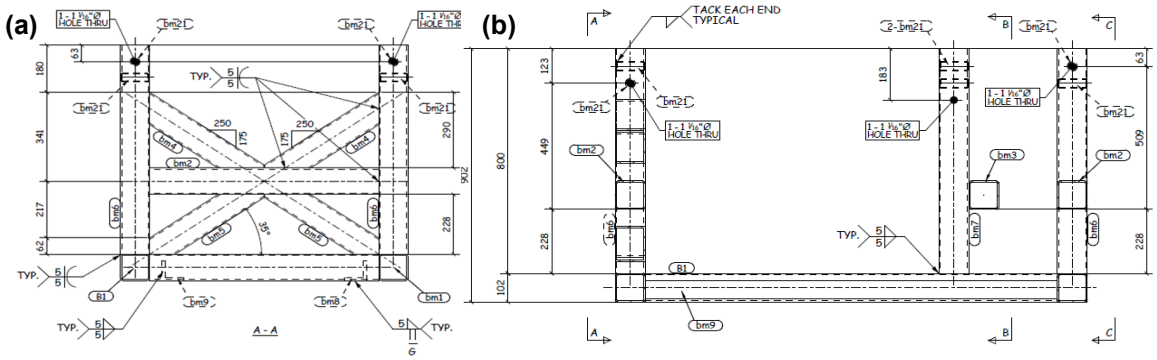

Figure 3.10: Test frame fabrication drawings of (a) section view A-A, (b) elevation view. All dimensions in mm.

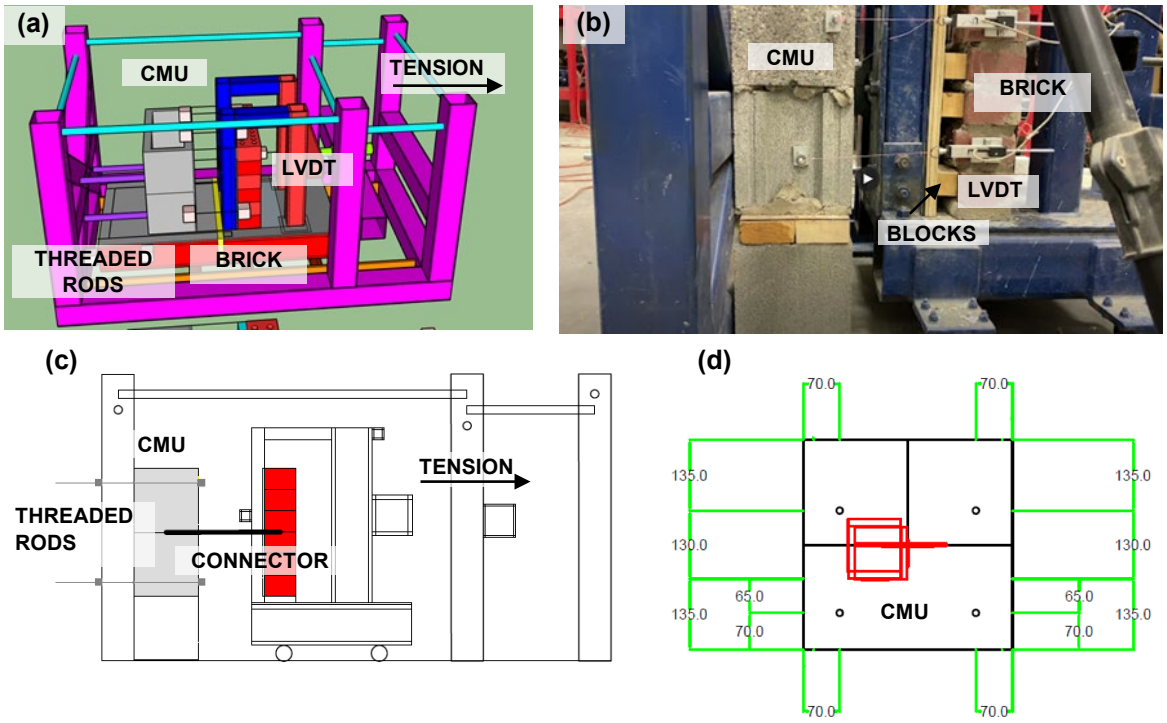

Figure 3.11: Tension testing with specimen in experimental frame of (a) initial conceptual design, (b) actual testing set up including blocks for even loading distribution, (c) actual test set up illustration, (d) threaded rod locations. All dimensions in mm.

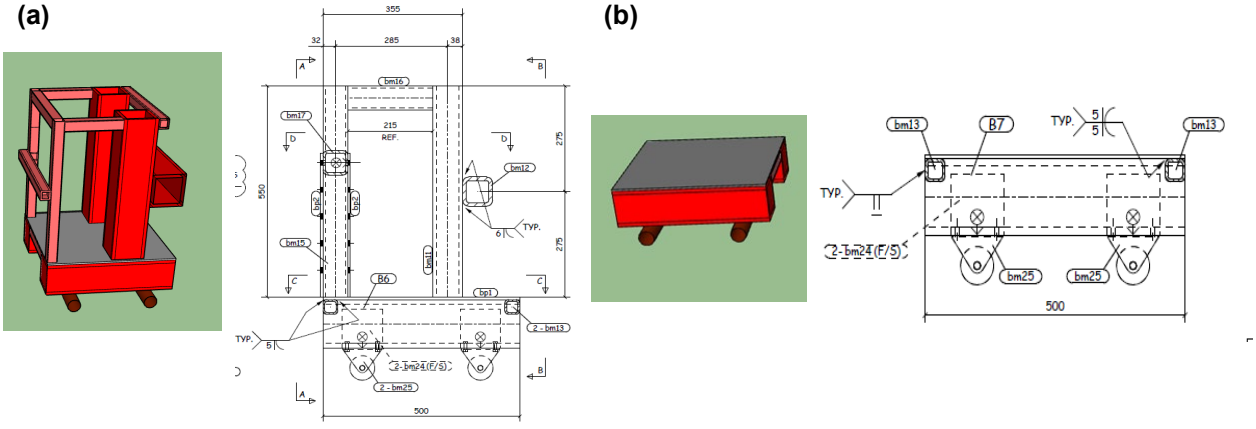

Figure 3.12: Test frame platform illustrations (a) modified platform, (b) standard platform. All dimensions in mm.

For tension tests, one end of the frame was drilled into to facilitate the placement of four Grade 2 (minimum yield strength, f_y, of 393 MPa) threaded rods with a diameter of 12.7 mm that were tightened before testing to hold the CMU wythe in place as shown in Figure 3.11(c). Four threaded rods were used to prevent localized failure of the CMU along its edges and to distribute load as

uniformly as possible. No localized failures were observed in tests so the four threaded rods were deemed sufficient to distribute applied load through the CMU.

Since some bricks in the wythe were jagged, rectangular blocks of leftover EPS were placed on the masonry courses to promote even distribution of load to the brick wythe in tension tests. Rectangular blocks were glued onto the brick wythes lining up with a wood layer of sheathing connected to the modified platform.

The setup was based on Hatzinikolas et. al (1979) but adjustments were made to their concept due to ease of specimen handling by using a more optimum loading setup and testing considerations. The main adjustment was that a second platform was not required due to a CMU with lumber placed on top being equivalent to provide a level surface for the CMU wythe portion of the specimen. A level surface was determined visually by having the connector level even with two different surfaces for both the veneer wythe and CMU wythe. Determining a level connector between mortar joints visually is also done in construction practice because it is not realistic to individually measure and determine a perfectly level connector with a level or plumb bob for every connector. The removal of the second platform was done to make the tension setup process easier and achieve more efficiency (tests that can be completed per day).

3.2.10 Test Setup and Instrumentation

A hydraulic Enerpac RCH123 jack was used to load specimens under tension or compression (Chapter 4). The jack was fit with a load cell to record load during each test. The maximum expected load was 30 kN which is less than the jack's capacity of 135 kN and fits into the load cell's range for recording. Six linear variable displacement transducers (LVDTs) were placed to measure relative movement between each wythe as shown in Figure 3.13. The maximum expected displacement is less than 25 mm which is the LVDT range.

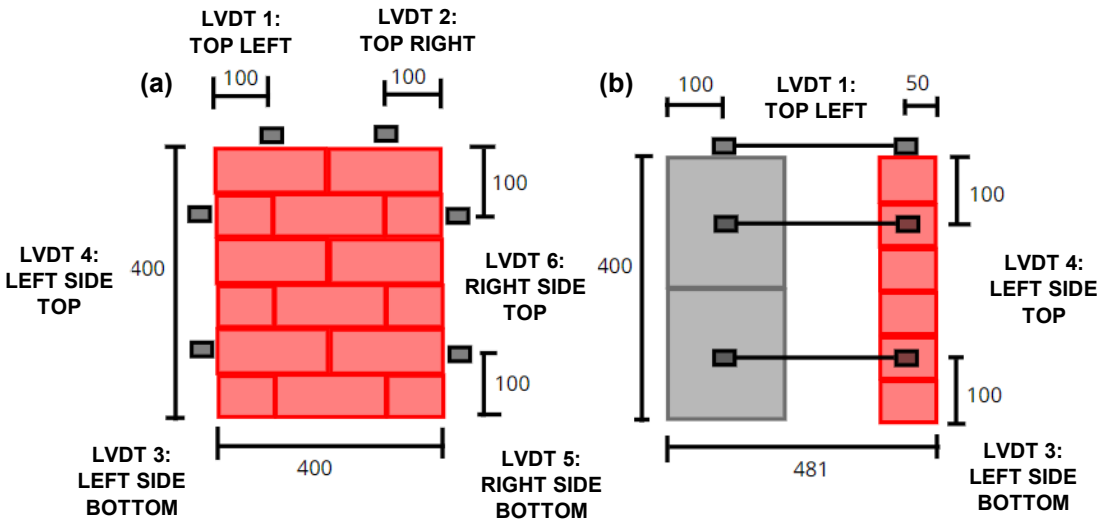

Figure 3.13: LVDT locations (a) cross section view (b) elevation view. All dimensions in mm.

The load rate was controlled manually using a hand pump during tests for all specimens as servo-hydraulic controls were unavailable at the time of testing. The average loading rate for the Z-ties, rectangular ties, plated connector with an upright orientation, plated connector lying down and inclined connector were 2.17 mm/min, 1.59 mm/min, 3.92 mm/min, 10.0 mm/min and 9.43 mm/min respectively. The individual tension loading rates and calculation method are provided in Appendix B.

When testing masonry specimens a surcharge load is required per CSA A370-14. The surcharge load simulates a nominal dead load that may be imposed on a connector near the top of a wall which is expected to be the critical location since increased gravity load at a lower location in a wall can increase connector anchorage through clamping (CSA A370, 2014). Weights available in 20 lb (0.09 kN) and 50 lb (0.22 kN) increments were placed on each wythe (Figure 3.14). A brick was placed on each wythe for weights to rest on due to the irregular shape of the weights interfering with instrumentation placement. The loading brick veneer dimensions were 400 by 100 mm, and the weight placed on the brick and CMU wythes were 0.31 kN (7.8 kPa) and 0.82 kN (10.3 kPa) respectively. 7.8 kPa was applied on the bricks from the weights and the self weight of the bricks (17 N each) on top increase this pressure to 10.3 kPa at the level of the connectors which is acceptable for CSA A370-14. A surcharge of 7.8 kPa was also applied on the inclined connectors from the weights with the self weight of the bricks increasing this pressure to 12 kPa for the lower inclined connector leg and 8.6 kPa for the upper inclined connector leg. The upper inclined

connector leg is less than the required 10 kPa which may lead to weaker responses than expected if it the upper connector leg tie was loaded to a larger surcharge compliant with CSA A370.

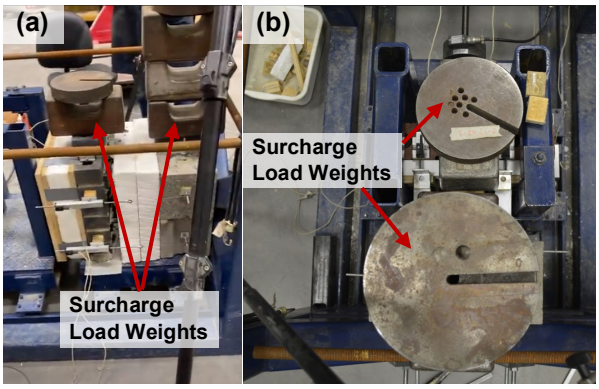

Figure 3.14: Surcharge load weight placement for test specimens (a)side view (b) top view

Two video iPhone cameras were also placed to have a better view of the different failure modes and to visually determine whether or not insulation bearing occurs (relevant for compression tests).

3.3 Tension Test Results

The primary failure mode under tension was either a breakout embedment failure or pull-out failure. The breakout embedment failure can be further classified into either a cone, angular, or tie breakout which is discussed in later sections. All plated connector specimens with a veneer tie except T-PV.CL experienced minor veneer tie yielding in addition to the primary failure mode. Table 3.3 summarizes the results from all tension tests for each specimen type and Figure 3.15 illustrates the tension load displacement plots for all specimens. A maximum displacement of 30 mm is shown on Figure 3.15 to show the peak load and an appropriate representation of the post peak tensile response for all connectors.

Table 3.3: Summary of test results under tension loading

Test ID	Ave. peak load, kN	Standard deviation, kN	CoV	Ave. displacement at peak load, mm	Average initial stiffness, kN/mm	Failure Mode
T-Z.CL	2.57	0.81	0.32	1.5	11.0	Cone breakout
T-Z.CN	1.84	0.47	0.26	1.6	8.9	Cone breakout
T-R.CL	1.92	1.09	0.57	0.6	4.8	Angular breakout
T-R.CN	1.95	0.62	0.32	0.9	6.2	Angular breakout
T-PV.CL	3.82	0.31	0.08	6.7	4.4	Tie breakout
T-PV.CN	4.40	0.37	0.08	7.2	3.5	Tie breakout/yielding
T-PH.CL	3.43	0.55	0.16	8.6	10.9	Pull-out
T-PH.CN	5.41	1.26	0.23	17.9	2.0	Pull-out
T-IN.CL	5.61	0.80	0.14	20.1	1.0	Pull-out/yielding
T-IN.CN	6.39	1.17	0.18	15.4	1.7	Pull-out/yielding

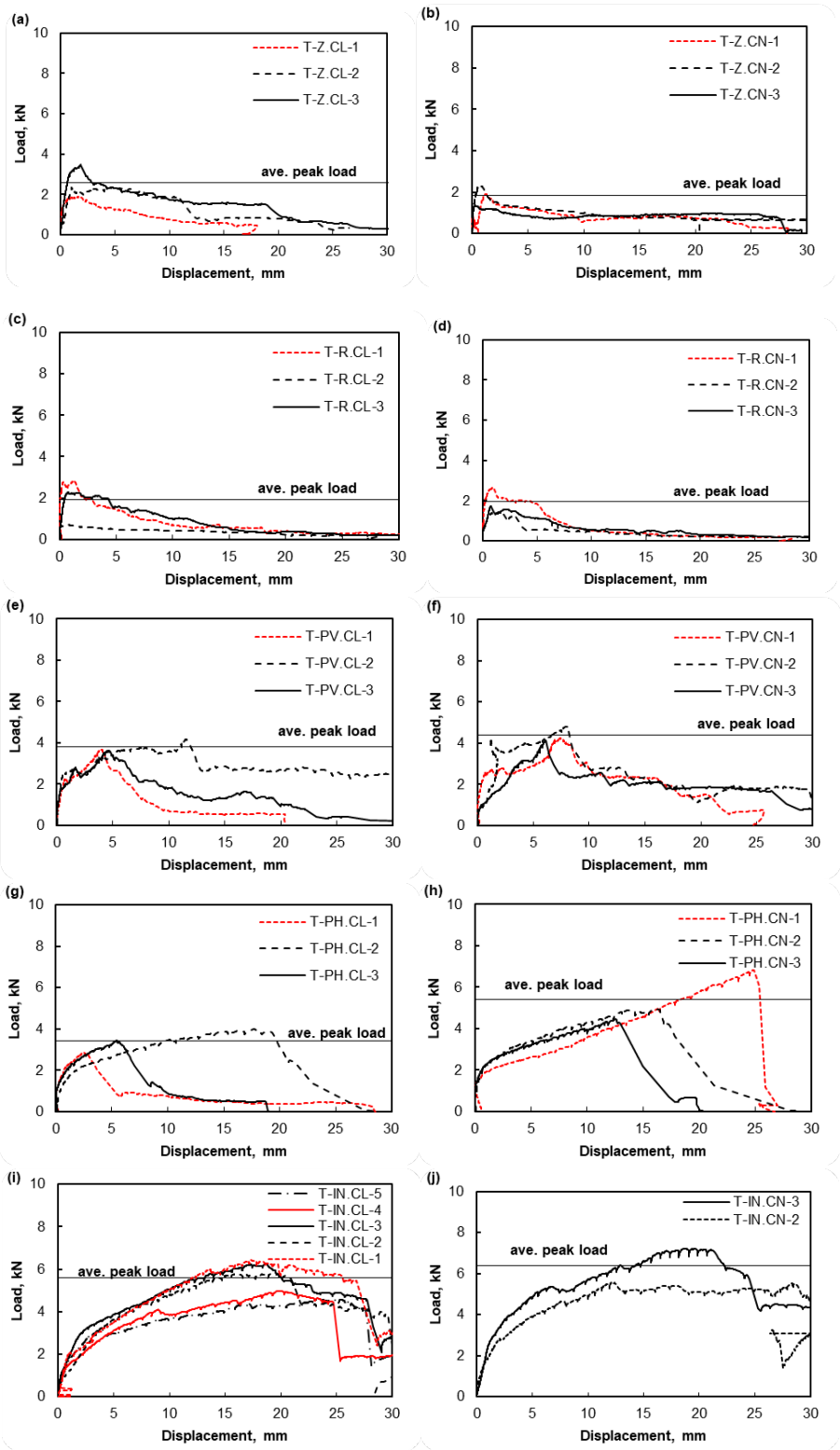

Figure 3.15: Tension load displacement plots for (a) Z tie with a clay veneer, (b) Z tie with a concrete veneer, (c) rectangular tie with a clay veneer, (d) rectangular tie with a concrete veneer, (e) plated connector with an upright orientation with a clay veneer, (f) plated connector with an upright orientation with a concrete veneer, (g) plated connector lying down with a clay veneer, (h) plated connector lying down with a concrete veneer, (i) inclined connector with a clay veneer, (j) inclined connector with a concrete veneer

More detailed explanations of each test are provided in the next sections. These explanations also include discussions on connector stiffness. This stiffness is taken as a secant between two points corresponding to 10% and 40% of the peak load. The secant method was found to be appropriate for evaluating connection stiffness of precast wall panels (Arevalo 2019) and calculated using Equation 3.1. The reason 10% is taken is because this is where settling is expected to have already taken place and 40% is the expected response before non-linearity occurs (proportional limit).

$$k_{secant} = \frac{F_{0.4peak} - F_{0.1peak}}{\Delta_{0.4peak} - \Delta_{0.1peak}} \quad \text{(Eq. 3.1)}$$

Six LVDT sensors were placed but the LVDT sensors selected for displacement averages for the specimens are averaged out over four LVDT sensors. Two extra LVDT sensors was mounted in case other LVDTs did not properly record displacements which occurred in some tests. A top pair and bottom pair were selected for the specimen displacement values to represent the overall displacement which is why an average is selected to offset rotations. There is one bottom LVDT sensor pair 3,5 and two top LVDT sensor pairs 1,2 or 4,6 to select from shown in Figure 3.13. The criteria for removing an LVDT in the calculated average is if there are constant value recordings, including zero, as load increases. Constant displacement readings were compared with other top LVDT sensor pair and bottom LVDT sensor pair readings to determine if it is recording a realistic response based on the other LVDTs. Figure 3.16(a) shows LVDT sensor pair 1,2 having bad agreement due to zero displacements compared to the other LVDTs which is why they were removed and not included in the selected LVDTs for the displacement average in Figure 3.16(b).

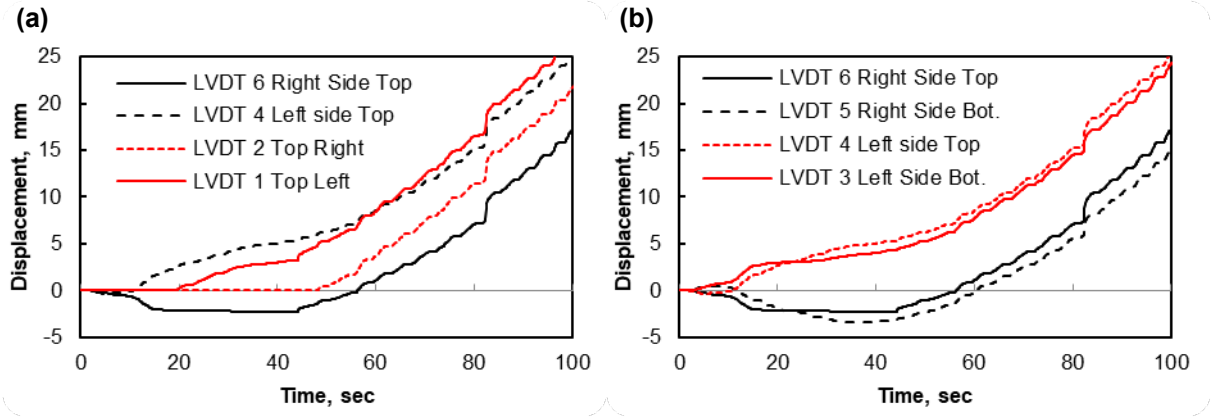

Figure 3.16: T-Z.CL-2 recorded displacements of (a) excluded LVDT sensors, (b) selected LVDT sensors to determine averages

3.3.1 Experimental Tension Results for the Z-tie Connector

Table 3.4 summarizes results for each of the Z-tie connectors and Figure 3.15 (a) and (b) illustrates the tension load displacement plots for each Z-tie specimen. Failure progression and modes for z-tie connectors under tension is shown in Figure 3.17.

Table 3.4: Experimental results for Z tie connectors with brick veneer and concrete veneer

Connector ID	Peak Load, kN	Displacement at peak load, mm	Initial Stiffness, kN/mm	Embedment Failure mode
T-Z.CL-1	1.90	1.70	26.6	Cone break out
T-Z.CL-2	2.34	1.06	1.76	Cone break out and pull-out
T-Z.CL-3	3.47	1.84	4.75	Cone break out
T-Z.CN-1	1.92	3.65	7.53	Cone break out
T-Z.CN-2	2.27	0.82	12.3	Cone break out
T-Z.CN-3	1.34	0.28	6.77	Cone break out or pull-out

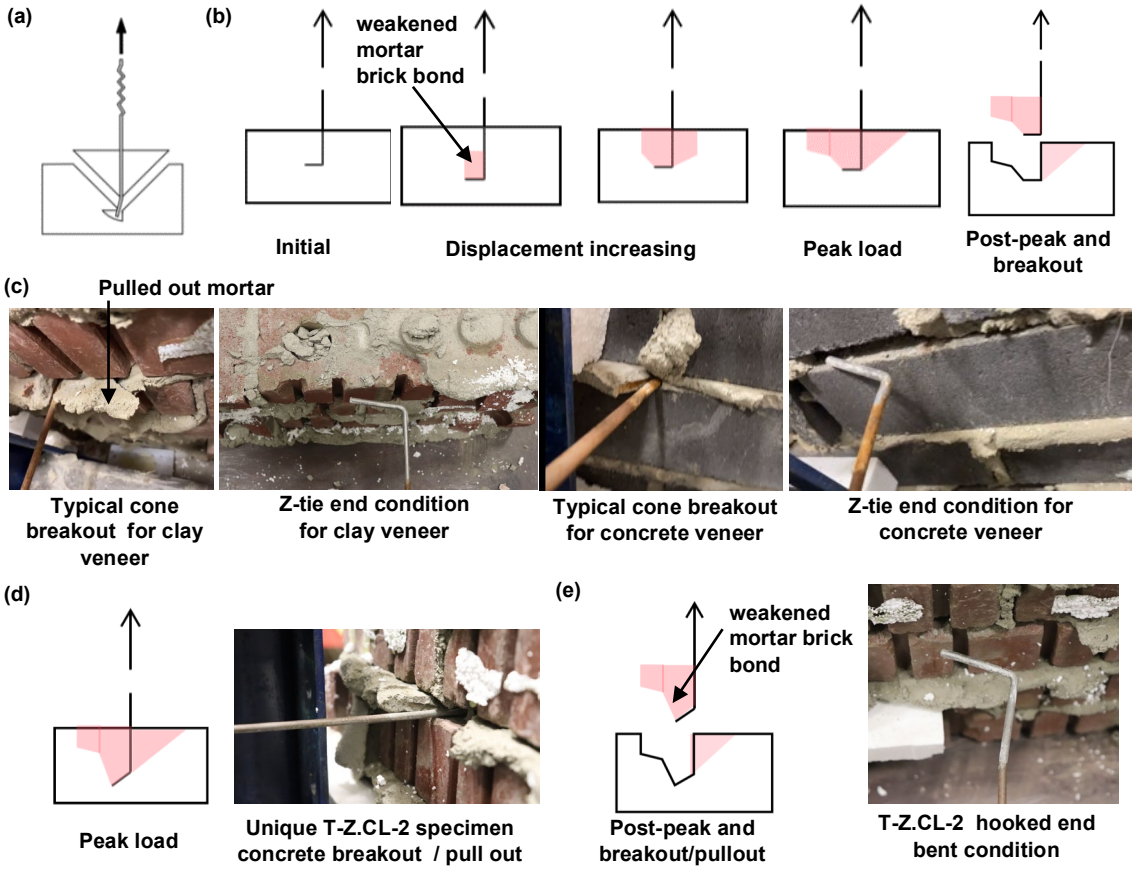

Figure 3.17: Plan view illustrations of tensile stress on Z tie and mortar joint of (a) idealized cone break-out failure from Arslan et al. (2021) (b) Z-tie tension failure progression, (c) representative failure photos of Z-tie connectors from tests, (d) different failure of T-Z.CL-2, (e) different failure of T-Z.CL-2.

T-Z specimens showed an initially high stiffness with essentially linear increase in load with deformation until peak load. Peak load for all T-Z specimens was associated with embedment failure in the mortar joint. This manifested initially as a drop in load caused by the mortar cracking

and separating from the bricks. After this, there was a prolonged gradual pull-out of the mortar contained within the hooked end of the Z-tie with load decreasing gradually as deformation increased. The decline after the average peak load in Figure 3.15(a) and (b) shows a post cracking tensile resistance (tension softening) through embedment failure in the mortar joint. Some T-Z specimens (shown in Figure 3.17(e) and (f)) had the Z-tie end bent during this process which is associated with yielding of the steel and the residual load at large deformations.

All clay and concrete brick veneer specimens except for T-Z.CL-2 experienced embedment cone breakout failure and is actually better described as a partial half cone breakout shown in Figure 3.17(d) which is different than the typically assumed cone shape formation of a prism of mortar radiating out with an ~45° failure angle and a constant tensile stress uniformly distributed over the projected area of the failure surface (Arslan et al., 2021) discussed in Section 2.3.1 and shown in Figure 3.17(a). T-Z.CL-2 experienced a hybrid cone breakout / pull-out failure. Pull-out failure is described as when the tie slides along the tie mortar interface as discussed in Chapter 2. All concrete veneer specimens had embedment cone breakout failures except for T-Z.CN-3 which had insufficient data to determine failure mode. The reported coefficient of variation from the auxiliary mortar cube testing is 0.29 shown in the Table 3.2 which is a suspected cause for the peak load variability due to the governing failure modes of cone break-out failure with different degrees of pull-out. Further complexities associated with bond strength between mortar and bricks is another concern for the observed variability. Specimens that experienced pull-out such as T-Z.CL-2 are shown in Figure 3.15(a) to have larger peak loads than specimens that did not. T-Z.CL-1 was the Z-tie specimen to most closely resemble a cone breakout failure shown in Figure 3.17(c). After peak load, half of the partial mortar cone came out after testing with the other half showing indications that it was about to come out (Figure C.1(b)) and it could be removed by hand which is due to the weakened bond with the brick shown in Figure 3.17 (d). All other specimens failed similarly to T-Z.CL-1 except T-Z.CL-2 which in addition to the typical breakout response, had bending in the tail portion of the Z-tie. The bend indicates that the tie was in the process of straightening due to combined local mortar crushing mortar and tie yielding, categorized by Arslan et al. (2021) as pull-out failure. A bent tie can also be an indicator of localized yielding of the tie and may explain why T-Z.CL-2 saw a load plateau after a while. Figure 3.17(d) and (f) show the degrees of pull-out that occurred amongst specimens.

3.3.2 Experimental Tension Results for the Rectangular Tie Connector

Table 3.5 summarizes the results for the rectangular tie connectors and Figure 3.15(c) and (d) illustrates the load displacement plots for each T-R specimen. Failure progression and modes for rectangular tie connectors under tension is shown in Figure 3.18.

Table 3.5: Experimental results for rectangular tie connectors with brick veneer and concrete veneer

Connector ID	Peak Load, kN	Displacement at peak load, mm	Initial Stiffness, kN/mm	Embedment failure mode
T-R.CL-1	2.80	0.33	3.83	Angular break-out
T-R.CL-2	0.70	0.78	5.62	see note[A]
T-R.CL-3	2.27	0.77	4.97	Angular break-out
T-R.CN-1	2.65	0.96	10.6	Angular break-out
T-R.CN-2	1.46	0.99	3.47	Angular break-out
T-R.CN-3	1.73	0.74	4.67	Angular break-out

[A] insufficient data to fully classify failure mode

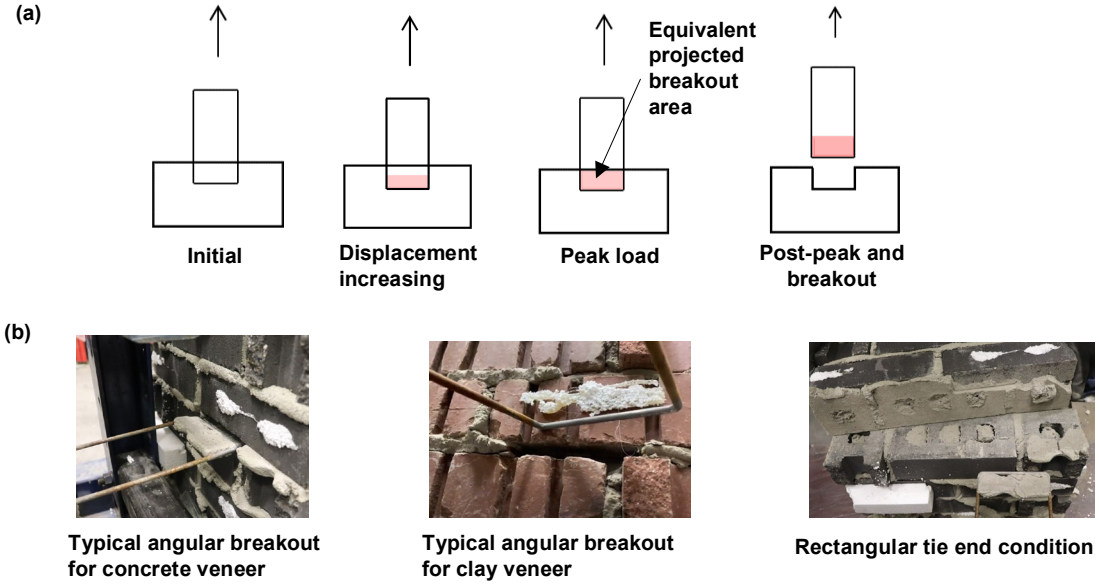

Figure 3.18: Plan view illustrations of tensile stress on rectangular tie and mortar joint of (a) rectangular tie tension failure progression, (b) representative failure photos of rectangular tie connectors from tests

The rectangular ties had similar responses and embedment failure modes like the Z-ties. The cross sectional area of material crossing the joint was twice that of the Z-ties but failure was still controlled by the tie's embedment depth into the veneer. The T-R connectors had half the embedment depth of the Z-ties (25 mm) due to a construction issue mentioned earlier and, unlike the Z-ties, had no signs of tie bending. This contributed to a reduced post-peak residual capacity compared to the Z-ties, as well as likely smaller peak loads than what would be expected if the

planned embedment length was used, as there was less friction during tie withdrawal. However there was still some degree of residual resistance as shown in Figure 3.15(c) and (d).

Instead of a cone failure mode as observed with the Z-tie specimens, the rectangular ties had a more angular embedment failure cone shape (closer to the rectangular tie shape) and is referred to as angular breakout failure in this thesis. Angular breakout in the T-R specimens occurred since the projected mortar breakout area was enclosed within the rectangular tie. Due to the enclosed shape, the 45° failure angle cannot be formed and instead has to 'pull-out' of the mortar joint overcoming both the bearing force from the rectangular tie end onto the mortar and frictional resistance between the mortar and tie itself. After the peak load, the angular cone pulled out by the rectangular tie end left a shape close to the outline as the rectangular connector itself shown in Figure 3.18(c).

All T-R specimens experienced angular breakout failures but T-R.CL-2, T-R.CL-3 and T-R.CN-2 did not have sufficient images to conclude angular breakout visually. Even though there was no visual verification for three specimens, the response between T-R.CL-3 and T-R.CL-1 and between T-R.CN-2 and T-R.CN-3, is enough to conclude angular breakout failure occurred. T-R.CL-2 is the only rectangular tie specimen with insufficient data to confidently classify as angular breakout and also had the lowest peak load.

The mortar's CoV(coefficient of variation) of 0.29 previously discussed with the T-Z specimens is a suspected cause why the T-R peak loads have a variance because the angular breakout failure mode relies on the mortar strength.

3.3.3 Experimental Tension Results for the Upright Plated Connector

Table 3.6 summarizes the results for the plated connectors with an upright orientation and Figure 3.15 (e) and (f) illustrates the load displacement plots for each T-PV specimen. Failure progression and modes for the upright plated connectors under tension is shown in Figure 3.19.

Table 3.6: Experimental results for plated connectors at an upright orientation with brick veneer and concrete veneer

Connector ID	Peak Load, kN	Displacement at peak load, mm	Initial Stiffness, kN/mm	Embedment failure mode
T-PV.CL-1	3.67	4.07	2.97	Tie break-out
T-PV.CL-2	4.18	11.5	5.44	Tie break-out / yielding
T-PV.CL-3	3.62	4.67	4.67	Tie break-out
T-PV.CN-1	4.24	7.44	8.69	Tie break-out/yielding
T-PV.CN-2	4.82	8.07	1.11	Tie break-out / yielding
T-PV.CN-3	4.13	6.10	0.76	Tie break-out

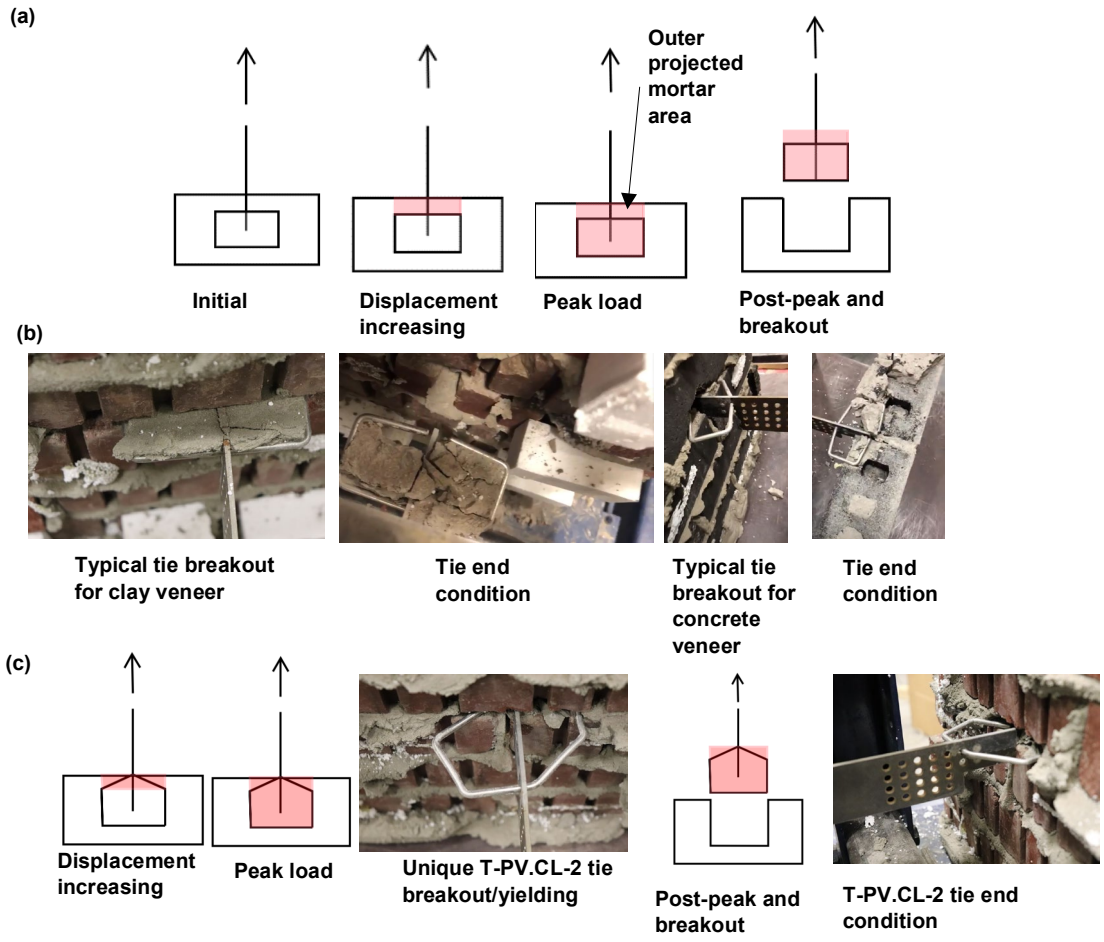

Figure 3.19: Plan view illustrations of tensile stress on plated connector with an upright orientation and mortar joint of (a) tension failure progression, (b) representative failure photos of plated connectors from tests, (c) different failure of T-PV.CL-2.

The T-PV specimens showed an initially high stiffness with essentially linear increase in capacity with deformation until a slight load drop is observed around 3 mm displacement for all specimens. The slight load drop was associated with embedment breakout failure in the mortar joint shown in Figure 3.19(a) and (b). After this load drop, forces redistribute to the other side of the embedment tie and load then began to increase with further displacement. Near peak load, the embedment tie yielded, reflected in permanent tie deformation, in some tests but not others as shown in Figure 3.19(c) and (e). After this, there was a prolonged gradual pull-out of mortar contained within the embedment veneer tie with load decreasing gradually as deformation increased. This post peak response shows that embedment tie yielding contributes to ductile behaviour due to the yielding specimens having the largest displacements at peak load.

All plated connector specimens had an angular breakout at the embedment veneer tie shown in Figure 3.19 (c) which will be defined as tie breakout. In addition to tie breakout, some embedment veneer ties yielded such as clay brick specimen T-PV.CL-2 shown in Figure 3.19(e) which had the highest observed permanent deformation followed by T-PV.CN-1,2. This hybrid failure mode is recorded as tie breakout/yielding.

The mean clay brick and concrete brick veneer peak load of 3.82 kN and 4.40 kN respectively both have a CoV of 0.08. Due to the veneer embedment tie yielding mechanism contributing to the governing failure mode and steel's expected low CoV, it is likely that the main reason the overall specimen's CoV is quite low due to the embedment veneer tie's steel material properties having less variability than the mortar bond. However the mortar coefficient of variance of 0.29 explained in depth in previous sections still does contribute to the overall specimen's CoV due to tie breakout occuring.

3.3.4 Experimental Tension Results for the Plated Connector Lying Down

Table 3.7 summarizes the results for the plated connectors with a lying down orientation and Figure 3.15 (g) and (h) illustrates the load displacement plots for each T-PH specimen. Failure progression and modes for the lying down connectors under tension is shown in Figure 3.20.

Table 3.7: Experimental results for plated connectors lying down with brick veneer and concrete veneer

Connector ID	Peak Load, kN	Displacement at peak load, mm	Initial Stiffness, kN/mm	Embedment failure mode
T-PH.CL-1	2.87	2.51	26.2	Pull-out
T-PH.CL-2	3.97	17.7	1.37	Pull-out
T-PH.CL-3	3.44	5.47	5.01	Pull-out
T-PH.CN-1	6.83	24.9	0.35	Pull-out
T-PH.CN-2	4.94	16.3	2.16	Pull-out
T-PH.CN-3	4.45	12.5	3.51	Pull-out

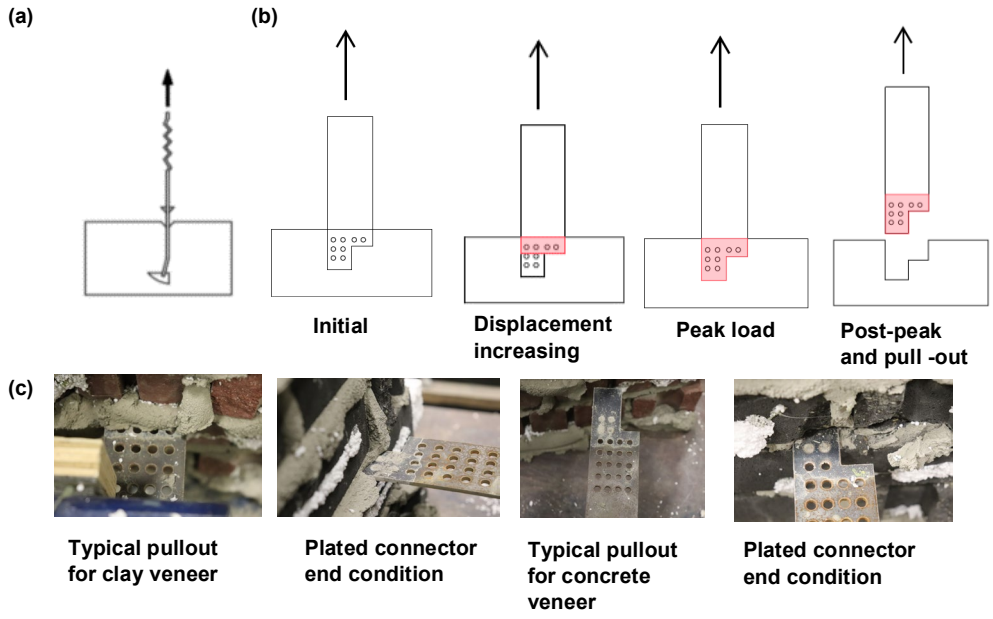

Figure 3.20: Plan view illustrations of tensile stress on plated connector lying down and mortar joint of (a)idealized pull-out failure from Arslan et al. (2021), (b) tension failure progression, (c) representative failure photos of plated connectors from tests

The T-PH specimens showed an initially high stiffness with a gradual increase in load with deformation until peak load. Peak load for all T-PH specimens was associated with pull-out embedment failure within the mortar joint shown in Figure 3.20. This manifested initially as a drop in load caused by mortar cracking around the connector. After this, there was a gradual pull-out of the connector shown in Figure 3.15(g) and Figure 3.20(c) as deformation increased explained by the frictional resistance of the mortar and connector itself.

All clay and concrete brick veneer specimens underwent a failure mode similar to the pull-out embedment failure described by Arslan et al. (2021) and shown in Figure 2.7(g) but differed as the ties had a different shape. Arslan et al. (2021) defined pull-out embedment failure as straightening of a connector due to local crushing of mortar and yielding of the tie followed by extensive slip. Arslan et al. (2021) further defined pull-out failure as occurring due to poor bonding along the inner interface between the tie and mortar which leads to extensive slip of the tie and the surrounding mortar does not have significant splitting or crushing. Since these connectors did not have hooks to provide additional anchorage, they only experience pull-out based on the second mechanism described by Arslan et al. (2021). The actual pull-out embedment failure that occurred is shown in Figure 3.20(c). T-PH.CL-2 and T-PH.CL-3 had no visual confirmation on the failure

mode however engineering judgement is used based on the load displacement data to classify this as pull-out failure.

3.3.5 Experimental Tension Results for Inclined Connector

Table 3.8 summarizes the results for the inclined connectors and Figure 3.15 (i) and (j) illustrates the load displacement plots for each T-IN specimen. Failure progression and modes for the inclined connectors under tension is shown in Figure 3.21.

Table 3.8: Experimental results for inclined connectors with brick veneer and concrete veneer

Connector ID	Peak Load, kN	Displacement at peak load, mm	Initial Stiffness, kN/mm	Embedment failure mode at top	Embedment failure mode at bottom
T-IN.CL-1	6.43	17.3	0.70	Leg pull-out with veneer tie yielding	Veneer tie yielding
T-IN.CL-2	5.78	19.1	0.77	Leg pull-out with veneer tie yielding	Leg pull-out with veneer tie yielding
T-IN.CL-3	6.26	18.6	1.60	Leg pull-out with veneer tie yielding	Veneer tie yielding
T-IN.CL-4	4.98	20.0	0.76	Leg pull-out with veneer tie yielding	Veneer tie yielding
T-IN.CL-5	4.58	25.4	1.42	Leg pull-out with veneer tie yielding	Leg pull-out with veneer tie yielding
T-IN.CN-2	5.56	12.1	1.35	Leg pull-out with veneer tie yielding	Leg pull-out with veneer tie yielding
T-IN.CN-3	7.22	18.7	1.98	Leg pull-out with veneer tie yielding	Leg pull-out with veneer tie yielding

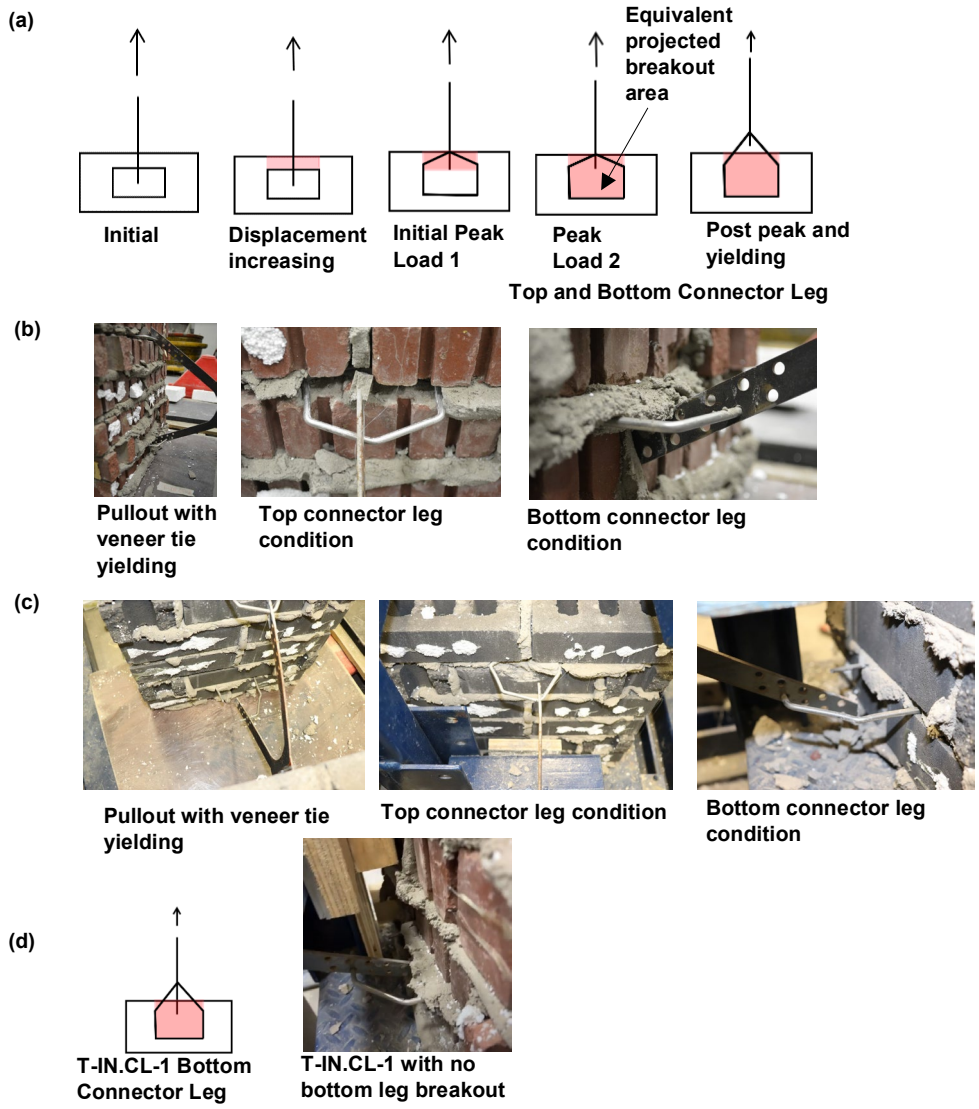

Figure 3.21: Plan view illustrations of tensile stress on inclined connector and mortar joint of (a) tension failure progression, (b) representative clay veneer failure photos of inclined connectors from tests, (c) representative concrete veneer failure photos of inclined connectors from tests (d) different failure of T-IN.CL-1

The T-IN specimens showed an initially high stiffness with a gradual increase in capacity with deformation until peak load shown in Figure 3.15(i) and (j). Peak load for all T-IN specimens was associated with connector leg pull-out embedment failure occurring together with embedment veneer tie yielding. Failure modes are illustrated in Figure 3.21. Like with T-PV connectors, a suspected cause for the gradual increase in load after the onset of tie yielding is due to the geometry changes in the embedment tie. Peak load was reached then followed by a drop in load due to mortar cracking around the connector leg. After this, there was a gradual pull-out of the connector leg similar to previously described ties. The plateau in the load-deflection response shows that tie

yielding contributes to ductile behaviour. There was also a potential contribution of increased ductility due to the connector yielding near the CMU interface shown in Figure C.20(e) and C.26 (c) in Appendix C.

Table 3.8 lists failure modes that occurred at the top and bottom connector leg due to differences with each occurring in some cases. All specimens had the top connector leg pulling out of the mortar joint in addition to veneer tie yielding. The failure mode differences between specimens are the bottom leg with the veneer tie yielding and either the bottom leg connector pulling out of the mortar joint or not pulling out prior to test ending. Similar to the plated connector in an upright orientation, the inclined connector experienced a combination of responses in the mortar joint/connector interface and the tie veneer interface. Without being able to visually confirm response within the mortar joint, the inclined connector legs underwent pull-out in the vertical mortar joint because the projected breakout area was minimal, shown by the embedment veneer still anchored into the horizontal mortar joint. Another reason why specimens are recorded as pull-out instead of cone breakout is because the vertical mortar joints where each 25 mm high connector leg is embedded in are 67 mm in height which does not have enough projected area to create the 45° failure cone angle.

3.3.6 Comparison of Response, Peak Loads, and Failure Modes between Parameters

Figure 3.22 illustrates individual representative specimens from each connector type taken from Figure 3.15. Representative specimens were selected based on whether they reasonably portray the general trend of the three specimens tested from that parameter.

T-Z.CL-2 and T-Z.CN-2 are selected to represent T-Z specimens which experienced cone breakout. Though some T-Z specimens had varying degrees of partial pull-out (Fig. 3.17(f)), the peak load variance is only 18.8% greater than T-Z-1 which experienced no partial pull-out. T-Z-2 may have a higher residual load capacity than T-Z-1 due to the associated yielding of the steel.

T-R.CL-3 and T-R.CN-3 are selected to represent T-R specimens which all experienced angular breakout. All T-R specimens were similar so any test may have been used in place of these ones (Fig. 3.17 (c),(d)).

T-PV.CL-3 and T-PV-CN-3 are selected to represent T-PV specimens which all experienced tie breakout. There were some T-PV specimens that underwent veneer tie yielding which seem to have a larger residual load capacity (Fig. 3.15 (e),(f)) due to yielding of the steel but they were not selected as representatives due to a larger peak load compared to other T-PV connectors. The

overall response before peak load for all T-PV connectors in Figure 3.15 (e) and (f) are similar with the exception of T-PV.CN-2 which is likely due to LVDT alignment issues.

T-PH.CL-3 and T-PH.CN-2 are selected to represent the T-PH specimens which all experienced pull-out failure. All T-PH specimens had similar responses up to peak load (Fig. 3.15 (g),(h)) however due to pull-out failure relying on the mortar joint strength bond, the response after peak loads differed between all T-PH specimens. T-PH.CL-2 and T-PH.CN-1 were not good representatives due to having the largest peak loads and post peak residual capacity within their specimen type. The remaining T-PH specimens are relatively similar in response.

T-IN.CL-3 and T-IN.CN-3 are selected to represent T-IN specimens which all experienced pull-out at the connector legs and veneer tie yielding. Figure 3.15 (i) and (j) shows all T-IN specimens are similar in response with the exception of T-IN.CL-1 which could be due to LVDT mis alignment. Even though there were varying degrees of pull-out at the bottom connector leg and the amount of yielding at the veneer tie, the general trend of a gradual increase at displacements greater than 20 mm is present in all clay and brick veneers.

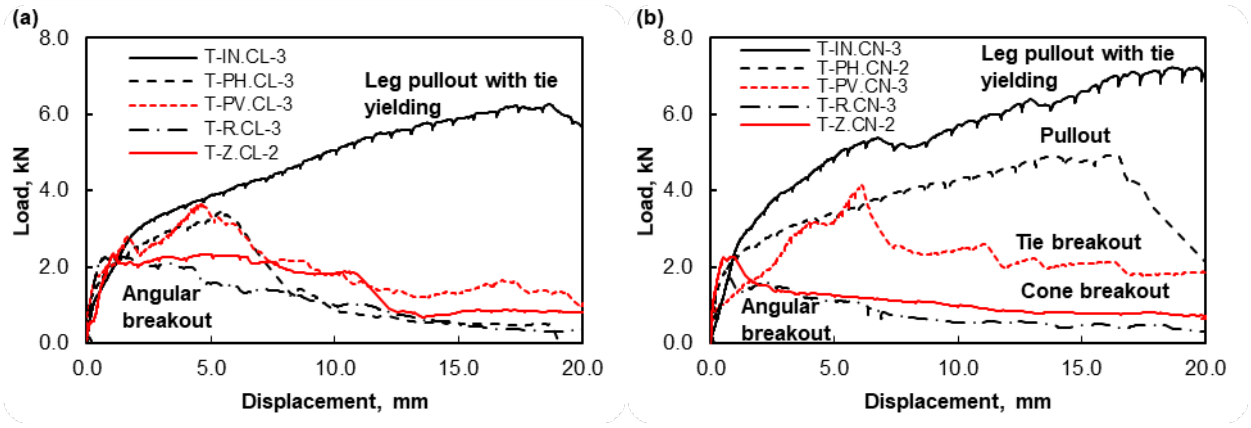

Figure 3.22: Tension load displacement plots of representative responses from each connector for (a) clay brick veneer, (b) concrete brick veneer

The average initial stiffness values for the T-Z and T-R tie connectors for the clay and concrete veneer (ranges from 4.8 to 11.0 kN/mm) are larger than the T-PV, T-PH and T-IN plated connector specimens (ranges from 1.0 to 4.4 kN/mm) except for T-PH.CL (10.9 kN/mm) shown in Table 3.3. This is attributed to the embedment veneer ties and slots within which would have larger initial deformations under low loads until slack in the slot is taken out. The initial stiffness (1.0 and 1.7 kN/mm) of the inclined T-IN specimens is the lowest amongst all the connector types tested which can be explained by the inclined connector having two embedment veneer ties at the top and

bottom connector leg compared to just one slot for the T-PV connector and no slots for the T-Z, T-R and T-PH connector types. Since T-PH did not have embedment veneer ties, it is expected that it would behave similarly to the T-Z and T-R tie connector types with a relatively high initial stiffness however the average initial stiffness of T-PH.CL and T-PH.CN are 10.9 kN/mm and 2.0 kN/mm. The T-PH.CN specimens do not have an average high initial stiffness as was expected which is shown in Figure 3.15 (g) and (h) with different specimen responses for T-PH.CL and T-PH.CN.

The overall average peak load values for the T-Z and T-R tie connectors for the clay and concrete veneer (1.84 to 2.57 kN) are smaller than the T-PV, T-PH and T-IN plated connector specimens (3.43 to 6.39 kN). The smaller values occur because the tie connectors were not a hybrid failure mode due to no embedment veneer ties creating veneer tie yielding occurring and thus controlled by the limited amount of projected breakout area. The variability in the amount of projected breakout area can be due to mortar strength, mortar bond with type of brick veneer, and the general connector shape around the projected breakout area which affects the tie connector specimens more than the plated connectors.

The mortar joint to clay brick veneer has a greater chance of a better bond than the concrete brick veneer due to water absorption (Drysdale and Hamid, 2013) as mentioned in Chapter 2. If the brick veneer has a better bond than the concrete veneer, this may also explain why the T-Z.CN specimens had a partial cone breakout failure in Figure C.4(a) compared to the T-Z.CL specimens in Figure 3.17(c) which had a more complete concrete cone breakout failure on both sides. T-Z.CL-2 showed minor degrees of pull-out in the form of the Z-tie end partially straightening had higher than expected peak loads seems to show that when pull-out behaviour is exhibited in failure, there is a higher peak load but also reinforces the previous point of a hybrid failure mode having higher expected peak loads. The T-R ties are limited to a maximum projected breakout area due to its enclosed shape however the initial high stiffness values combined with the general load displacement tie connector trends in Figure 3.15 (a), (b), (c) and (d) show that if similar tie connectors with non-hybrid breakout failure modes were embedded deeper into the mortar joint, a higher peak load can be achieved due to higher projected breakout areas resulting in a similar response as the T-Z and T-R connectors.

The angular breakout due to the embedment veneer tie for the plated connectors is similar to the rectangular tie's angular breakout with the projected mortar breakout area being enclosed by

the shape of the embedment veneer tie in Figure 3.19(a) and is referred to as tie breakout in this thesis for the plated connectors. The only difference with the plated connectors is since the embedment veneer tie is fully embedded into the mortar joint, there is a portion of the projected mortar breakout area that is outside of the veneer tie shown in Figure 3.19 (a). Tie breakout hybrid failure occurs as a combination of the embedment veneer tie yielding to a degree and the connector breakout at the vertical mortar joint which all contribute to a higher peak load response when compared to the tie connectors. Table 3.3 shows that T-PH.CN's peak loads are the largest when comparing connector types not including the T-IN connectors which have two anchorage points. A reason for this could be that pull-out resistance for the T-PH.CN connectors is further strengthened by the connector holes which promote mini circular 'breakout' areas that add to the load that is required for slip to occur.

The CoV for the T-Z and T-R tie connectors for the clay and concrete specimens (0.26 to 0.57) are higher than the T-PV, T-PH and T-IN values for the clay and concrete plated connector specimens (0.08 to 0.23). The CoVs for all specimens can be compared to the CoV of the mortar auxiliary testing value of 0.29 and are more influenced by the mortar's variability for the T-Z and T-R tie connectors than for the plated connectors.Due to the mortar strength variability which affects breakout crack formation, there are differences in how the mortar breaks out which in turn affects the projected break-out area which also affects the frictional resistance during pull-out both referenced by Arslan et al. (2021).The mortar strength variability is shown by the mortar cube testing which has a CoV of 0.29. This is mainly due to temperature variability from the environment. Masonry mortar already has variability from factors such as water dosing and intensity of mixing however it is believed the reason in this case and found in research is reduced and elevated temperature of fresh mortars (Golaszewska et al. 2020). During the first 72 hours after mixing, lower temperatures decrease the hydration and hardening speed of cement paste in mortars and increased temperatures affect mortar mostly by causing rapid hydration on the surface of cement particles, which could obstruct the hydration of deeper layers of cement particles (Golaszewska et al. 2020). Since specimens were constructed in an outdoor environment over a two-month construction phase with temperature differences as high as 34° C throughout the day, mortar variability due to temperature is expected due to the mortar cubes for auxiliary testing being taken throughout the construction phase. Even in a controlled environment, the CoV of tests by Arslan et al. (2021) was 0.15. Muhit et al. (2022) noted the high variability of mortar joint strength

in their experiments citing Heffler et al. (2008) who discussed that the brick/mortar interface predominately governs the strength of clay brick masonry and that the strength of the brick/mortar interface is governed by workmanship and variability in brick suction rate. Each brick on a pallet potentially possesses different amounts of surface dust and varying exposure to weather conditions because of its location on a pallet which in turn may affect suction rate (Heffler et al., 2008). The CoVs for the T-PV plated connectors are all less than the T-Z and T-R tie connectors due to the embedment tie veneer yielding mechanism . Steel yielding is more predictable than embedment breakout and controls the failure load more for the plated connectors.

3.3.7 Comparison of experimental values with previously developed expressions

Hatzinikolas et al (1979) proposed an empirical equation for tensile and compression capacity of masonry ties as described in Section 2.3.1 and repeated here for convenience. K is a constant related to the diameter of the horizontal rod which is 1.0 for a 3.66 mm rod and 1.25 for a 4.76 mm rod, d represents the distance from the horizontal rod to the face of the mortar joint, f_m is the compressive strength of mortar, f_c is the compressive stress due to vertical load at the level considered, v is the coefficient of friction, μ represents the bond strength l represents the length of embedment and r is the tie diameter.

$$P_{ult} = 6Kd^2\left(0.15\sqrt{f_m} + vf_c\right) + \mu 2\pi rl \qquad \text{(Eq. 3.2)}$$

Arslan et al. (2021) proposed equations that represent three failure modes as described in Section 2.3.1. The failure modes from Arslan et. al (2021) are tie failure, cone break out failure, and pull-out failure but the governing failure mode for all tension specimens in this current study between Equation 3.3, 3.4 and 3.7 is cone break out failure. Due to the high variability in shear strength of mortar, a range of 0.10 and 0.17 is used (Alecci et. al., 2013, Zimmermann and Strauss, 2011). Equation 3.4 determines the masonry cone breakout failure with a 45°breakout angle assumption. The first term in Equation 3.4 defines the tensile break out of the mortar and the remaining terms related to the friction coefficient and mortar shear strength (Arslan et. al., 2021). $0.332\sqrt{f_m}$ represents the mortar tensile strength, A_{pt} is the projected breakout area calculated with Equation 3.5 and 3.6 due to the projected breakout restricted by the thickness of the mortar joint which is a limited space between bricks (Arslan et. al., 2021). The cone breakout failure of Equation 3.4, 3.5 and 3.6 has variables t which is the thickness of the mortar joint, $l_b$is the embedment length of the

tie, A_w is the effective area of the cone of the mortar, μ is the coefficient of friction, f_{v0} is the initial shear strength of mortar and f_p is the precompression level acting orthogonally to the interface (Arslan et. al., 2021). Arslan et. al (2021) also noted that the initial shear strength and coefficient of friction vary for different masonry typologies.

$$N = A_s f_u \quad \text{(Eq. 3.3)}$$

$$N = 0.332 A_{pt} \sqrt{f_m} + 2\left(\mu f_p + f_{v0}\right) A_w \quad \text{(Eq. 3.4)}$$

$$A_{pt} = 2 l_b t + {l_b}^2 \left(\frac{\pi\theta}{180} - sin\theta\right) \quad \text{(Eq. 3.5)}$$

$$\theta = 2\sin^{-1}\left(\frac{t/2}{l_b}\right) \quad \text{(Eq. 3.6)}$$

$$N = 1.5 f_m l_h d + a\sqrt{f_m}\pi(l_h + l_b)d + \frac{12EI\emptyset}{l_c d^3} \quad \text{(Eq. 3.7)}$$

Table 3.9 compares the test peak loads of each specimen to the predicted capacity from Equation 3.2, and the predicted capacity from Equation 3.4 with a range of f_{v0} between 0.10 and 0.17 MPa used.

The tested connectors that did not undergo hybrid failure modes and were governed by a cone breakout failure (T-Z and T-R) are most controlled by the mortar strength parameter in Equation 3.4. Due to the tested Z-tie and rectangular tie specimens having the same embedment length, mortar thickness, and surcharge stress the only parameter that affects the cone breakout capacity in Equation 3.4 is mortar strength however it is important to note there are other factors not included in the equation such as load misalignment and how well mortar consolidated around the connector. Other parameters such as projected break-out and effective area would ideally have not as much variance between specimens though the projected break-out area assumes a 45° cone and the test observations showed that other shapes, such as half a cone, were observed. The projected break-out area is related to mortar crack formation which is also a function of mortar strength.

Figure 3.23 shows plots for each subset connector type separated by tie, plated connector, and inclined connector because each subset differs greatly by cross sectional properties or failure mode. The model peak load in Figure 3.23 compared against tests is based on Equation 3.4 except for Figure 3.23(a) and (b) which includes Equation 3.2 from Hatzinikolas et al. (1979) since those tests (Z-tie and rectangular tie) are in the scope of Hatzinikolas et al (1979)'s work. Even though pull-out failure occurred in some tests, pull-out (Equation 3.7) did not govern model failure in the plated connectors.

Table 3.9: Comparison of experimental peak loads with empirical equations from previous research under tension

Test ID	Experimental peak load, kN	Failure Mode	T.P.[A] ratio Eq. 3.2	T.P. ratio Eq. 3.4 f_{v0} = 0.17	T.P. ratio Eq. 3.4 f_{v0} = 0.10
T-Z.CL	2.57	Cone break-out	0.81	1.13	1.34
T-Z.CL-1	1.90	Cone break-out	0.60	0.83	0.99
T-Z.CL-2	2.34	Cone break-out and pull-out	0.74	1.03	1.22
T-Z.CL-3	3.47	Cone break-out	1.10	1.53	1.81
T-Z.CN	1.84	Cone break-out	0.58	0.81	0.96
T-Z.CN-1	1.92	Cone break-out	0.61	0.85	1.00
T-Z.CN-2	2.27	Cone break-out	0.72	1.00	1.18
T-Z.CN-3	1.34	Cone break-out or pull-out	0.42	0.59	0.70
T-R.CL	1.92	Angular break-out	0.64	2.09	2.31
T-R.CL-1	2.80	Angular break-out	0.94	3.04	3.37
T-R.CL-2	0.70	--	0.23	0.76	0.84
T-R.CL-3	2.27	Angular break-out	0.76	2.47	2.73
T-R.CN	1.95	Angular break-out	0.65	2.12	2.35
T-R.CN-1	2.65	Angular break-out	0.89	2.88	3.19
T-R.CN-2	1.46	Angular break-out	0.49	1.59	1.76
T-R.CN-3	1.73	Angular break-out	0.58	1.88	2.08
T-PV.CL	3.82	Tie break-out	--	1.68	1.99
T-PV.CL-1	3.67	Tie break-out	--	1.62	1.91
T-PV.CL-2	4.18	Tie break-out / yielding	--	1.84	2.18
T-PV.CL-3	3.62	Tie break-out	--	1.59	1.89
T-PV.CN	4.40	Tie break-out/yielding	--	1.94	2.29
T-PV.CN-1	4.24	Tie break-out / yielding	--	1.87	2.21
T-PV.CN-2	4.82	Tie break-out / yielding	--	2.12	2.51
T-PV.CN-3	4.13	Tie break-out	--	1.82	2.15
T-PH.CL	3.43	Pull-out	--	1.51	1.79
T-PH.CL-1	2.87	Pull-out	--	1.26	1.49
T-PH.CL-2	3.97	Pull-out	--	1.75	2.07
T-PH.CL-3	3.44	Pull-out	--	1.52	1.79
T-PH.CN	5.41	Pull-out	--	2.38	2.82
T-PH.CN-1	6.83	Pull-out	--	3.01	3.56
T-PH.CN-2	4.94	Pull-out	--	2.18	2.57
T-PH.CN-3	4.45	Pull-out	--	1.96	2.32
T-IN.CL	5.61	Leg pull-out / tie yielding	--	2.17	2.59
T-IN.CL-1	6.43	Leg pull-out / tie yielding	--	2.48	2.96
T-IN.CL-2	5.78	Leg pull-out / tie yielding	--	2.23	2.66
T-IN.CL-3	6.26	Leg pull-out / tie yielding	--	2.42	2.88
T-IN.CL-4	4.98	Leg pull-out / tie yielding	--	1.92	2.29
T-IN.CL-5	4.58	Leg pull-out / tie yielding	--	1.77	2.11
T-IN.CN	6.39	Leg pull-out / tie yielding	--	2.47	2.94
T-IN.CN-2	5.56	Leg pull-out / tie yielding	--	2.15	2.56
T-IN.CN-3	7.22	Leg pull-out / tie yielding	--	2.79	3.32

[A] T.P. represents Test to Predicted ratio

Equation 3.4 is mostly conservative for all scenarios when comparing to the test values. Even though Figure 3.23(a) and (b) have large variability, it shows that the Z ties and rectangular ties for clay brick veneers follow Equation 3.4 and are more conservative than Eq. 3.2. Another reason

for shift in higher capacity in connectors with typical ties to plated connectors in tension is that Arslan's expression considers mortar embedment failure well by adopting the concrete cone model found in the Canadian concrete design standard (CSA A23.3:19) but the plated connectors in tension also failed with embedment veneer tie yielding which may contribute to the larger capacity.

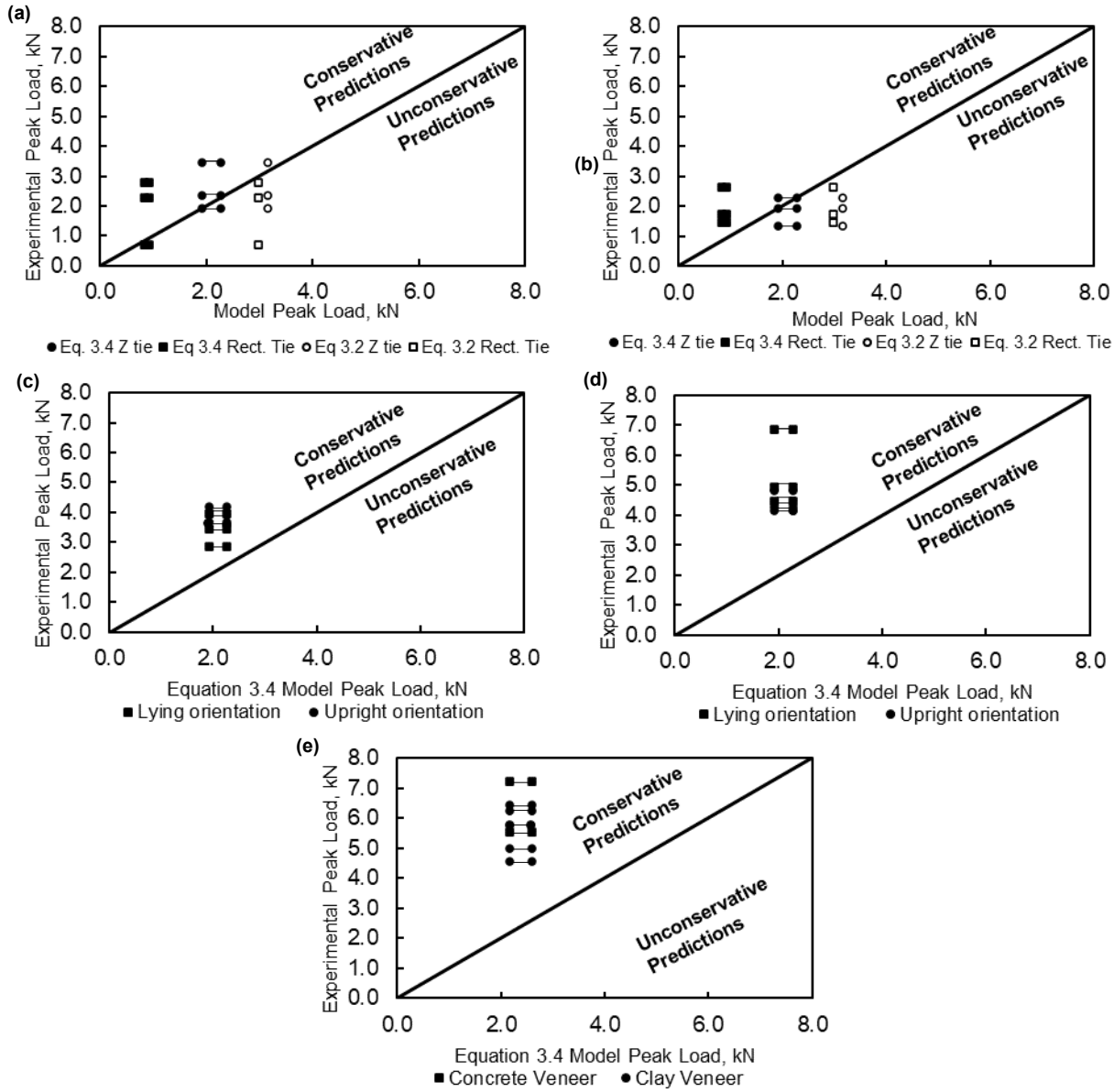

Figure 3.23: Experimental model comparison for (a) tie connectors T-Z and T-R clay veneer specimens (b) tie connectors T-Z and T-R concrete veneer specimens (c) plated connectors T-PH and T-PV clay veneer specimens, (d) plated connectors T-PH and T-PV concrete veneer specimens, (e) inclined connectors T-IN

3.3.8 Effect of Connector Cross Sectional Area

Initially, a larger cross-sectional area was expected to lead to larger capacities. The rectangular tie would likely have had a larger peak load if not for the lower 25 mm embedment length into the mortar joint compared to the other specimens. However, the failure modes for all connectors were either breakout or pull-out failure which is not necessarily a function of connector cross-sectional area but instead related to the shape of the concrete breakout area. The concrete breakout area can be increased using embedment veneer ties instead of relying on the connector's own cross sectional area.

The inclined connector had two embedment veneer ties. Embedment veneer ties increased capacity since there was more anchorage in the mortar joints. Even though the primary tension failure mode remained as an embedment failure, we can observe that none of the connector specimen's use more than 36% of the expected yielding capacity (calculated based on the connector yield strength in Section 3.2.7) from cross sectional area. Therefore it would be more effective to reduce cross sectional area if possible for material savings without losing connector capacity. Alternatively, larger or more embedment veneer ties may be used to increase breakout area and increase capacity for ties beyond those seen in these tests.

Table 3.10: Comparison of experimental peak loads by cross sectional area

Test ID	Connector Net Cross Sectional Area, mm^2	Mean Tensile Experimental Peak Load, kN	Expected Axial Yielding Capacity, kN	Experimental Peak Load / Yielding Ratio, %
T-IN.CN	75	6.39	18	36
T-IN.CL	75	5.61	18	32
T-PH.CN	75	5.41	18	31
T-PV.CN	75	4.40	18	25
T-PV.CL	75	3.82	18	22
T-PH.CL	75	3.43	18	20
T-Z.CL	18	2.57	10	25
T-R.CN	36	1.95[A]	20	10
T-R.CL	36	1.92[A]	20	10
T-Z-CN	18	1.84	10	18

[A]T-R specimens have a lower (25 mm instead of 50 mm) embedment length than all other specimens

3.3.9 Tension Capacity Comparison of Connectors with Previous Experiments

Similar to Table 3.9, Table 3.11 compares the test mean tension peak loads of clay brick and concrete brick connector specimens and the previous test tension results from Hatzinikolas et al. (1979), Arslan et al. (2021), and Choi and LaFave (2004). The calculated expected capacity from Equation 3.4 assumes an initial mortar shear strength of 0.10 MPa. When selecting specimens from

previous research, variables that were closest to this thesis program were chosen such as embedment length, mortar strength and type of masonry structural backing to properly compare.

Table 3.11: Comparison of experimental (from this study) and previous (from others) peak loads with empirical equations under tension loading

Test ID	Mean experimental peak load, kN	Equation 3.4 f_{v0} = 0.10, kN
T-IN	5.8	2.2
T-PH	4.4	1.9
T-PV	4.1	1.9
Type G[A]	2.3	1.4
T-R	1.9	0.8
SSTE[B]	1.8	2.5
L Tie[C]	2.9	2.9
T-Z	2.2	1.9
Type H[D]	0.7	1.4

[A]One rectangular tie 3.66 mm rod specimen from Hatzinikolas et. al. (1979)
[B]SSTE22 and SSTE16 corrugated metal strip tie specimen 22 gauge and 16 gauge from Choi and LaFave (2004)
[C]Four L tie specimens from Arslan et al. (2021)
[D]Two Z tie 4.76 mm rod specimens from Hatzinikolas et al. (1979)

An individual plot is made of average tensile values from this experiment of each type of connector in Figure 3.24 with results from previous research. There is limited research for plated masonry connectors under axial loading as only tie connectors from previous research were available for Figure 3.24. The model peak load is found from Equation 3.4 with a $f_{v0} = 0.10$.

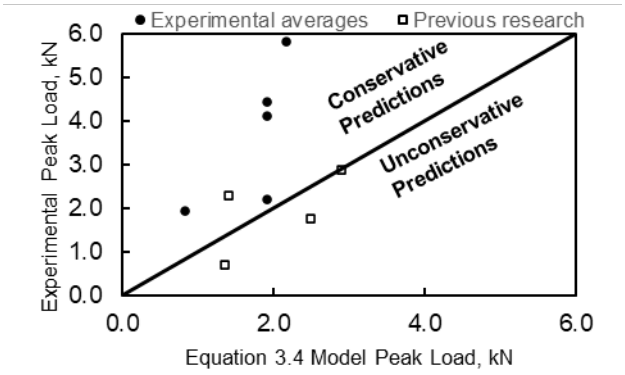

Figure 3.24: Experimental tension peak loads equation 3.4 model comparison from multiple research programs

Equation 3.4 is closer to unity with the actual recorded experimental values recorded for Z- and rectangular ties whereas the calculated values for the plated connectors have the most conservative predictions. Since there is a lower expected capacity in plated connectors using Equation 3.4, designers would over design plated connectors if using conservative values from tie connector

design tables. The test values for the plated connector are larger than the ties due to better anchorage. As a bonus, the plated connectors with veneer ties gives a warning of failure. To accurately predict the expected capacity of plated connectors with veneer ties, design checks for anchorage, yielding of the connector, and yielding of the embedment tie must be taken into account in future expressions.

3.3.10 Exterior Wythe Material Considerations and Future Investigations

The specimens were exposed to the outside for a long period of time during both winter and summer months which mimic realistic scenarios of wall exposure and construction during all seasons. Ahmadi and Reisi (2020) compared the durability of concrete bricks against fired clay bricks and concluded that concrete bricks had better durability based on water absorption and freeze-thaw durability tests. Drysdale and Hamid (2013) noted that during initial contact between mortar and a masonry unit, the unit absorbs some water from the mortar and creates a more "intimate" contact associated with a good bond between the materials. There is evidence to suggest that masonry units that do not draw mortar into intimate contact through initial water absorption will not develop a good bond (Drysdale and Hamid, 2013). Since clay bricks have higher absorption rate than concrete bricks, specimens that failed due to embedment failure in the veneer are expected to have larger peak load for the clay brick specimens than concrete brick specimens. Whether or not this durability affects structural behaviour should be researched more in the future. The various failure modes seen in Table 3.9 show that the T-Z specimens, which underwent cone breakout failure, have greater mean peak load for the clay brick veneer of 2.57 kN than the concrete brick peak load of 1.84 kN. For the T-R specimens there is minimal difference between the peak load of 1.92 kN for clay brick and 1.95 kN for concrete brick which all underwent angular breakout failure. All other plated connector specimens had clay brick veneer peak loads lower than the concrete brick veneer however all plated connector specimens had either a different failure mode of pull-out or yielding of the tie veneer within the plated connector. A caveat is that variability in the results was large so additional studies should be conducted to better establish this potential trend.

3.4 Chapter Conclusions

The observed tensile failure mode for all specimens were a type of embedment failure (breakout or pull-out) within the mortar joint. All connectors experienced a form of breakout failure except for T-PH and T-IN which underwent pull-out failures. The breakout failure modes can be further

categorized as cone breakout for T-Z, angular breakout for T-R, tie breakout for T-PV.CL and tie breakout/yielding for T-PV.CN. The mortar to brick and mortar to connector interfaces were observed to be the most critical components affecting capacity.

Even though the T-R specimens had a 25 mm embedment length, half that of the other connectors, the angular breakout failure mode observed is more so attributed to the T-R connector shape. This enclosed area can be seen as an equivalent 'projected breakout area' which restricts a 45° cone breakout from occurring. T-Z specimens may have equal to or greater tensile resistance than T-R specimens by adjusting the shape of the hooked end in the veneer to enhance anchorage. Breakout was not possible for T-PH specimens because those connectors were anchored in a different way. T-IN specimens had pull-out as the governing failure mode because due to the two connector legs distributing tension to the top and bottom veneer ties. Veneer ties gave a larger angular breakout resistance than the lower pull-out resistance from individual connector legs. The T-IN connectors had a larger capacity then all the connectors due to the two anchorage locations at each end of the inclined connector contributing to the higher tensile resistance. T-PV specimens experienced tie breakout because there was only one anchorage location for the veneer tie. It can be argued that if there were two anchorage locations by adjusting the height dimensions to accommodate two anchorage locations, the response would be similar to the inclined connector.

Due to not utilizing more than 36% of the full axial yield tensile capacity shown in Table 3.10, it would be effective to reduce the cross-sectional area if possible for material savings while keeping the same capacity. Alternatively, more larger or otherwise more detailed embedment veneer ties to increase connector capacity.

The observation that a brick veneer offers more connector tension resistance than a concrete veneer due to a higher absorption rate for clay brick which promotes a better bond could not be concluded as variability in the tests was too large. More studies should be completed to investigate this possibility later.

T-Z and T-R connectors have amongst the largest initial stiffness compared to the plated connectors T-PV and T-IN which can be explained by the lack of an embedment veneer tie. The slot and embedment tie had larger initial deformations under low loads until slack in the slot was taken out.

Expressions from Hatzinikolas et al. (1979) were unconservative for T-Z and T-R specimens. Arslan et al. (2021) had conservative cone breakout predictions when assuming a mortar shear

strength f_{vo} of 0.10 MPa. The tested to model peak load ratio is closer to unity when a mortar shear strength f_{vo} of 0.17 MPa is assumed for T-Z and T-R.

A more accurate equation model can be developed in future for connectors with embedment veneer ties since the veneer tie yielded in some tests which leads to peak load being reached. A less conservative connector capacity equation, which also includes tie yielding, should be proposed since current design capacity from A370:14 use an empirical resistance factor giving a connector capacity of 0.6 kN for a material embedment failure mode under axial loading.

The tension load displacement responses of connectors all had variability between specimens that were identical. However, the T-R and T-PV specimens gave the most consistent response when compared to other connectors based on similar load displacement curves and having the lowest difference between the overall average peak load of the specimen type and each individual specimen. A likely reason for this is due to the expected enclosed mortar breakout area of the tie connector itself (T-R) and the embedment veneer tie (T-PV) being predictable.

Ways to increase tension capacity for connectors that underwent breakout failure modes can be achieved by increasing the projected breakout area which can be done by increasing the embedment depth or by changing the shape of the connector's end that's embedded into the veneer wythe. Ideally the connector's end embedded into the veneer wythe would not be enclosed (T-R), would not contain an 'enclosed' embedment veneer tie (T-PV and T-IN) and forms a 'T' shape instead of an 'L' shape (T-Z) which will give a higher capacity breakout closer to the expected idealized 45 degree cone. For connectors that underwent pull out failure (T-PH), an increase in embedment depth would increase tension capacity. All connectors would have a higher tensile capacity if mortar strength was increased.

4. EXPERIMENTAL INVESTIGATION OF DOUBLE WYTHE MASONRY WALL WITH DIFFERENT CONNECTORS UNDER COMPRESSION

4.1 Introduction

As discussed in Section 3.1, due to connection vulnerability under out of plane loading for cavity walls, connector behaviour needs to be better understood. This chapter will focus on the response of the connectors under compression. The same test frame presented in Chapter 3 was used with a key difference being that insulation was a part of the specimen construction due to its potential contribution to resistance when connectors are under compression in the transverse direction. There is minimal research on how much the insulation contributes but there is previous research on non-masonry wall systems discussed indicating that insulation provides increased connector stability in the longitudinal direction under compression (Dias et al. 2019, Lawson et al. 2020, Du et al. 2022, Carstens and Pahn 2022). The tested connectors are longer than connectors from previous test research programs due to the larger insulation thickness of 150 mm and an air cavity of 25.4 mm. This is done due to expected future energy code requirements resulting in an increase of insulation. Four different connectors are tested in compression. Peak loads and deformations will be compared to previous research where applicable.

4.2 Experimental Program

Thirty one specimens were tested in compression. The compression specimens have the same parameters as the tension specimens discussed in Section 3.2 except for the addition of 150 mm thick insulation in the compression specimens due to an expected contribution from insulation to the compression behaviour.

The same four connectors in Figure 3.1 and the same specimen dimensions and construction (Figure 3.2) described in Chapter 3 were used for compression testing. The compression specimen test matrix shown in Table 4.1 uses the same test identifier format, connector type, diameter, thickness, brick embedment and veneer brick material parameters as the tension test matrix previously shown and described in Section 3.2.6. The main difference is that C-IN.CN-4 has no insulation so that the complete specimen response during compression loading can be viewed with no obstructions from the insulation.

Table 4.1: Compression test matrix

Test Identifier	Connector type	Connector Diameter / Thickness, mm	Nominal connector area, mm^2	Embedment in Brick Veneer, mm	Veneer brick material
C-Z.CN-1,2,3	Z-tie	4.8	18	50	Concrete
C-Z.CL-1,2,3	Z-tie	4.8	18	50	Clay
C-R.CN-1,2,3	Rectangular tie	4.8	36	25	Concrete
C-R.CL-1,2,3	Rectangular tie	4.8	36	25	Clay
C-PV.CN-1,2,3	Plated connector	3.0	150	50	Concrete
C-PV.CL-1,2,3	Plated connector	3.0	150	50	Clay
C-PH.CN-1,2,3	Plated connector	3.0	150	50	Concrete
C-PH.CL-1,2,3	Plated connector	3.0	150	50	Clay
C-IN.CN-1,2,3,4[A]	Inclined connector	3.0	150	20	Concrete
C-IN.CL-1,2,3	Inclined connector	3.0	150	20	Clay

[A] C-IN.CN-4 has no insulation

The first designation specifies C for Compression and T for Tension (for this chapter only C is considered). The second specifies R for a rectangular tie, Z for Z-tie, PH for plate connector placed lying down (H = horizontal), PV for plate connector placed upright (V = vertical) and IN for inclined connector. The third specifies CL for clay brick veneer and CN for concrete brick veneer. The final numbers specify the specimen ID number. All specimens had three identical specimens to investigate variability except for the C-IN.CN specimens having one extra without insulation to record observations during loading. An example of this test identifier format is C-Z.CL-2 which represents a compression wall specimen with a Z-Tie connector of clay brick veneer and the second specimen of that type tested.

The material properties in Table 3.2 and specimen fabrication process in Section 3.2.8. were also the same for the compression specimens with the addition of the insulation. The same testing frame and platforms in Figure 3.10 and Figure 3.12 were used for compression loading however adjustments were made to accommodate the compression specimen being loaded onto the experimental frame shown in Figure 4.1.

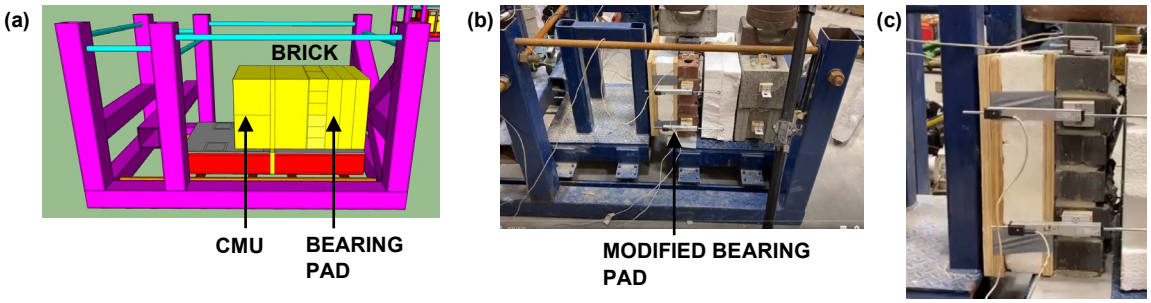

Figure 4.1: Compression testing with specimen in experimental frame of (a) initial conceptual design, (b) actual testing set up, (c) modified compression bearing pad.

For the compression tests, the CMU wythe beared against the test frame during loading. Due to the difficulty in placing both wythes on separate platforms, as done in Chapter 3, a modified compression bearing pad was made to transfer compression to the brick veneer wythe. The modified compression bearing pad had the same 400 mm width and 400 mm height dimensions as a typical specimen's cross section shown in Figure 3.13 (a) and was made of two layers of plywood sheathing with EPS insulation in between to achieve the desired thickness when applying uniform loading as shown in Figure 4.1(c). This was done to place all wythes on one platform allowing for easier work with loading specimens onto the test frame. Teflon was placed underneath the brick veneer to prevent sliding during compression loading because of its low friction surface.

The same hydraulic Enerpac RCH123 jack described in Section 3.2.10 was used along with the same LVDT instrumentation and placements in Figure 3.13. The average loading rate for the Z-ties, rectangular ties , plated connector with an upright orientation, plated connector lying down and inclined connector were 3.8 mm/min, 8.9 mm/min, 1.8 mm/min, 3.1 mm/min, and 2.6 mm/min respectively. The individual compression loading rates are provided in Appendix B which are calculated from 25% of the peak load up to the peak load.

The same weights described in Figure 3.14 of Chapter 3 are placed onto the brick veneer also to satisfy surcharge load requirements from CSA A370-14.

When determining peak loads, loads were recorded after insulation bearing were not considered in this thesis's discussion as they are not representative of the connector response. The compression load-displacement figures for some connectors had a decrease in load followed by later increase to a new peak load larger than those reported at displacements exceeding 15 mm. Visual verification and engineering judgement was used to determine that these secondary peaks loads were from insulation bearing. The specified air cavity width for every specimen is 25.4 mm except for C-IN.CN-4 which had a 175 mm air cavity due to no insulation present. The actual air cavity widths were less than 25.4 mm in some locations due to mortar joint extrusions and brick units extruding which is common in construction. The average recorded displacements at peak load for all connector types ranged from 0.9 mm to 8.4 mm shown in Table 4.1 which is well below 50% of the cavity width and representative of connector response and not insulation bearing.

4.3 Experimental Compression Results

The primary failure mode under compression loading for all specimens is buckling except for C-PH specimens which underwent piercing. Table 4.2 summarizes results from all compression tests for each specimen type and Figure 4.2 illustrates the compression load displacement plots for all specimens. A maximum displacement of 20 mm is shown on Figure 4.2 to show the peak load and an appropriate representation of the post peak compression response for all connectors. The maximum average displacement at peak load is 8.4 mm and increases in load occurring at displacements closer to 20 mm is attributed largely to insulation bearing.

Table 4.2: Summary of test results under compression loading

Test ID	Ave. peak load, kN	Standard deviation, kN	CoV	Ave. displacement at peak load, mm	Average initial stiffness, kN/mm	Failure Mode
C-Z.CL	3.1	1.0	0.33	0.9	9.9	Connector buckling
C-Z.CN	3.2	0.3	0.09	1.5	1.7	Connector buckling
C-R.CL	7.7	1.2	0.16	8.2	1.0	Connector buckling
C-R.CN	6.6	0.4	0.06	3.6	9.6	Connector buckling
C-PV.CL	10.0	2.7	0.27	2.8	4.2	Connector buckling
C-PV.CN	9.6	1.6	0.17	1.9	29.5	Connector buckling
C-PH.CL	8.0	2.6	0.32	6.6	4.1	Piercing
C-PH.CN	8.6	0.4	0.05	4.8	1.7	Piercing
C-IN.CL	9.4	0.5	0.05	8.4	3.1	Connector buckling
C-IN.CN-1,2,3	7.2	1.9	0.26	2.3	13	Connector buckling
C-IN.CN-4[A]	9.5	N/A	N/A	1.9	9.7	Connector buckling

[A] C-IN.CN-4 has no insulation

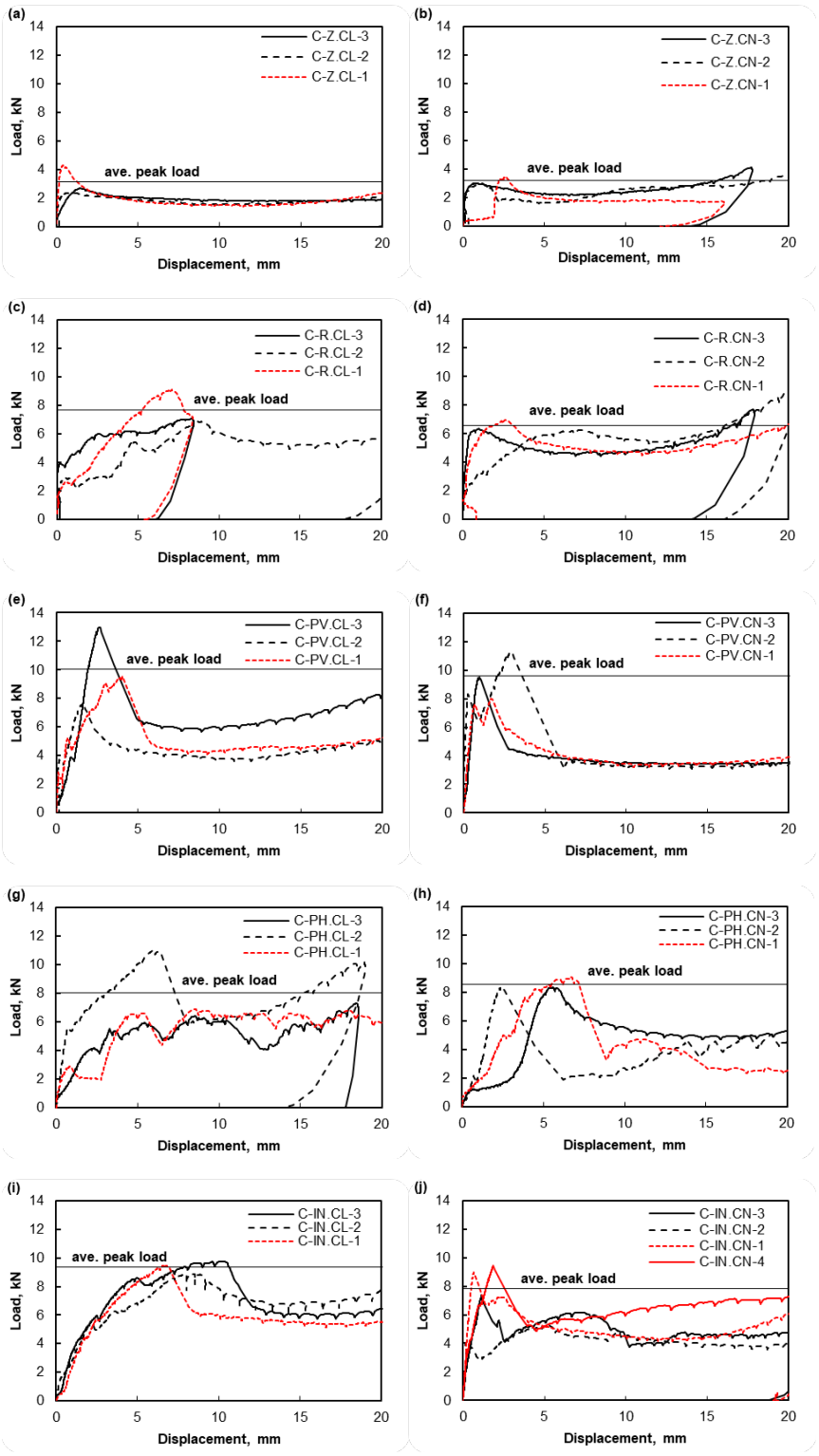

Figure 4.2: Compression load displacement plots for (a) Z tie with a clay veneer, (b) Z tie with a concrete veneer, (c) rectangular tie with a clay veneer, (d) rectangular tie with a concrete veneer, (e) plated connector with an upright orientation with a clay veneer, (f) plated connector with an upright orientation with a concrete veneer, (g) plated connector lying down with a clay veneer, (h) plated connector lying down with a concrete veneer, (i) inclined connector with a clay veneer, (j) inclined connector with a concrete veneer

Explanation of test observations including failure modes, test events, and connector stiffness are provided in the next sections. The same secant method approach from Section 3.3 corresponding to 10% and 40% of the peak load was used to assess stiffness. Due to negative displacements resulting in a negative slope because of LVDT alignment issues during testing when calculating the initial stiffness value for C-Z.CL-2, C-R.CL-3, C-R.CN-1, and C-PV.CL-2, the initial stiffness value is instead taken at 40% of the peak load to the peak load which is more representative of the specimen's stiffness value. The initial stiffness value of C-Z.CL-1 and C-R.CN-3 is also calculated at 40% to peak load solely because the adjusted initial stiffness value is more representative of the initial response than if taken at 10% to 40%. The same LVDT selection process described in Section 3.3 was used for determining the displacement averages for the compression specimens.

4.3.1 Experimental Compression Results for the Z Tie Connector

Table 4.3 summarizes results for each of the Z-tie connectors and Figure 4.2 (a) and (b) illustrates the compression load displacement plots for the Z-tie specimens.

Table 4.3: Experimental results for Z-tie connectors with brick veneer and concrete veneer

Connector ID	Peak Load, kN	Displacement at peak load, mm	Initial Stiffness, kN/mm	Failure mode
C-Z.CL-1	4.3	0.39	7.6	Connector buckling
C-Z.CL-2	2.4	0.87	1.6	Connector buckling
C-Z.CL-3	2.7	1.45	3.9	Connector buckling
C-Z.CN-1	3.5	2.57	0.56	Connector buckling
C-Z.CN-2	3.0	1.04	1.92	Connector buckling
C-Z.CN-3	3.0	0.75	2.46	Connector buckling

The C-Z specimens showed an initially high stiffness except for C-Z.CN-1 which had a high stiffness occurring only after a displacement of 1.5 mm. There was a linear increase in capacity with deformation until peak load. Peak load for all C-Z specimens was associated with connector buckling. There was then a gradual drop in load as expected from buckling. A reason for the gradual drop post buckling could be that since the T-Z connectors are closer to fixed-fixed boundary conditions due to being embedded within the mortar joint, plastic hinges are formed to mitigate the drop. The overall residual capacities are similar, converging to approximately 2 kN when a displacement of 6 mm is reached.

.

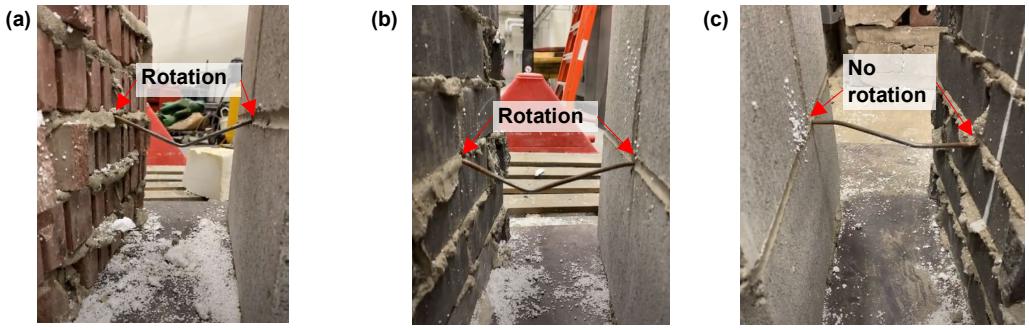

Figure 4.3: Z-tie illustrations of (a) typical buckling for clay brick specimens, (b) typical buckling for concrete veneer specimens, (c) unique C-Z.CN-2 buckling with a horizontal displacement

4.3.2 Experimental Compression Results for the Rectangular Tie Connector

Table 4.4 summarizes results for each of the rectangular tie connectors and Figure 4.2 (c) and (d) illustrates the compression load displacement plots for the rectangular tie specimens.

Table 4.4: Experimental results for rectangular tie connectors with brick veneer and concrete veneer

Connector ID	Peak Load, kN	Displacement at peak load, mm	Initial Stiffness, kN/mm	Failure mode
C-R.CL-1	9.1	7.1	1.4	Connector buckling
C-R.CL-2	6.9	9.0	1.1	Connector buckling
C-R.CL-3	7.1	8.4	0.5	Connector buckling
C-R.CN-1	7.0	2.6	1.8	Connector buckling
C-R.CN-2	6.3	7.3	4.0	Connector buckling
C-R.CN-3	6.4	1.0	4.2	Connector buckling

The C-R specimens showed an initially high stiffness followed by a gradual increase in capacity with deformation until peak load. Peak load for all C-R specimens was associated with connector buckling. There was then a gradual drop in load as expected from buckling and the similar post peak responses to the T-Z connector including formation of plastic hinges. This is due to similar tie connector boundary conditions (fixed-fixed) and the low buckling capacity of the selected ties. The overall residual capacities converge to approximately 5.5 kN when a displacement of 6 mm is reached except for C-R.CL-1,3 which underwent an abrupt decrease in capacity.

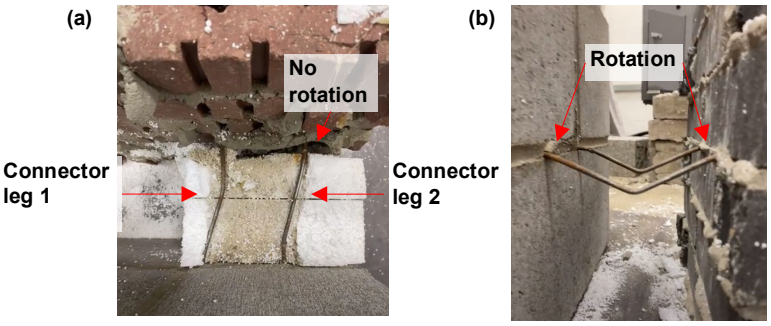

Figure 4.4: Rectangular-tie illustrations of (a) typical buckling for clay brick specimens with a horizontal deflection, (b) typical buckling for concrete veneer specimens with a vertical deflection

4.3.3 Experimental Compression Results for the Plated Connector with an Upright Orientation

Table 4.5 summarizes the results for each of the plated connectors with an upright orientation and Figure 4.2 (e) and (f) illustrates the compression load displacement plots for the upright plated connectors.

Table 4.5: Experimental results for plated connectors with an upright orientation with brick veneer and concrete veneer

Connector ID	Peak Load, kN	Displacement at peak load, mm	Initial Stiffness, kN/mm	Failure mode
C-PV.CL-1	9.5	4.1	5.6	Connector buckling
C-PV.CL-2	7.6	1.6	2.9	Connector buckling
C-PV.CL-3	13.0	2.6	4.0	Connector buckling
C-PV.CN-1	8.0	1.7	16.6	Connector buckling
C-PV.CN-2	11.2	2.9	62.0	Connector buckling
C-PV.CN-3	9.5	1.0	10.0	Connector buckling

The C-PV specimens showed an initially high stiffness and remained largely linear until peak load. Interestingly, C-PV.CL-1,2 and C-PV.CN-1,2 have a small load drop prior to the peak load followed by linear responses to peak load as shown in Figure 4.2(e) and (f) which may be due to the mortar within the embedment veneer tie bearing against the embedment veneer tie but then this mortar breaks off which shifts load to the veneer tie until the connector buckled. See Figure C.49 (a-c) in Appendix C for more details. Peak loads for all C-PV specimens was associated with connector buckling. There was then an abrupt drop in load. as expected. from buckling. The tie connectors (C-Z and C-R) had a gradual drop post peak when compared to the C-PV connector. A reason why the C-PV connector had an abrupt drop in load could be due to the post peak resistance contribution from plastic hinges not being a significant factor. The buckling capacity of C-PV connectors are noticeably larger than the load needed to cause plastic hinge formation and thus not a factor in resistance after yielding when compared to the tie connectors (C-Z and C-R) which is

why C-PV has a abrupt decrease. The residual capacity response converged to approximately 5.0 kN after around a 5 mm displacement was reached.

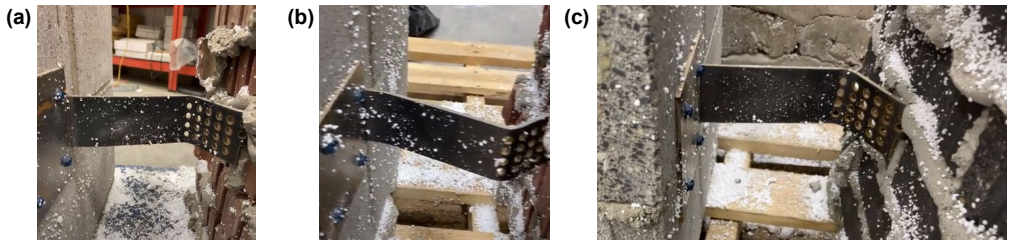

Figure 4.5: Plated connector with an upright orientation illustrations of (a) typical buckling of clay brick veneer specimens, (b) unique C-PV.CL-2 buckling in opposite direction, (c) typical buckling of concrete brick veneer specimens

4.3.4 Experimental Compression Results for the Plated Connector with a Lying Down Orientation

Table 4.6 summarizes results for each of the plated connectors with a lying down orientation and Figure 4.2 (g) and (h) illustrates compression load displacement plots for the lying plated connectors.

Table 4.6: Experimental results for plated connectors with a lying down orientation with brick veneer and concrete veneer

Connector ID	Peak Load, kN	Displacement at peak load, mm	Initial Stiffness, kN/mm	Failure mode
C-PH.CL-1	6.6	5.4	0.7	Piercing
C-PH.CL-2	11.0	5.9	9.7	Connector buckling
C-PH.CL-3	6.4	8.5	1.8	Piercing
C-PH.CN-1	9.0	6.7	1.5	Piercing
C-PH.CN-2	8.4	2.4	2.8	Connector buckling
C-PH.CN-3	8.3	5.4	0.7	Piercing

All clay and concrete brick veneer specimens are recorded as piercing failures except for C-PH.CL-2 and C-PH.CN-2 which underwent buckling. The C-PH specimens that buckled showed an initially high stiffness followed by a gradual increase in load with deformation until peak load. There was then an abrupt drop in load, as expected, from buckling. The piercing C-PH specimens showed a lower initial stiffness when compared to buckling with an overall more gradual increase in load with deformation until peak load. The overall residual capacity after buckling converged to approximately 5 kN when after about 6 mm of displacement.

Clay brick veneer specimens C-PH.CL-1,3 had piercing failures because the connectors had no indications of buckling and the mortar joint showed signs of piercing failure shown in Figure 4.6 (a) and (c) where the mortar joint is clearly disturbed and breaking. Arslan et al. (2021)

characterized piercing failure as a situation where a portion of mortar punches out from beneath the connector as further explained and illustrated in Section 2.4.2 and Figure 2.10(b). A reason why buckling was not the primary governing failure mode for all specimens could be because of the mortar strength properties due to the variability in mortar mixing on site. Piercing failure is directly proportional to mortar strength so if there is a lower strength with a mortar batch the piercing failure mode would govern.

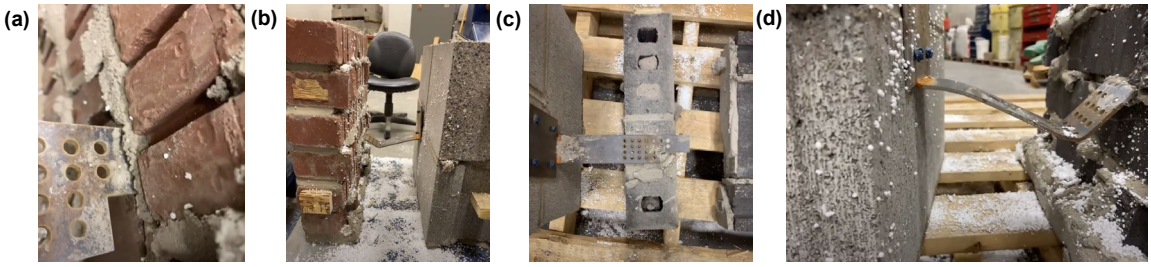

Figure 4.6: Plated connector with a lying down orientation illustration of (a) typical piercing failure of clay brick specimens, (b) unique buckling of C-PH.CL-2, (c) typical piercing failure of concrete brick specimens, (d) unique buckling of C-PH.CN-2

4.3.5 Experimental Compression Results for the Inclined Connector

Table 4.7 summarizes results for each of the inclined connectors and Figure 4.2 (i) and (j) illustrates the compression load displacement plots for the inclined connectors.

Table 4.7: Experimental results for inclined connectors with brick veneer and concrete veneer

Connector ID	Peak Load, kN	Displacement at peak load, mm	Initial Stiffness, kN/mm	Failure mode
C-IN.CL-1	9.4	6.5	3.2	Connector buckling
C-IN.CL-2	8.9	8.4	2.4	Connector buckling
C-IN.CL-3	9.8	10.3	3.6	Connector buckling
C-IN.CN-1	9.0	0.70	19.1	Connector buckling
C-IN.CN-2	5.3	5.2	11.8	Connector buckling
C-IN.CN-3	7.4	1.1	8.1	Connector buckling
C-IN.CN-4[A]	9.5	1.9	9.7	Connector buckling

[A] C-IN.CN-4 has no insulation

The C-IN.CL specimens showed an initially high stiffness followed by a gradual increase in load with deformation until peak load. The C-IN.CN specimen's response was the same except for having a higher initial stiffness with an abrupt increase in load until peak load. There was then a gradual drop in load as expected from buckling. The overall residual capacity was around 6 kN when a displacement of 15 mm was reached.

All clay and concrete brick veneer specimens are recorded as connector buckling failures. There were minimal signs of the embedment veneer ties at the top and bottom yielding except for in C-IN.CN-4 which had a noticeable bottom embedment veneer tie yielding.

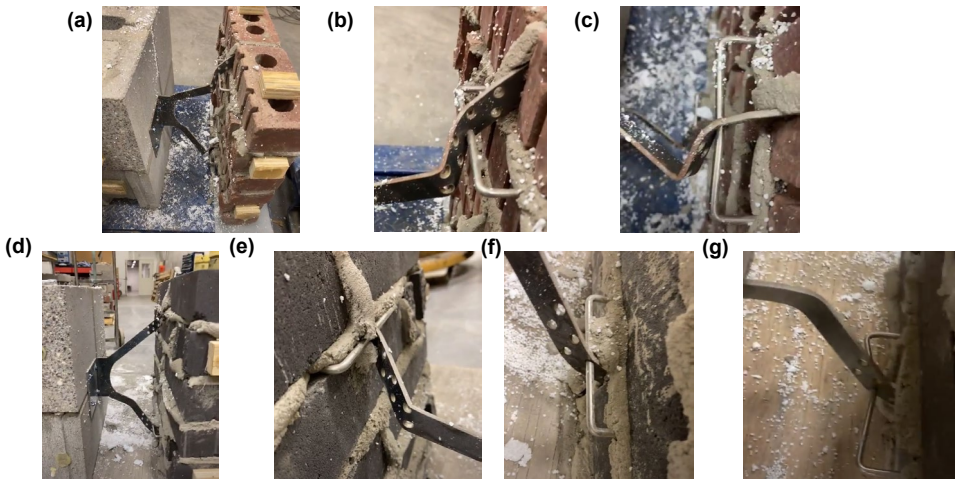

Figure 4.7: Inclined connector illustrations of (a) typical buckling failure mode of clay brick veneer specimens, (b) typical condition of top leg connector after buckling for clay brick veneer specimens, (c) typical condition of bottom leg connector after buckling for clay brick veneer specimens, (d) typical buckling failure mode of concrete brick veneer specimens, (e) typical condition of top leg connector after buckling for concrete brick veneer specimens, (f) typical condition of bottom leg connector after buckling for concrete brick veneer specimens, (g) unique C-INC.CN-4 bottom leg connector condition with embedment tie yielding

4.3.6 Comparison of Response, Peak Loads, Failure Modes between Parameters

Figure 4.8 shows an illustration of individual representative specimens from each connector type taken from Figure 4.2 similar to the approach used in Section 3.3.6. All connectors experienced connector buckling except for the C-PH.CL-1,3 and C-PH.CL-1,3 which underwent piercing failure. Piercing failure of C-PH connectors is shown in the figure.

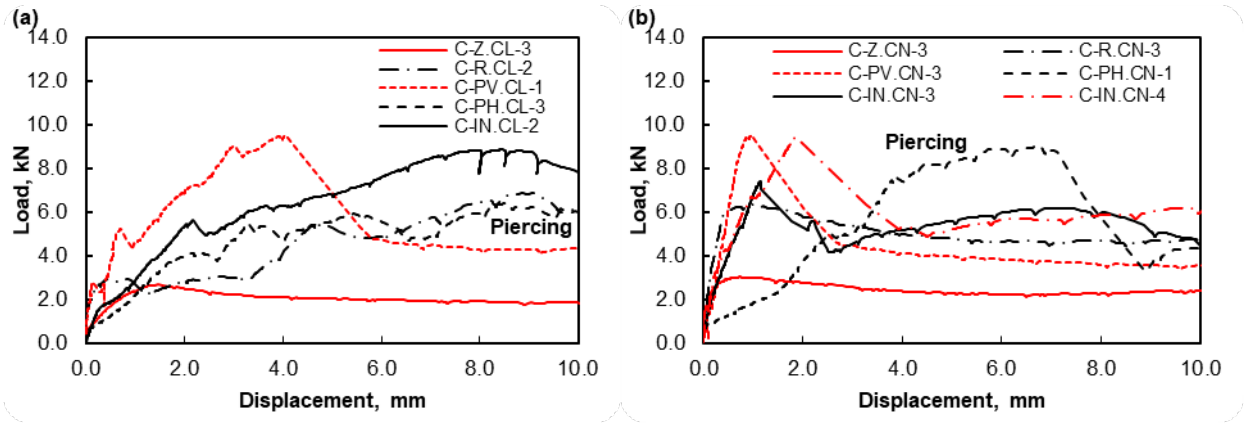

Figure 4.8: Compression load displacement plots of representative responses from each connector for (a) clay brick veneer, (b) concrete brick veneer

The average peak load's for C-Z.CL, C-R.CN, C-R.CL and C-R.CN are 3.1 kN, 3.2 kN, 7.7 kN, 6.6 kN respectively with CoV of 0.33, 0.09, 0.16 and 0.06 respectively shown in Table 4.1. The total average peak load of the C-R specimens are the second lowest amongst all connector types and approximately double the peak load of the C-Z tie's. This is because even though the material and geometric properties are similar for C-R and C-Z, C-R has two connector legs crossing the cavity which are expected to distribute load in half.

The average peak loads of C-PV.CL, C-PV.CN, C-PH.CL, C-PH.CN, C-IN.CL and C-IN.CN are 10 kN, 9.6 kN, 8.0 kN, 8.6 kN, 7.2 kN and 7.8 kN respectively with a CoV of 0.27, 0.17, 0.32, 0.05, 0.05 and 0.24. A key difference with the C-PH connectors is that four of the six specimens were piercing failure and not buckling failure observed with all the other connectors.

The variance between individual specimen's peak loads with the same connector type associated with buckling can be explained by differences in the actual effective length factor, k, accidental eccentricity, and potential added resistance due to EPS insulation.

The restraint conditions within the mortar can differ from one test to the next which affects k for restraint but even the connector lengths may differ slightly from test to test. Accidental eccentricity in the specimens is due to no connector being perfectly straight and perpendicular to the wythe faces. The additional resistance due to increased stability from the EPS insulation also may affect capacity but vary between tests depending on how tight the insulation was placed around connectors.

Other factors, such as connector elastic modulus, dimensions, and yield strength vary slightly as well but are not expected to be differ greatly from one test to the next. Whether the connector

buckles about different axes (Figure 4.3 or 4.4) is irrelevant due to previously explaining each specimen can have different accidental eccentricities which would cause buckling about different axes from one test to the next in the same set of specimens.

The initial response of all connectors have scatter when comparing between specimens of the same type with the exception of C-IN.CL which has the least amount of scatter initially. The initial response of the C-PV connectors is shown in Figure 4.8 with a large initial stiffness scatter between C-PV.CL specimens and C-PV.CN specimens which could be due to the LVDT placement and loading not perfectly uniformly distributed. There is a large scatter amongst all post peak responses except for the C-Z connector type shown in Figure 4.2 and C-PV.CN connector type shown in Figure 4.2 (f) which could also be due to loading placement.

4.3.7 Comparison of Experimental Values with Euler buckling

Hatzinikolas et al. (1979) proposed Equation 4.4 for mortar in block failure capacity of masonry ties further described in Section 2.4.1. However, test specimens in this program were all governed by buckling except for four of the six C-PH connectors which underwent piercing. Arslan et al. (2021) also proposed compression expressions in Equation 4.1, 4.2 and 4.3 for buckling, piercing and punching respectively as previously described in Section 2.4.2. Equation 4.1 use the critical Euler buckling load and accounts for initial deformation, Equation 4.2 represents piercing failure (bearing failure),and Equation 4.3 represents the punching failure based on the ACI empirical relationship for concrete punching failure (Arslan et al. 2021).

$$N = \frac{\pi^2 EI}{K^2 l_c^2} - \frac{12EI}{l_c d^3} \quad \text{(Eq. 4.1)}$$

$$N = A_1\left(f_m + 12.5 f_t\left(\sqrt{\frac{A_2}{A_1}} - 1\right)\right) \quad \text{(Eq. 4.2)}$$

$$N = 0.332\sqrt{f_m}uc \quad \text{(Eq. 4.3)}$$

$$P_{ult} = 6Kd^2\left(0.15\sqrt{f_m} + vf_c\right) + \mu 2\pi rl \quad \text{(Eq. 4.4)}$$

Arslan et al. (2021) does not consider surcharge loads in their compression equations. However Hatzinikolas et al. (1979) considers surcharge effects in Equation 4.4 as the f_c term described in Section 2.4.1. Buckling however can potentially be affected by surcharge due to affecting the rotational restraint at the connector ends. The amount of rotational restraint affects the effective lengths for buckling but quantifying this restraint is outside of the scope of this thesis.

A k-value of 0.7 is selected for the C-Z and C-R tie connectors since this represents a more realistic partially-fixed condition even though the tie connector is embedded within the mortar joint idealized by fixed boundary conditions, there is always a partial rotation since no boundary condition is ever perfectly fixed. Any observed rotation in the illustrations of the tie end conditions occurred after buckling initiated. The plated connector C-PV, C-PH and C-IN specimens are closer to a fixed-pin condition with a k of 0.7 due to the plated connectors being fastened to the CMU wythe with four fasteners which is closest to a fixed condition relative to the rigidity of the veneer boundary condition due to no rotation occurring at the connector/CMU interface. The brick wythe having the connector embedded within the mortar joint together with a embedment tie veneer is closest to a pinned condition since rotation does occur at this interface. In the case of the C-PV connector, this could be due to the plated connector moving along the embedment veneer tie's slot location.

Each individual leg of the inclined connector failed by buckling shown in Figure 4.7 however there is also a tendency for lateral torsional buckling to occur. The buckling load is 4.8 kN with a horizontal component of 5.8 kN to buckle. The total resistance is double since there are two legs totalling 11.7 kN. Figure 4.9 shows the connectors experimental peak loads compared to a critical buckling load with each connectors idealized k values however there are factors which affect the assumed k value for the inclined connector such as the transition point of 33 mm (Figure 3.2 b) between connector legs at the CMU which provides end restraint resistance and also the usage of embedment veneer ties. Table 4.7 compares the experimental peak load to the expected critical buckling load of each connector type. P_y represents the expected compression yielding load for each connector type calculated as the product of the yield strength and cross-sectional area.

Table 4.8: Comparison of experimental connector peak loads to Euler buckling

Test ID	Moment of inertia, mm^4	Mean Experimental Peak Load, kN	Expected buckling load, kN	Test to Predicted Ratio	P_y, kN
C-Z.CL	26	3.2	3.4	0.94	10.3
C-Z.CN	26	3.2	3.4	0.94	10.3
C-R.CL	52	7.7	6.8	1.13	20.6
C-R.CN	52	6.6	6.8	0.97	20.6
C-PV.CL	112	10.1	14.4	0.70	35.1
C-PV.CN	112	9.6	14.4	0.67	35.1
C-PH.CL	112	8.0	14.4	0.55	35.1
C-PH.CN	112	8.6	14.4	0.60	35.1
C-IN.CL	112	9.4	7.7[A]	1.22	28.6[B]
C-IN.CN	112	7.8	7.7[A]	1.01	28.6[B]

Modulus of elasticity: tie = 197 000 MPa and Plate = 194 000 MPa. Length, l = 175 mm. Tie diameter, d = 4.80 mm and plate thickness, t = 3.0 mm. Effective length factor, k = 0.7 for all connectors

[A] the horizontal component of the overall two connector legs assuming an individual connector leg diagonal resultant buckling load of 4.8 kN with a one leg horizontal component of 3.9 kN

[B] the horizontal yielding component of the overall two connector legs assuming an individual connector leg diagonal resultant yielding load of 17.6 kN with a one leg horizontal component of 14.3 kN

Yield strength of steel: Tie's f_y = 569 MPa and Plate's f_y = 234 MPa

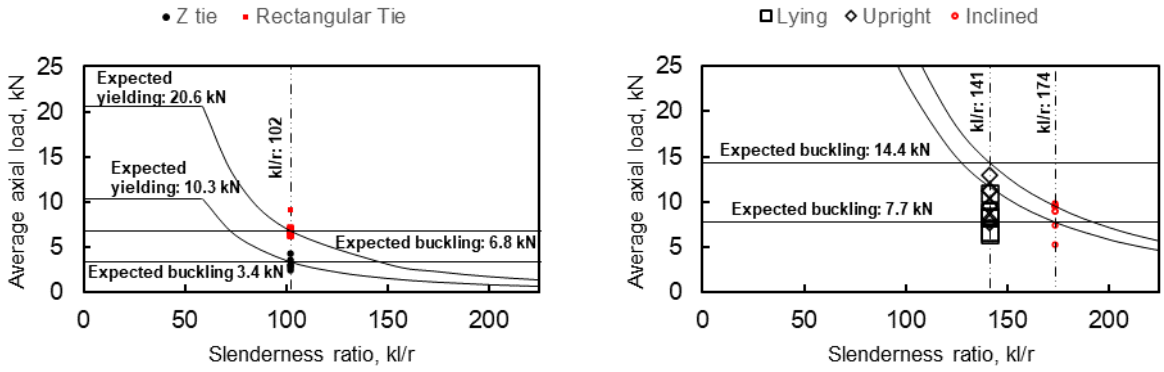

Figure 4.9: Average axial load versus slenderness ratio for (a) C-Z and C-R ties with k=0.7, and (b) C-PH, C-PV, C-IN with k=0.7

Figure 4.10 plots the recorded load displacement response to an expected bilinear yielding short column response of each connector if the connector were idealized as a piecewise equation assuming a slenderness ratio small enough to prevent buckling failure as shown in Equation 4.5. E is the modulus of elasticity of the steel connector, A is the cross-sectional area of the steel connector, L is the length of the connector taken as 175 mm which is the cavity length, δ is the axial displacement and δ_y is the yield displacement.

$$P_y = \begin{cases} \dfrac{\delta EA}{L}, & \delta < \delta_y \\ P_y, & \delta \geq \delta_y \end{cases} \qquad \text{(Eq. 4.5)}$$

Figure 4.10 indicates that the overall load displacement response for all connectors is elastic buckling even though there is scatter when comparing load displacement responses between identical specimens because the buckling load occurs well before the yielding response which is what occurs for elastic buckling.

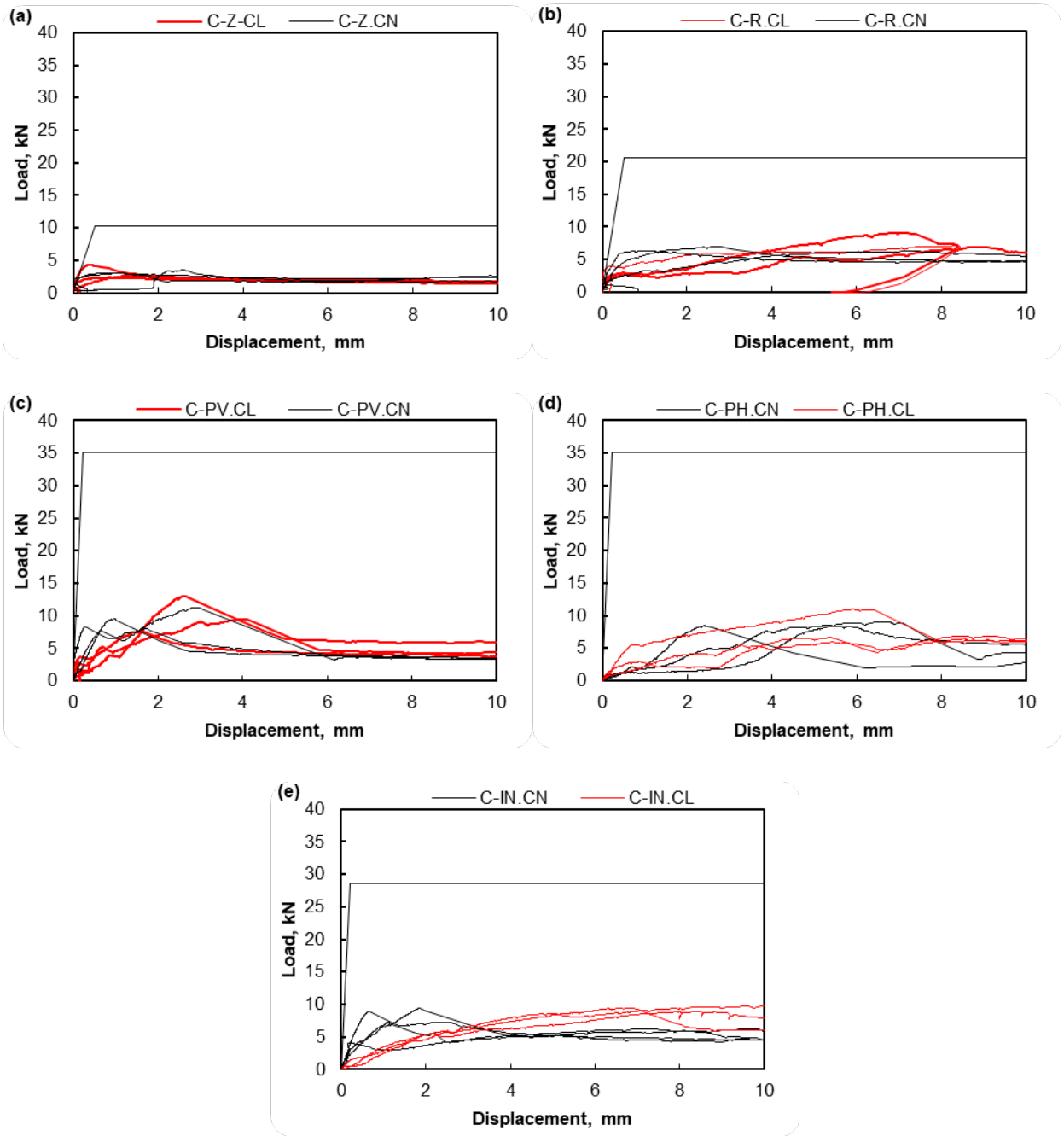

Figure 4.10: Compression response of clay brick and concrete brick veneers for specimen (a) C-Z, (b) C-R, (c) C-PV, (d) C-PH, (e) C-IN

The average experimental peak loads for the C-Z and C-R tie specimens are within a test to predicted ratio variance of 13% while the C-PV and C-IN plated connector tie specimens have at most a 45% variance shown in Table 4.7 which can be due to resistance from another source that is not due to the connector. C-PH has the highest test to predicted ratio variance with unity amongst all connector types of 0.58 however the governing observed failure mode is piercing failure. C-Z has the lowest test to predicted ratio variance with unity of 0.94 due to the less complexity of failure mechanisms and predictability of steel material properties when compared to the other connector types.

4.3.8 Compression Capacity Comparison of Connectors with Previous Experiments

Table 4.8 compares the combined experimental mean compression peak loads for connector systems with clay brick and concrete brick with results from previous research. All specimens in Table 4.8 had a buckling failure mode except for the Type H Z tie specimen and Type G rectangular tie specimen from Hatzinikolas et al. (1979) which were governed by embedment failure. Choi and LaFave (2004) defined their flexural buckling failure mode as closing at the 90°tie bend followed by bending at the middle and at the mortar side of the tie to accommodate the angle closing which is due to the low 25.4 mm cavity width when compared to the other tie specimens from previous research. All connectors from previous research were either fastened on one wythe and embedded into a mortar joint on the other wythe or embedded within a mortar joint at both wythes therefore an idealized effective length factor of 0.7 was assumed when calculating the Euler buckling load as discussed in Section 4.3.7.

Table 4.9: Comparison of experimental and previous research peak loads to Euler buckling

Test ID	Mean experimental peak load, kN	Expected buckling load, kN	Failure mode	Cavity width, mm	Mortar strength, MPa
NSCO28[A]	0.2	0.7	Flexural buckling	25.4	5.2
NSCO22, SSCO22[B]	0.6	5.9	Flexural buckling	25.4	5.2
Side-fixed sheet metal tie[C]	1.0	0.6	Axial buckling	50	15
Type H[D]	1.5	3.6	Embedment breakout	100	9.4
CS-1,2,3,4 CB50[E]	1.7	0.9	Connector buckling	80	5.7
C-Z.	3.2	3.4	Connector buckling	175	16.9
Type G[F]	4.4	3.2	Embedment breakout	150	14.8
C-R	7.1	6.8	Connector buckling	175	16.9
C-PH	8.3	14.4	Piercing	175	16.9
C-PV	9.8	14.4	Connector buckling	175	16.9
C-IN	8.5	7.7[G]	Connector buckling	175	16.9

[A] One corrugated metal tie 0.4x22 mm specimens from Choi and LaFave (2004).
[B] Two corrugated metal tie 0.8x22 mm specimens from Choi and LaFave (2004).
[C] One side-fixed sheet metal 0.9mm by 6mm specimen from Muhit et al. (2021).
[D] Two Z tie 3.66 mm rod specimens from Hatzinikolas et al. (1979) governed by embedment failure.
[E] Five L tie 3.6 mm rod specimens from Arslan et al. (2021)
[F] One rectangular tie 3.66 mm rod specimen from Hatzinikolas et al. (1979) governed by embedment failure.
[G] The horizontal component of the overall two connector legs assuming an individual connector leg diagonal resultant buckling load of 4.8 kN with a one leg horizontal component of 3.9 kN

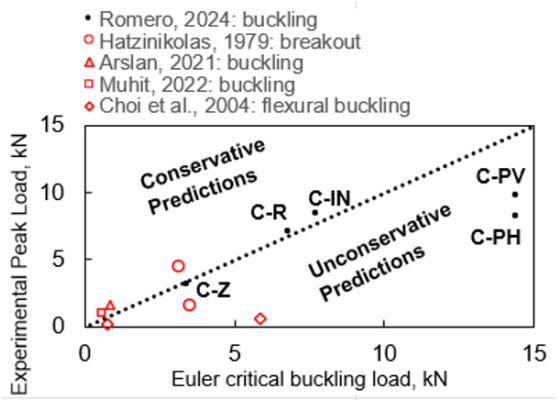

Figure 4.11: Current study and previous research compression peak load comparison with Euler buckling

When comparing the peak average test loads from previous research under compression to theoretical Euler critical loads, the actual peak load value follows a trend shown in Figure 4.11 for most specimens except for specimens which either underwent flexural buckling (Choi and LaFave, 2004) or embedment breakout failure (Hatzinikolas et al., 1979). The plated connectors (C-PV and C-PH) were the furthest from unity of all connector types in the current study.

Figure 4.11 shows that if a specimen buckles under compression, Euler's buckling equation is an appropriate model to predict the load of all connector types except for C-PV and C-PH . C-PH should be excluded due to piercing being the governing failure mode. A reason why C-PV connector types are not close to unity could be due to the actual k value being higher than the

idealized value of 0.7. The assumed k value would have to be 0.85 to achieve a buckling load of 9.8 kN. This shows the assumed fixed end for the C-PV connectors is only partially fixed which agrees with the C-PV illustrations in Figure C.45 to C.50 which shows the CMU/connector interface and veneer/connector interface rotating to some degree and not entirely fixed.

4.3.9 Exterior Wythe Material Considerations and Eccentricity Effects

There does not appear to be a correlation between different type of veneers and buckling resistance shown in Figure 4.10. The reason for this is because the buckling resistance is proportional to effective length, geometric, and material properties. Even though the veneer material type can affect the strength and stiffness of the mortar bond with the embedded connector (Drysdale et al. 2005, Ahmadi and Reisi 2020) which indirectly affects the effective length portion within the mortar joint (at most 50 mm), the combined effects of the connector's geometry, material properties and accidental eccentricity are larger factors in the buckling resistance.

Unintended eccentricities are present in all specimens because of unavoidable variances between specimens from alignment of the connector during construction, installation into the test frame, and loading. Larger eccentricity results in smaller load than the expected buckling load which would decrease the test to predicted ratios which ranged from 0.94-1.13 for the tie connectors (C-Z and C-R), ranged from 0.55-0.70 for the plated connectors (C-PV and C-PH) and ranged from 1.01-1.22 for the C-IN inclined connectors which shifts the current study data points in Figure 4.11 to the more unconservative prediction region. The plated connectors would be most affected by this however since all specimens that failed by buckling were well within the expected elastic buckling region (Figure 4.10),.even if eccentricity was zero, the overall failure loads of the connectors is expected to remain as elastic buckling. Any future adjustment for unintended eccentricities would be primarily for the C-PV connector types since C-PH was not governed by buckling. If an adjustment were to be made for the unintended eccentricity, the other connector types would be shifted more to the conservative prediction region in Figure 4.11.

4.4 Chapter Conclusions

The observed compression failure mode for all specimens is elastic buckling failure except for C-PH.CL-1,3 and C-PH.CN-1,3 which experienced piercing failure. The plated connector laid flat on the brick wythe with less chance of misalignment which creates less chance of eccentricities that reduce buckling resistance with the specimen. This connector also directly beared against mortar instead of an embedment tie or other bend which made piercing more likely. The large

amount of scatter in the actual buckling peak load can be attributed to different actual effective length factors, different eccentricities created due to mis-alignment, and non-uniform loading conditions between specimens.

The C-Z and C-R tie connectors have the lowest average compression peak loads and the C-IN and C-PV plated connectors have the largest average compression peak.

A more realistic effective length for C-Z and C-R tie connectors is 0.7 which is appropriate for the end conditions because even though the ties are embedded into the mortar joint which is idealized as fixed, there is always partial rigidity in reality. Even though some tie specimens are visually seen as having rotation at the ends suggesting pinned conditions, this occurred after buckling. . A more realistic effective length value for the for the inclined connector (C-IN) is 0.7 for pinned and fixed end conditions. C-PH and C-PV had the largest variance with the expected buckling load when assuming a k of 0.7 due to undergoing a piercing failure mode instead of buckling and C-PV likely having a slightly larger effective length closer to 0.85.

There is expected additional compression resistance due to the increased insulation providing expected stability however the exact amount cannot be quantified using methods explored in this test. The C-IN.CN-4 specimen with no insulation had the second highest peak load amongst all inclined connectors, which indicates that insulation may not contribute much to this resistance though further study is needed to make a conclusion. When viewing an entire wall system, the increased compression resistance from stability due to insulation may be significant due to scaling effects and the selected masonry connector spacing used in the overall wall. The amount of stability provided by insulation for compression resistance is also dependent on the density of the insulating material with this study's rigid foam insulation (EPS) density of 24 kg/m^3 in comparison to rockwool insulation density ranging from 27 – 40 kg/m^3 and fibreglass batt insulation density ranging from 10 – 14 kg/m^3 however whether insulation is blown in can greatly affect the insulation density.

Euler buckling and piercing failure (Arslan et al. (2021) expressions were compared to the test values. Results indicate that the piercing failure expression should be adjusted for plated connectors. Similar to Chapter 3, a less conservative connector design capacity equation may be considered since current design capacity from A370:14 uses an empirical resistance factor that gives a connector capacity load of 0.6 kN for buckling failure under axial load which, by extension, may lead to needing considerably more or larger connectors in a full wall given the expression's

conservatism. Complete compression tension load responses can also be developed to validate expected behaviour of other connectors with similar geometry and adjusted if different material properties are used.

The compression load displacement responses of connectors all had variability between specimens that were identical. However, the C-Z and C-R connectors gave the most consistent response when compared to other connectors based on similar load displacement curves and having the lowest difference between the overall average peak load of the specimen type and each individual specimen. A likely reason for this is the effective length is more consistent for tie specimens due to embedment on both sides being more uniform with less variables involved compared to plated connectors which either underwent a different failure mode (C-PH) or had the connector itself embedded into the mortar joint with the embedment veneer tie (C-PV and C-IN) which affects the true effective embedment length.

Ways to increase compression capacity for connectors that underwent elastic buckling would be to increase the flexural stiffness (EI) of the connector itself or decrease the cavity which decreases the connector's effective length (kl). For connectors that underwent piercing failure (C-PH), the cross-sectional dimensions of the connector end embedded within the veneer wythe can be increased or increasing the mortar strength would increase the compression capacity.

5. SUMMARY AND CONCLUSIONS

This chapter provides a summary, conclusion, and recommendation from the experimental investigation of masonry connectors within a cavity wall system specimen under tension and compression loading.

5.1 Summary

Chapter 2 presented a literature review on masonry walls and masonry connectors with a focus on tension and compression loading. Chapter 3 discussed details on the masonry connectors used during tension and compression testing. Details on the test frame designed and constructed for this test program were also presented in Chapter 3. Tension tests were presented on five connector types in Chapter 3: Z-tie (T-Z) and rectangular tie (T-R) connectors were tested due to their conventional use in masonry cavity walls. A plated connector, representative of connectors used in contemporary walls, was tested in both horizontal (T-PH) and vertical (T-PV) orientations along with an inclined connector (T-IN) which is a novel approach designed to act more as a shear connector in future walls. Results such as peak load and displacement were observed and recorded. Stiffness was calculated from the recorded peak loads and displacements and general trends were observed. Chapter 4 focused on the compression loading that was done on the same connectors in Chapter 3 including Z-tie (C-Z), rectangular (C-R), horizontal plate connector (C-PH), vertical plate connector (C-PV), and a novel inclined connector (C-IN). Failure modes and peak loads were discussed and related to simple design-oriented expressions from past studies.

5.2 Conclusions

The following conclusions are drawn in this thesis:

1. Previous testing on walls with connectors is included in the literature review. The literature review determined that there are gaps in masonry connector capacities under axial loading which is a reason why conservative and empirical capacity design equations are relied on by masonry codes and standards. There is also a lack of existing knowledge in differentiating connectors with different geometries and material properties. This accomplished *Item 1* of the research objective.
2. The T-Z and T-R connectors experienced embedment breakout failure further classified into cone breakout and angular breakout respectively. The T-PV connectors experienced veneer tie breakout failure and the T-PH and T-IN connectors experienced pull-out failure. The tie connectors had the smallest average peak loads when compared to the plated connectors.

Even though all connectors relied on mortar bond strength to some degree due to the governing failure mode being a type of embedment failure, the T-IN and T-PV connectors had the highest average peak loads with high displacements at peak load when compared to T-Z and T-R connectors. The main reason for this is due to embedment veneer ties which increased the effective concrete breakout area and provided more deformation capability due to the free play from the slot that the embedment veneer tie went into. Due to not utilizing the full axial yield tensile capacity, it would be effective to reduce the cross sectional area and utilizing an embedment veneer tie shape that will achieve the required effective concrete breakout area which increases the embedment tension capacity of the connector. This accomplished *Item 2 and 3* of the research objective.

3. In compression, all specimens experienced Euler buckling except for four out of a total of six horizontal plate specimens that underwent piercing failure. Even though there is a large amount of scatter between clay and concrete specimens, the overall observed response for all specimens that buckled is most similar to elastic buckling. Scatter can be attributed to different actual effective length factors, different eccentricities created due to mis-alignment and non-uniform loading conditions between specimens. As expected, tie connectors had the lowest peak loads when compared to the plated connectors. Idealized effective length factors for the tie (C-Z and C-R), and inclined (C-IN) connectors were verified when compared to the experimental values to be 0.70. The plated connectors (C-PV and C-PH) had the largest variance from the expected buckling load when assuming a k of 0.7 which can be attributed to C-PH undergoing a piercing failure and C-PV having a k closer to 0.85. C-PV brick and concrete veneer specimens had the largest peak loads (10.0 kN and 9.6 kN respectively). However, C-IN brick and concrete veneer inclined connectors performed similarly (9.4 kN and 7.8 kN respectively). If larger compression resistance is required, an inclined connector would be an acceptable connector design due to performing similarly to the C-PV connector with the largest peak loads however its effective length would have to be adjusted when calculating buckling capacity so as to avoid an unconservative buckling prediction. This accomplished *Item 4* and 5 of the research objective.
4. Comparisons of peak loads under tension for tests in this study with previously developed expressions determined that the cone breakout approach adjusted by Arslan et al.(2021) is conservative. A correlation of a better mortar bond with the connector and thus a larger peak

load for different veneer types was not observed. This accomplished part of *Item 5* of the research objective.

5. Chapter 4 compared experimental and previous research peak loads to the expected Euler buckling load. A linear elastic buckling response was observed for all specimens that underwent buckling. This accomplished the rest of *Item 5* of the research objective.

Overall, this thesis presented experimental results evaluating a cavity wall system with cavity widths reflecting recent energy code updates and their behaviour with different connectors. Trends such as a larger tensile capacity being associated with a larger projected breakout area for the tie connectors is observed. Results show that even though the tie connectors have lower capacity when compared to the plated connectors, if the tie end shapes were adjusted for a projected breakout area equal to or greater than the plated connectors, the capacity may be around the same despite the smaller cross sectional area used. The T-IN connectors were amongst the largest in average peak loads for tensile resistance. The compression results for all connectors had a consistent elastic buckling response between identical specimens excluding the C-PH connectors which underwent piercing failure. This is due to buckling being dependent on the flexural stiffness of the connector itself which has low variability when compared to mortar and the effective length being fairly uniform due to specimens being constructed the same. Similarly, the tension results for all connectors had consistent breakout responses between identical specimens excluding the T-PH which underwent pull-out failure. Even though the mortar strength has variability, the projected mortar breakout areas were consistent (T-Z and T-R) due to the connectors being fabricated the same and even with the embedment veneer tie undergoing yielding in some cases (T-PV and T-IN). Overall, the rectangular connector (T-R and C-R) had the most consistent tension and compression response out of all connectors due to a predictable enclosed mortar breakout area under tension and a consistent effective length due to proper tie placement during specimen construction for compression. The cone breakout model proposed by Arslan et al. (2021) is close to the recorded tensile peak loads recorded. There seemed to be no increase in peak loads between brick veneer and clay brick veneer under both tension and compression loading. The tie connectors had the lowest compression capacity as expected due to lower material properties (EI). Idealized k values for the tie connectors(C-Z and C-R) and inclined connectors (C-IN) were found to be 0.7. However, the actual k value for C-PV is closer to 0.85 and the C-PH expected compression peak load prediction should be adjusted so that piercing failure governs instead of buckling Due to the

overall axial failure modes in tension and compression being located at the veneer mortar joint for breakout failure and along the connector itself for connector buckling respectively, a change of structural backing would not be expected to change the axial response significantly for the plated connectors with fasteners. If the structural CMU wythe were instead wood studs (common in residential construction) or steel studs (common in commercial construction) then the axial response when using the plated connectors in both orientations and the inclined connector would be expected to have similar results assuming the same cavity widths are used and fastener failure at the structural backing does not occur. A complete axial response combining tension and compression for all connector specimens show that tensile embedment breakout and pull-out are the governing axial failure modes. The current connector design capacity equation from A370:14 which uses an empirical resistance factor of 0.6 kN for material embedment failure mode is shown to be conservative compared to the measured experimental values in this thesis. The inclined connector had the highest overall tension resistance. The plated connectors (C-PH and C-PH) and the inclined connector (C-IN) had similar overall compression responses. The tie connectors were consistently lower in capacity under tension and compression when compared to the other connectors. If the best connector is judged by the highest overall resistance in both tension and compression, the inclined connector performed the best due to the tensile failure modes governing over compression failure modes. However, the amount of shear resistance in a connector to be researched in future research work for composite behaviour is needed to decide whether a specific connector is better over another for an overall composite wall system. If the overall wall system is non-composite which requires only the lateral load transfer between wythes, then the axial behaviour of the inclined connector shows better performance than other connectors.

5.3 Recommendation for Future Work

The experimental program studied the response of a typical cavity wall system under tension and compression. This was the first investigation on these connectors with shear loading and thermal analysis later completed by Bello (2023). There are several recommendations for future work that are based on the outcomes of this thesis. Determining how much shear load is transferred within each connector transversely using the tension and compression peak loads and failure modes as limits that should not be exceeded. A more systematic approach in predicting capacities of different connector types can be taken in design as opposed to relying on the current connector design

capacity equation from A370:14 which is shown to be conservative for both tension and compression loading when compared to the experimental connector values.

Expressions that includes the contribution and possible failures of the embedment veneer tie in connectors is recommended to better predict the expected capacity. Current expressions only take into consideration the main body of the connector's cross-sectional dimensions and properties. Finite element modelling of the interaction with embedment veneer ties (micro modelling specifically) as well as more reliability analysis are potential options beyond further testing.

If more specimens were constructed, the novel inclined connector should be tested with different angles. These test results show that the governing axial failure mode is embedment tensile breakout failure so by increasing the angle, less connectors may be needed in the overall wall system. However, a balance is needed in setting a maximum angle as increasing angle increases effective length and may shift the failure mode to buckling. Determining the angle where this transition is expected would be the first step in determining optimal layouts of connectors in a full wall. However, connector shear response and capacities will also need to be considered for full wall systems.

Although insulation is expected to contribute to the wall system's compression resistance, it is difficult to quantify and C-IN-4 (the only specimen without insulation) had the lowest experimental peak load at 9.5kN. As insulation thicknesses increase due to code requirements, further research is required on whether the insulation contribution is negligible to compression peak loads to accurately predict expected compression peak load.

The results were too variable to provide conclusions on whether the veneer material type affected the compression response and the tension response. At times the concrete brick veneer had a higher axial resistance in identical specimens instead of the expected clay brick veneer having more resistance based on water absorption assumptions previously mentioned in Chapter 2. Due to mortar properties such as mortar strength affecting the governing tensile failure modes, the type of veneer material that is in contact with mortar and how it affects the mortar strength and/or mortar bond can be investigated along with contact strength. Investigating how the axial response changes by increasing or decreasing the mortar strength within the veneer masonry joints can also provide modifications to the existing breakout expressions by Arslan et al. (2021) and Hatzinikolas et al. (2021) which both rely on empirical relationships for mortar strength.

REFERENCES

Ahmadi, S.F., and Reisi, M. 2020. "Comparison of mechanical and durability properties of concrete and fired facing bricks". *Proceedings of the Institution of Civil Engineers - Structures and Buildings*. **173**(7): 512–522. doi:10.1680/jstbu.18.00144.

Alberta Masonry Council. 2023. Concrete Masonry Units. Available from https://albertamasonrycouncil.ca/masonry-types/concrete-masonry-units/. [accessed 6 April 2023].

Alecci, V., Fagone, M., Rotunno, T., and De Stefano, M. 2013. "Shear strength of brick masonry walls assembled with different types of mortar". *Construction and Building Materials*. **40**: 1038–1045. doi:https://doi.org/10.1016/j.conbuildmat.2012.11.107.

Amirzadeh, A., Strand, R.K., Hammann, R.E., and Bhandari, M.S. 2018. "Determination and Assessment of Optimum Internal Thermal Insulation for Masonry Walls in Historic Multifamily Buildings". *Journal of Architectural Engineering*. **24**(3). doi:10.1061/(asce)ae.1943-5568.0000320.

Arevalo, S. 2019. "Experimental Investigation of Thermal Bowing for Concrete Insulated Wall Panels". MSc. thesis, University of Alberta, Edmonton, Canada.

Arslan, O., Messali, F., Smyrou, E., Bal, E., and Rots, J.G. 2021. "Mechanical modelling of the axial behaviour of traditional masonry wall metal tie connections in cavity walls". *Construction and Building Materials*, **310**: 125205. Elsevier. doi:10.1016/J.CONBUILDMAT.2021.125205.

ASTM International. 2023. "ASTM C31/C31M-23 Standard Practise for Making and Curing Concrete Test Specimens in the Field." West Conshohocken, PA, USA

Bello, A.L.B. 2023. "Longitudinal Shear and Thermal Resistance of Novel and Conventional Ties in Cavity Walls". MSc. Thesis, University of Alberta, Edmonton, Canada.

Bennett, B. 2016. "Global Impacts Of CCMPA and CMDCS National Research Investments". Available from https://ccmpa.ca/wp-content/uploads/2016/05/GLOBAL-IMPACTS-OF-CCMPA-AND-CMDCS-NATIONAL-RESEARCH-INVESTMENTS.pdf. [accessed 6 April 2023].

Brick Industry Association. 2003. Tech Notes 44B - Wall Ties for Brick Masonry. Reston, VA, USA

Brown, R.H., and Elling, R.E. 1979. “Lateral Load Distribution in Cavity Walls”. Fifth International Brick Masonry Conference. Washington, D.C., USA, pp. 351–359.

Buildex Tapcon. 2013. Tapcon Performance Tables. Available from https://www.tapcon.com/getattachment/828aae2c-7c49-4a52-869d-9e2c618c152a/charts_performancetables_maxiset_v0-0_cp. [accessed 8 April 2023].

Burrows, J., and Canada Mortgage and Housing Corporation. 2013. Canadian Wood-Frame House Construction. In 2005.

Bush, T.D., and Stine, G.L. 1994. “Flexural Behavior of Composite Precast Concrete Sandwich Panels With Continuous Truss Connectors”. *PCI Journal*, **39**(2): 112–121.

Canadian Concrete Masonry Producers Association. 2013. Thermal properties & design Details.

Carstens, S., and Pahn, M. 2022. “Durability of GFRP connectors under sustained compression load for use in sandwich walls”. *Acta Polytechnica CTU Proceedings*, **33**: 58–62. doi:10.14311/APP.2022.33.0058.

CCMP. 2013. Metric Technical Manual. Thermal properties & design details.

Choi, Y.-H., and LaFave, J.M. 2004. “Performance of Corrugated Metal Ties for Brick Veneer Wall Systems”. *Journal of Materials in Civil Engineering*, **16**(3): 202–211.

Classic Rock Face Block. 2021. History of Rock Face Block. Available from https://classicrockfaceblock.com/news/history-of-rock-face-block/. [accessed 8 April 2023].

Cruz-Noguez, C. 2020. Masonry Centre Newsletter. Available from https://www.masonrycentre.ca/app/uploads/Masonry-Centre-Spring-2020-Newsletter-3.pdf. [accessed 6 April 2023].

CSA (Canadian Standards Association). 2019. “CSA A23.2:19 Test methods and standard practises for concrete.” Mississauga, ON, Canada.

CSA (Canadian Standards Association). 2014. “CSA A82:14 Fired Masonry Brick made from clay or shale.” Mississauga, ON, Canada.

CSA (Canadian Standards Association). 2014. “CSA A165 SERIES-14 CSA Standards on concrete masonry units.” Mississauga, ON, Canada.

CSA (Canadian Standards Association). 2014b. “CSA A370:14 Connectors for Masonry.” Mississauga, ON, Canada.

CSA (Canadian Standards Association). 2013. “CSA G40.20-13/G40.21-13 General requirements for rolled or welded structural quality steel / Structural quality steel.” Mississauga, ON, Canada.

CSA (Canadian Standards Association). 2014a. “CSA S304-14 Design of masonry structures.” Mississauga, ON, Canada

Dias, Y., Mahendran, M., and Poologanathan, K. 2019. “Full-scale fire resistance tests of steel and plasterboard sheathed web-stiffened stud walls”. *Thin-Walled Structures*, **137**: 81–93. doi:10.1016/j.tws.2018.12.027.

Drysdale, R., Hamid, A., and Baker, L. 2005. Masonry Structures Behavior and Design. In First. Canadian Masonry Design Centre.

Du, E., Shu, G., Qin, L., Lai, B., Zhou, X., and Zhou, G. 2022. “Experimental investigation on fire resistance of sandwich composite walls with truss connectors”. *Journal of Constructional Steel Research*, **188**: 107052. doi:10.1016/j.jcsr.2021.107052.

Dunlop, C. 2014. Brick Houses - Solid Masonry vs. Brick Veneer. Available from https://www.carsondunlop.com/inspection/blog/brick-houses-solid-masonry-vs-brick-veneer/. [accessed 6 April 2023].

Einea, A., Salmon, D.C., Tadros, M.K., and Culp, T. 1994. “A New Structurally and Thermally Efficient Precast Sandwich Panel System”. *PCI Journal*, **39**(4): 90–101.

FERO Corporation. 2014. Stud Shear Connector Technical Notes. Edmonton.

Gołaszewska, M., Gołaszewski, J., Cygan, G., and Bochen, J. 2020. “Assessment of the Impact of Inaccuracy and Variability of Material and Selected Technological Factors on Physical and Mechanical Properties of Fresh Masonry Mortars and Plasters”. Materials (Basel, Switzerland), **13**(6). doi:10.3390/ma13061382.

Goudarzi, N. 2016. “Effect of Z-shaped Steel Plate Connectors on Out-of-Plane Flexural Behaviour of Precast Insulated Concrete Panels”.PhD. thesis, University of Alberta, Edmonton, Canada.

Hatzinikolas, M., Korany, Y., and Brzev, S. 2005. Masonry Design for Engineers and Architects. In 4th edition. Canadian Masonry Publications, Edmonton.

Hatzinikolas, M., Longworth, J., and Warwaruk, J. 1979. “Strength and behaviour of metal ties in 2-wythe masonry walls”. : 1455–1466.

Hibbeler, R.C. 2011. Mechanics of Materials. In 8th edition. Edited by M. Horton and C. McDonald. Prentice Hall.

International Masonry Institute. 2008. Shelf Angle Detail.

Ismaiel, M., Chen, Y., Cruz-Noguez, C., and Hagel, M. 2022. "Thermal resistance of masonry walls: a literature review on influence factors, evaluation, and improvement". *Journal of Building Physics*, **45**(4): 528–567. doi:10.1177/17442591211009549.

Izquierdo, K., Mohsenijam, A., and Cruz-Noguez, C. 2023. "Model trees and stepwise regressions for accurate in-plane shear strength predictions of partially grouted masonry walls". *Canadian Journal of Civil Engineering*, **50**(6): 475–487. doi:10.1139/cjce-2022-0162.

Laird, D.A., Drysdale, R.G., Stubbs, D.W., and Sturgeon, G.R. 2005. "The New CSA S304.1-04 "Design of Masonry Structures." *10th Canadian Masonry Symposium*. Banff, AB, Canada, pp. 1-10.

Lawson, R.M., Way, A.G.J., Heywood, M., Lim, J.B.P., Johnston, R., and Roy, K. 2020. "Stability of light steel walls in compression with plasterboards on one or both sides". *Proceedings of the Institution of Civil Engineers - Structures and Buildings*, **173**(6): 394–412. doi:10.1680/jstbu.18.00118.

Lourenço, P., Milani, G., Tralli, A., and Zucchini, A. 2007. "Analysis of masonry structures: review of and recent trends in homogenization techniques". *Canadian Journal of Civil Engineering*, **34**(11).

Lourenço, P.B. 2002. "Computations on historic masonry structures". *Progress in Structural Engineering and Materials*, **4**(3): 301–319. doi:https://doi.org/10.1002/pse.120.

Mariscal, R.D.J.G. 2022. "Study of a Slender Masonry Wall Tested in an Innovative Device". MSc. thesis, University of Alberta, Edmonton, Canada.

McGinley, W.M., and Hamoush, S. 2008. "Seismic Masonry Veneer: Quazi-Static Testing of Wood Stud Backed Clay Masonry Veneer Walls". In Structures Congress 2008. American Society of Civil Engineers, Reston, VA. pp. 1–10.

Metwally, Z., Zeng, B., and Li, Y. 2022. "Probabilistic Behavior and Variance-Based Sensitivity Analysis of Reinforced Concrete Masonry Walls Considering Slenderness Effect". *ASCE-ASME Journal of Risk and Uncertainty in Engineering Systems, Part A: Civil Engineering*, **8**(4). doi:10.1061/AJRUA6.0001273.

Muhit, I.B., Stewart, M.G., and Masia, M.J. 2022. “Probabilistic constitutive law for masonry veneer wall ties”. *Australian Journal of Structural Engineering*, **23**(2): 97–118. doi:10.1080/13287982.2021.2021628.

Naito, C., John, H., Beacraft, M., and Bewick, B. 2012. “Performance and Characterization of Shear Ties for Use in Insulated Precast Concrete Sandwich Wall Panels”. *Journal of Structural Engineering*, **138**(1): 52–61.

Natural Resources of Canada. 2020. Energy Fact Book 2020-2021. In 2020-10-06.

O’Hegarty, R., West, R., Aidan, R., and Oliver, K. 2019. “Composite behaviour of fibre-reinforced concrete sandwich panels with FRP shear connectors”. *Engineering Structures*, **198**.

Pessiki, S., and Mlynarczyk, A. 2003. “Experimental Evaluation of the Composite Behavior of Precast Concrete Sandwich Wall Panels”. *PCI Journal*, **48**(2): 54–71.

Razvi, S., and Saatcioglu, M. 1994. “Strength and deformability of confined high-strength concrete columns”. *ACI Structural Journal*, **91**: 678–687.

Reneckis, D., LaFave, J., and Clarke, W.M. 2004. “Out-of-plane performance of brick veneer walls on wood frame construction”. *Engineering Structures*, **26**(8): 1027–1042.

Roppel, P., Lawton, M., and Norris, N. 2012. “Thermal Performance of Building Envelope Details for mid-and high-rise buildings”. *ASHRAE Transactions*, **118**(2): 569–584.

Satko, J. 2007. History of Insulation with Masonry. Illinois.

Shrive, N.G., and Sturgeon, G. 2001. Masonry Education in Canadian Post-Secondary Institutions. In 9th Canadian Masonry Symposium. Fredericton.

Altair (2021), S-FRAME (2022.0)[Computer software]. https://altair.com/s-frame

Tobriner, S. 1984. “A History of Reinforced Masonry Construction Design to Resist Earthquakes”, 1755 - 1907. *Earthquake Spectra*, **1**(1): 125–149.

Tomlinson, D. 2015. “Behaviour Of Partially Composite Precast Concrete Sandwich Panels Under Flexural And Axial Loads”. PhD. thesis, Queen’s University, Kingston, ON, Canada.

Zhang, F., Liu, X., Ge, F.-W., and Cui, C. 2023. “Investigation on the Ductility Capacity of Concrete Columns with High Strength Steel Reinforcement under Eccentric Loading”. *Materials* (Basel, Switzerland), **16**(12). doi:10.3390/ma16124389

Zimmermann, T., and Strauss, A. 2011. Variation of Shear Strength of Masonry with Different Mortar Properties. In Eleventh *North American Masonry Conference*. Minneapolis, MN, USA, pp. 1-14.

APPENDIX A: AUXILLIARY TESTING

The grout properties were determined by cylinder testing similar to how concrete cylinders are tested. Grout cylinder samples were taken at various stages during the wall specimen construction. All cylinders except cylinder 1 and 2 were end grinded. End grinding is a cylinder preparation procedure done before testing to create a uniform bearing testing surface. End grinding is recommended by both CSA A23.2:19 (CSA Group, 2019) and ASTM C31(ASTM, 2023) testing standards.

Table A.1: Grout cylinder testing results

Grout cylinder ID	Peak load, kN	Peak stress, MPa	Failure mode
1*	220.6	28.1	--
2*	220.4	28.1	Shear failure
3	244.1	31.1	Shear failure
4	218.1	27.8	Cone and shear failure
5	193.1	24.6	Cone and split failure
6	211.0	26.9	Cone and shear failure
7	245.3	31.2	Shear failure
Mean Values	221.8	28.3	--
Standard Deviation	18.3	2.3	
CoV	0.08	0.08	

* Not end grinded

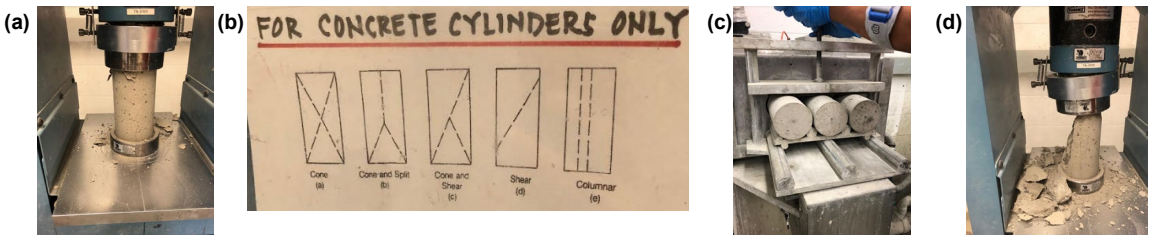

Figure A.1: Auxiliary grout cylinder testing (a) setup, (b) possible cylinder failure modes, (c) cylinder end grinding, (d) cylinder shear failure

The mortar properties were determined by mortar cube testing using CSA A23.2:19 (CSA Group, 2019). Mortar cube samples were taken at various stages during the wall specimen construction. Every mortar cube sample except 3,5 and 7 did not have a void.

Table A.2: Mortar cube testing results

Mortar Cube ID	Peak load, kN	Peak stress, MPa
1	54.4	21.8
2	57.1	22.9
3*	33.3	13.3
4	52.0	20.8
5*	53.8	21.5
6	37.0	14.8
7*	28.1	11.3
8	25.8	10.3
9	37.6	15.1
Mean Values	42.1	16.9
Standard Deviation	12.2	4.90
CoV	0.29	0.29

* Void was present in sample

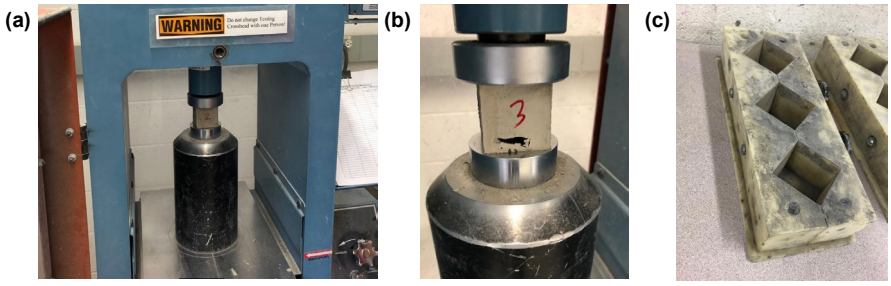

Figure A.2: Auxiliary mortar cube testing (a) setup, (b) close up view of mortar cube, (c) mortar cube container

The concrete masonry unit properties were determined by standard CMU prism testing as per the CSA S304-14 standard (CSA Group, 2014a). The closest representation to this thesis's experimental specimens is the 2 course ungrouted specimens however 2 course grouted specimens and a single block's prism's results were also recorded. The testing was done by Mahmoud Elsayed, Alan Alonzo and Rafael Gonzalez.

Table A.3: Concrete masonry unit testing results

Prism ID	Peak stress for 2 course ungrouted, MPa	Peak stress for 2 course grouted, Mpa	Peak stress for one block, MPa
1	16.6	18.2	22.6
2	18.2	21.5	21.1
3	15.7	17.7	24.8
4	16.1	16.5	27.3
5	19.0	18.4	24.7
Mean Value	17.1	18.5	24.1
Standard Deviation	1.42	1.85	2.36
CoV	0.08	0.10	0.10

Figure A.3: Auxiliary concrete masonry unit specimen testing of (a) two course ungrouted, (b) two course grouted, (c) one block from Elsayed, Alonzo and Gonzalez experimental work

The connector's steel properties were tested by Benedict Egbon. He determined that the steel for the embedded tie and connector(both plate and inclined) had a yield strength of 569±8.52 and 234±5.53 MPa respectively. The steel rebar had a yield strength of 429±2.45 MPa and the elastic modulus of the tie and connector were 197±6.6 GPa and 194±9.4 GPa respectively.

APPENDIX B – LOADING RATES

The individual loading rates are calculated from 25% of the peak load up to the peak load except for T-Z.CN-3 which is calculated from 40% of the peak load due to the T-Z.CN-3 data measuring a recording beyond 25% at zero displacement.

Table B.1: Loading rates for tension specimens of tie connectors

Connector ID	Loading Rate mm/min	Connector ID	Loading Rate mm/min
T-Z.CL-1	3.74	T-R.CL-1	0.93
T-Z.CL-2	1.57	T-R.CL-2	1.72
T-Z.CL-3	1.95	T-R.CL-3	1.29
T-Z.CN-1	2.87	T-R.CN-1	0.91
T-Z.CN-2	2.07	T-R.CN-2	2.46
T-Z.CN-3	0.84*	T-R.CN-3	2.23

load rate calculated from 40% of the peak load

Table B.2: Loading rates for tension specimens of plated connectors

Connector ID	Loading Rate mm/min	Connector ID	Loading Rate mm/min	Connector ID	Loading Rate mm/min
T-PV.CL-1	4.01	T-PH.CL-1	4.49	T-IN.CL-1	8.79
T-PV.CL-2	6.35	T-PH.CL-2	12.8	T-IN.CL-2	8.46
T-PV.CL-3	1.78	T-PH.CL-3	4.21	T-IN.CL-3	8.37
T-PV.CN-1	2.89	T-PH.CN-1	18.3	T-IN.CL-4	11.2
T-PV.CN-2	3.78	T-PH.CN-2	11.2	T-IN.CL-5	13.0
T-PV.CN-3	4.71	T-PH.CN-3	8.97	T-IN.CN-2	8.54
				T-IN.CN-3	7.68

Table B.3: Loading rates for compression specimens of tie connectors

Connector ID	Loading Rate mm/min	Connector ID	Loading Rate mm/min
C-Z.CL-1	1.87	C-R.CL-1	10.5
C-Z.CL-2	2.60	C-R.CL-2	12.8
C-Z.CL-3	9.51	C-R.CL-3	7.69
C-Z.CN-1	4.00	C-R.CN-1	7.30
C-Z.CN-2	3.02	C-R.CN-2	11.6
C-Z.CN-3	2.18	C-R.CN-3	3.42

Table B.4: Loading rates for compression specimens of plated connectors

Connector ID	Loading Rate mm/min	Connector ID	Loading Rate mm/min	Connector ID	Loading Rate mm/min
C-PV.CL-1	2.78	C-PH.CL-1	2.48	C-IN.CL-1	2.09
C-PV.CL-2	1.86	C-PH.CL-2	4.58	C-IN.CL-2	4.67
C-PV.CL-3	1.51	C-PH.CL-3	4.93	C-IN.CL-3	4.99
C-PV.CN-1	1.61	C-PH.CN-1	3.12	C-IN.CN-1	0.45
C-PV.CN-2	2.22	C-PH.CN-2	1.27	C-IN.CN-2	3.55
C-PV.CN-3	0.60	C-PH.CN-3	2.22	C-IN.CN-3	0.88
				C-IN.CN-4*	1.83

only compression specimen with no insulation in between wythes

APPENDIX C – SPECIMEN PHOTOS

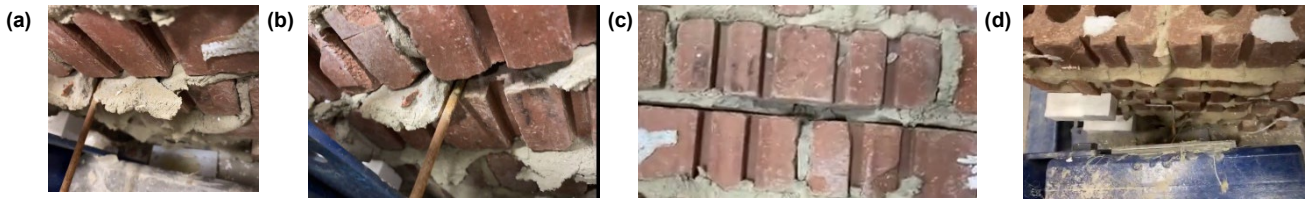

Figure C.1: T-Z.CL-1 after testing (a) top view, (b) alternative top view, (c) mortar joint condition, (d) elevated view of specimen

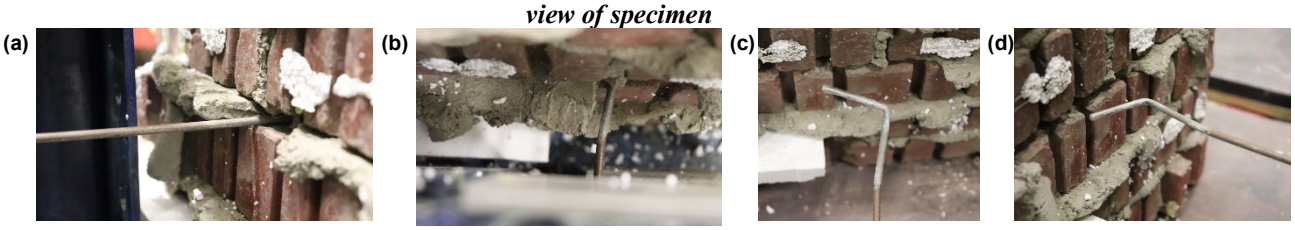

Figure C.2: T-Z.CL-2 after testing (a) side view, (b) top view, (c) bent Z-tie view, (d) bent Z-tie alternative view

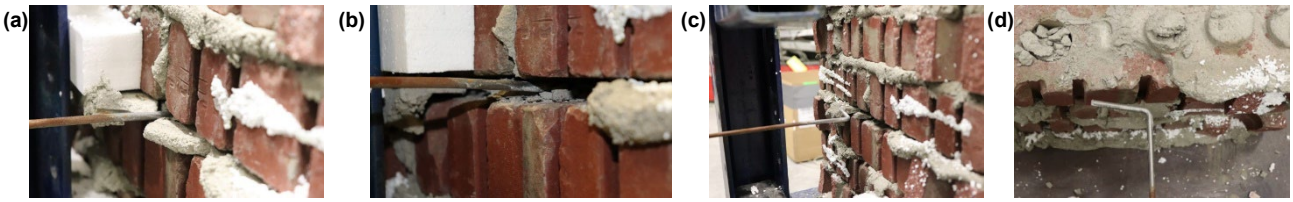

Figure C.3: T-Z.CL-3 after testing (a) side view, (b) side view with left mortar joint intact, (c) side view during removal of connector from veneer, (d) top view during removal of connector from veneer

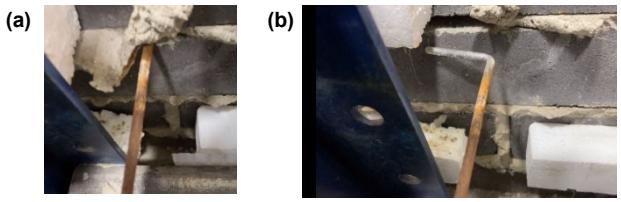

Figure C.4: T-Z.CN-1 after testing (a) top view, (b) top view of removal of connector from veneer

Figure C.5: T-Z.CN-2 after testing (a) connector brick interface, (b) alternative view of connector brick interface, (c) removal of connector from veneer

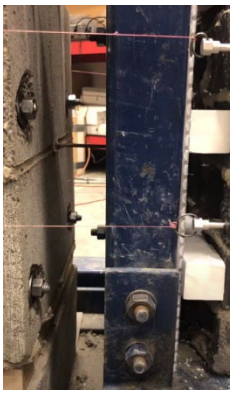

Figure C.6: T-Z.CN-3 specimen view

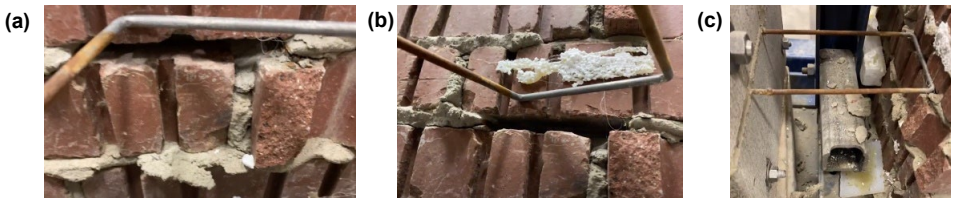

Figure C.7: T-R.CL-1 after testing of (a) embedment failure, (b) horizontal mortar joint pull-out after connector removal, (c) top view after connector removal

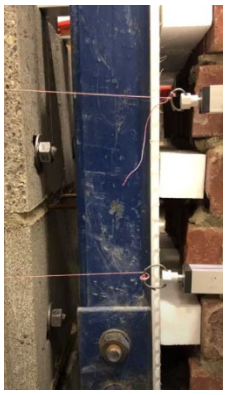

Figure C.8: T-R.CL-2 specimen side view

Figure C.9: T-R.CN-1 after testing of (a) embedment failure, (b) top view of embedment failure, (c) top view after connector removal

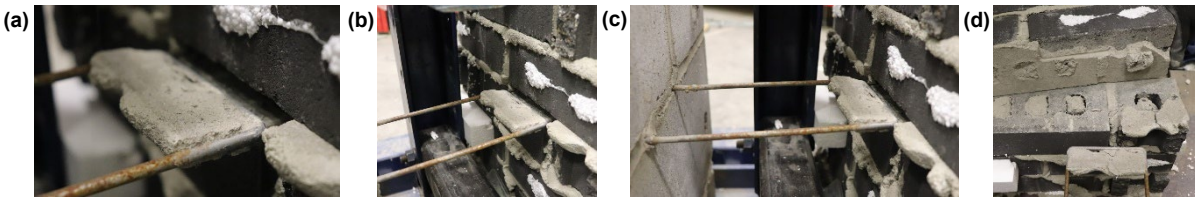

Figure C.10: T-R.CN-3 after testing of (a) embedment failure, (b) zoomed out view of embedment failure, (c) side view of embedment failure, (d) horizontal mortar joint condition after connector removal

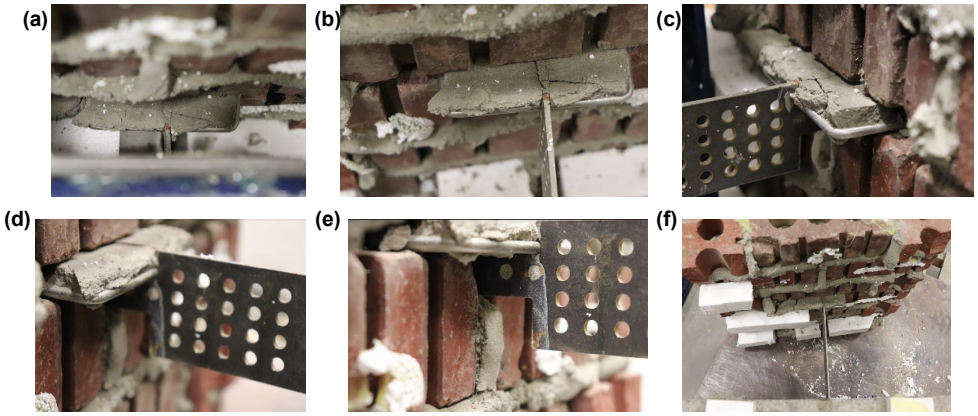

Figure C.11: T-PV.CL-1 after testing of (a) top view of embedment failure, (b) alternative view of embedment failure, (c) side view, (d) alternative side view, (e) lower connector portion view, (f) top view

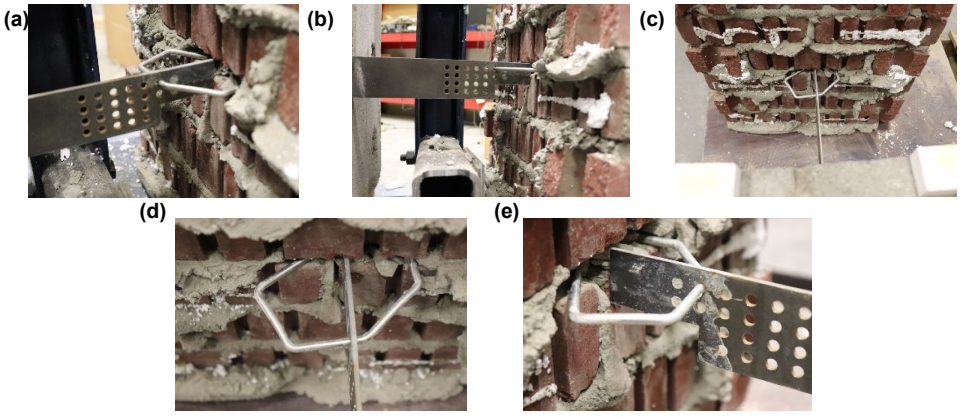

Figure C.12: T-PV.CL-2 after testing of (a) embedment tie yielding, (b) side view, (c) top view, (d) top view close up of connector, (e) alternative side view of embedment tie yielding

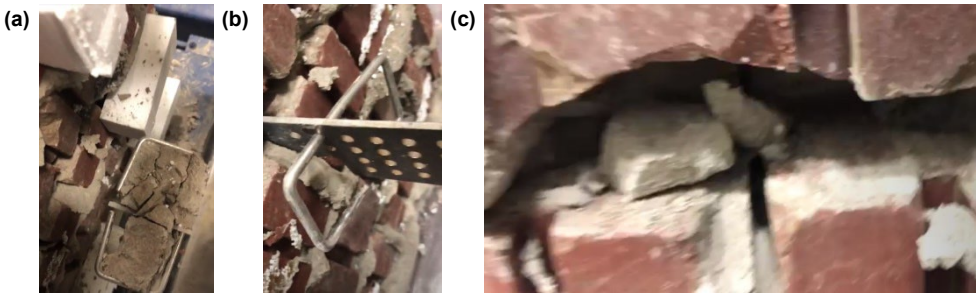

Figure C.13: T-PV.CL-3 after testing of (a) embedment tie veneer failure, (b) tie connector condition, (c) horizontal mortar joint condition after removal of connector

Figure C.14: T-PV.CN-1 connector condition after testing and veneer removal

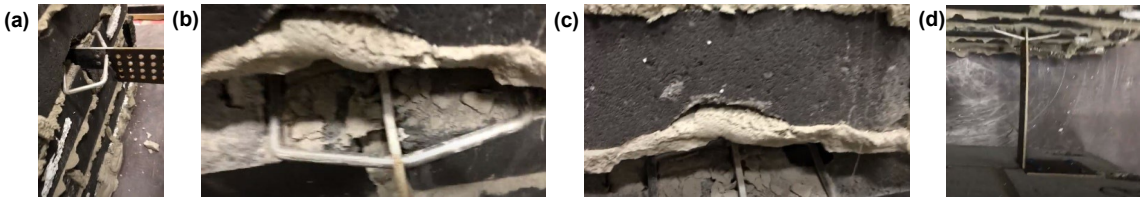

Figure C.15: T-PV.CN-2 after testing of (a) embedment tie failure, (b) horizontal mortar joint condition, (c) alternative view of mortar joint condition, (d) top view

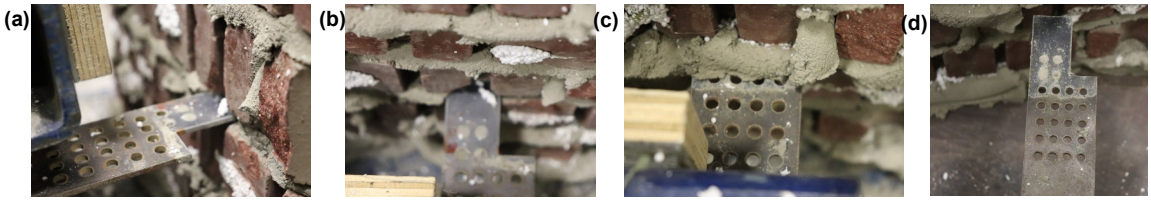

Figure C.16: T-PH.CL-1 after testing of (a) elevated side view, (b) top view, (c) alternative top view, (d) top view after connector removal from veneer

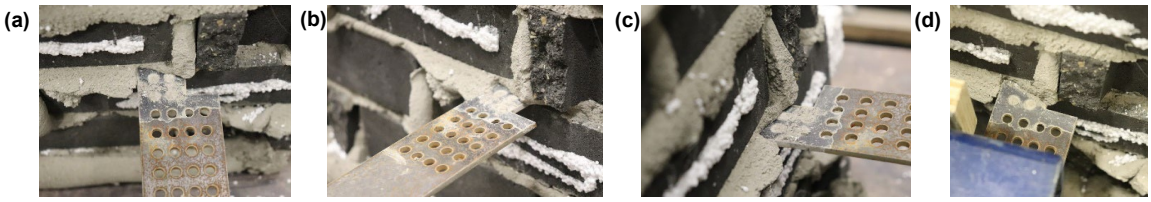

Figure C.17: T-PH.CN-1 after testing of (a) top view, (b) elevated side view, (c) alternative elevated side view, (d) top view

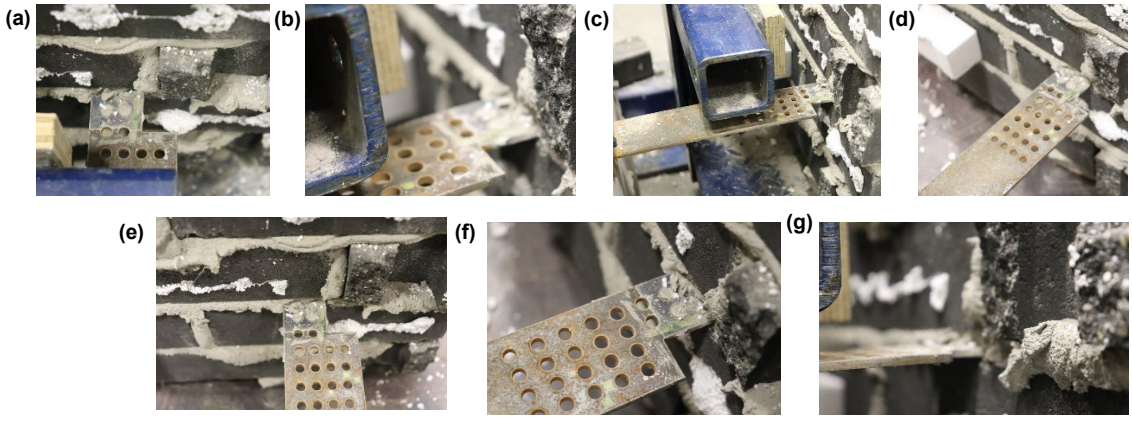

Figure C.18: T-PH.CN-2 after testing of (a) top view, (b) elevated side view, (c) zoomed out elevated side view, (d) zoomed out alternative elevated side view, (e)top view, (f)alternative elevated side view, (g) side view

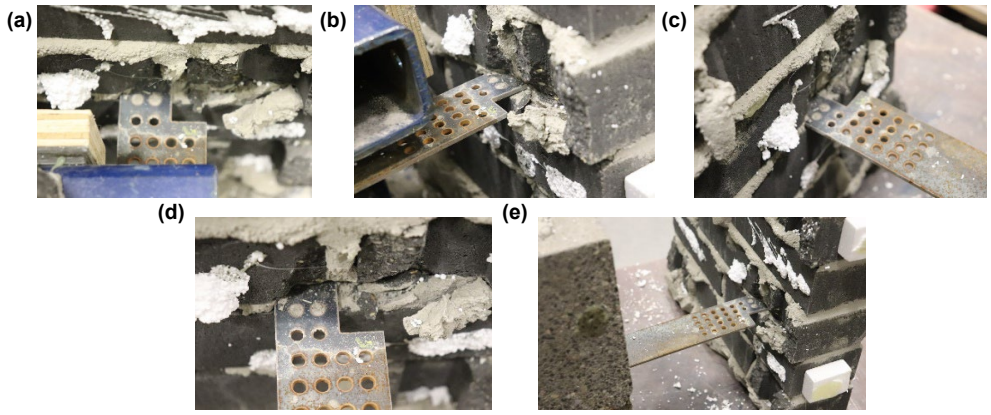

Figure C.19: T-PH.CN-3 after testing of (a) top view, (b) elevated side view, (c) alternative elevated side view, (d) connector condition after testing, (e)zoomed out view of elevated side view

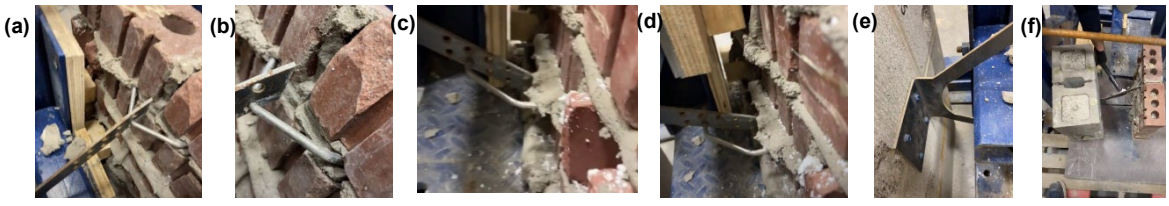

Figure C.20: T-IN.CL-1 after testing of (a) top embedment tie yielding, (b) zoomed in view of top embedment tie, (c) bottom embedment tie yielding, (d) alternative view of bottom embedment tie, (e)inclined connector CMU interface, (f) top view of inclined connector after frame removal

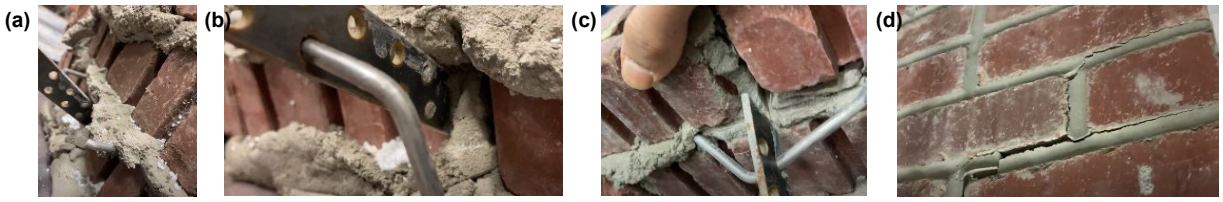

Figure C.21: T-IN.CL-4 after testing of (a) bottom embedment tie yielding, (b) bottom embedment tie condition after removal from veneer, (c) top embedment tie yielding, (d) mortar joint condition at outside face of clay brick veneer

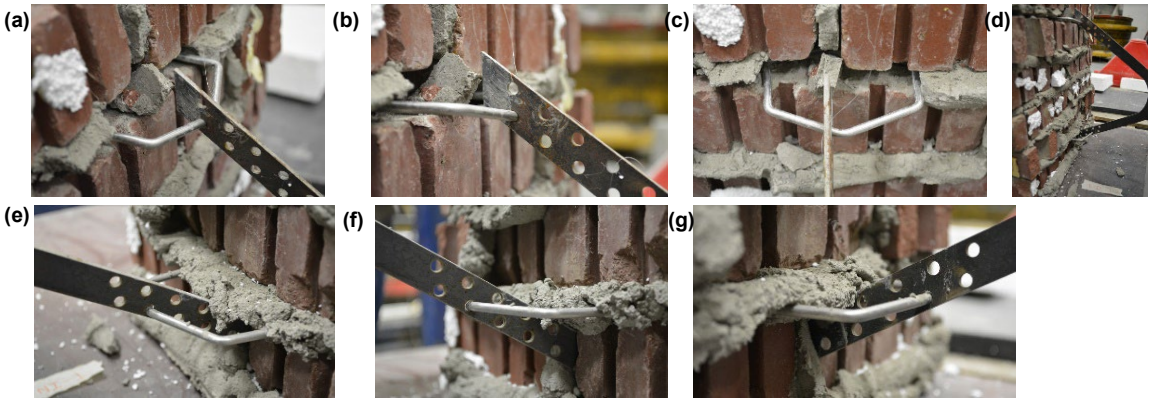

Figure C.22: T-IN.CL-2 after testing of (a) side view of top embedment tie yielding, (b) alternative side view of top embedment tie yielding, (c) top view of embedment tie, (d)inclined connector after testing, (e) bottom embedment tie, (f) alternative view of bottom embedment tie, (g) alternative view 2 of bottom embedment tie

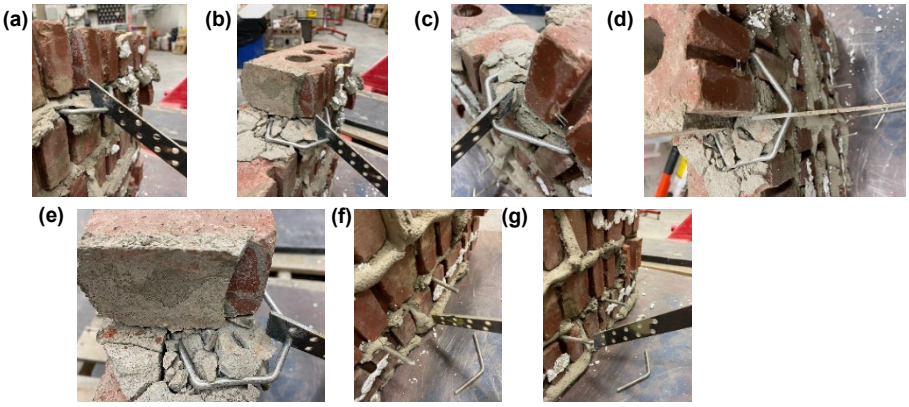

Figure C.23: T-IN.CL-3 after testing of (a) top embedment veneer tie yielding, (b) top embedment veneer tie condition, (c) alternative view of top embedment veneer tie condition, (d) top view of top embedment tie, (e)alternative top view of top embedment tie, (f) bottom embedment tie condition, (g) alternative view of bottom embedment tie condition

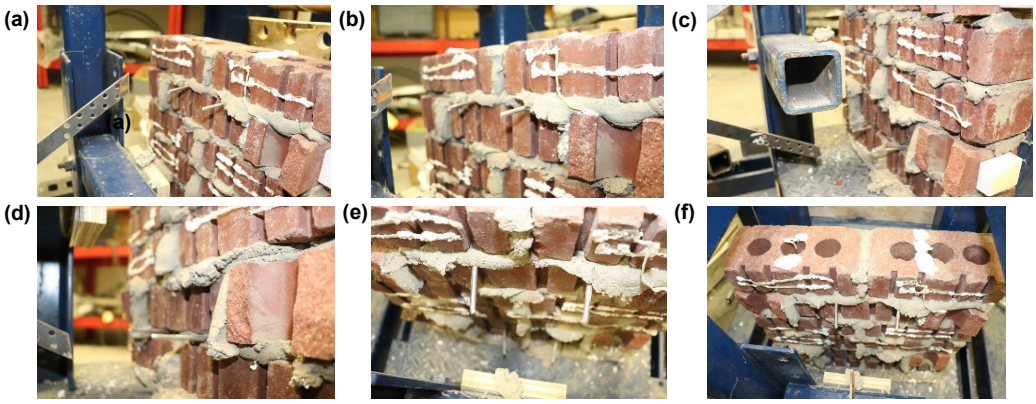

Figure C.24: T-IN.CL-5 after testing of (a) side view of top embedment veneer tie yielding, (b) alternative side view of embedment tie yielding, (c) side view of bottom embedment veneer tie yielding, (d) alternative side view of bottom embedment tie yielding, (e)top view of top and bottom embedment ties after testing, (f) alternative top view of yielded top and bottom embedment ties

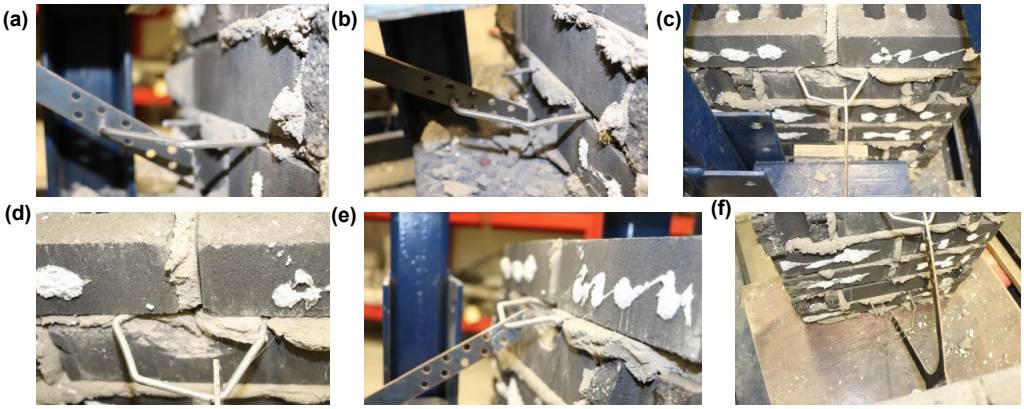

Figure C.25: T-IN.CN-2 after testing of (a) side view of bottom embedment veneer tie yielding, (b) alternative side view of bottom embedment veneer tie yielding, (c) top view of connector condition after testing, (d) top embedment veneer tie yielding, (e) zoomed in view of top embedment veneer tie yielding, (f) side view of top embedment veneer tie yielding

Figure C.26: T-IN.CN-3 after testing of (a) top embedment veneer tie yielding, (b) alternative top view of top embedment veneer tie yielding, (c) connector CMU interface condition

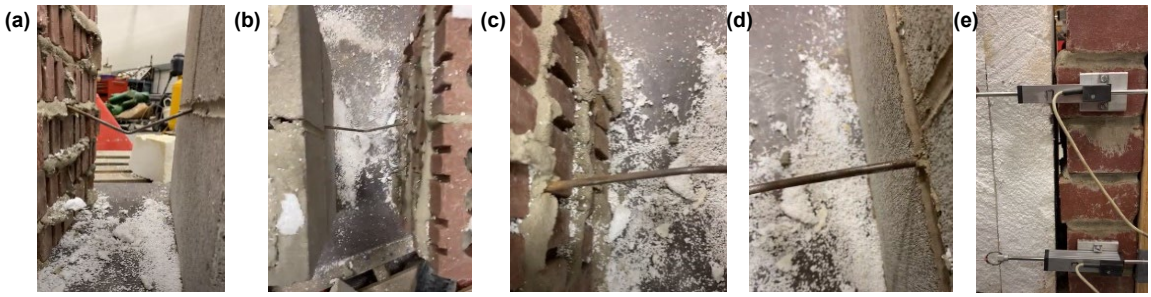

Figure C.27: C-Z.CL-1 after testing of (a) side view, (b) top view, (c)connector brick veneer interface, (d) connector CMU interface, (e) specimen view during testing

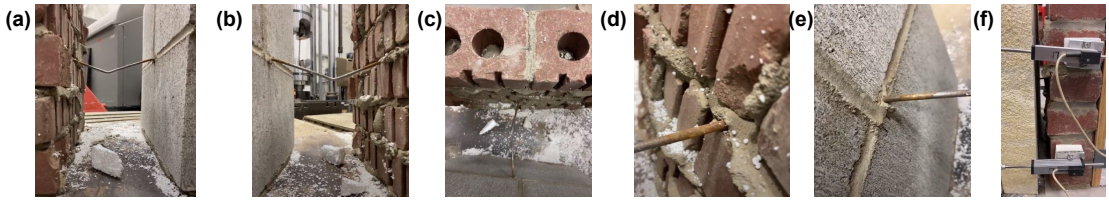

Figure C.28: C-Z.CL-2 after testing of (a) side view, (b) alternative side view, (c) top view, (d)connector brick veneer interface, (e) connector CMU interface, (f) specimen view during testing

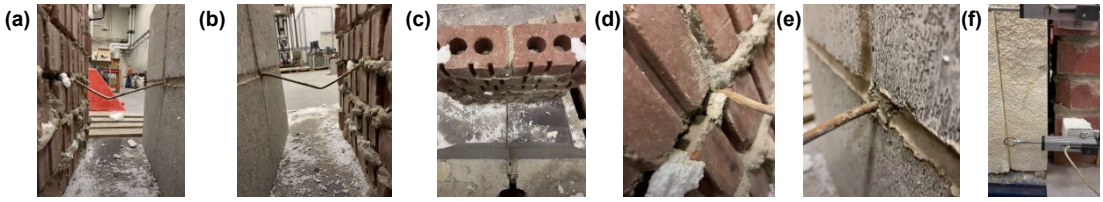

Figure C.29: C-Z.CL-3 after testing of (a) side view, (b) alternative side view, (c) top view, (d) connector brick veneer interface, (e) connector CMU interface, (f) specimen view during testing

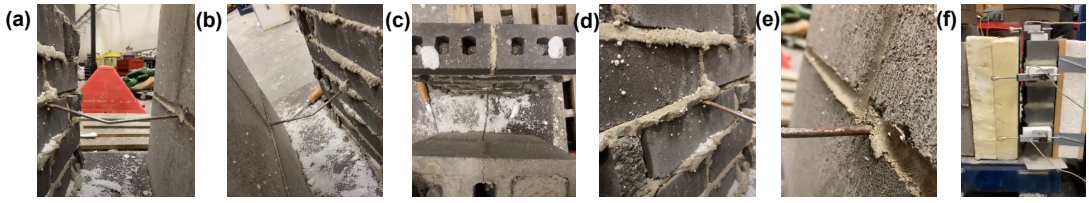

Figure C.30: C-Z.CN-1 after testing of (a) side view, (b) alternative side view, (c) top view, (d) connector brick veneer interface, (e) connector CMU interface, (f) specimen view during testing

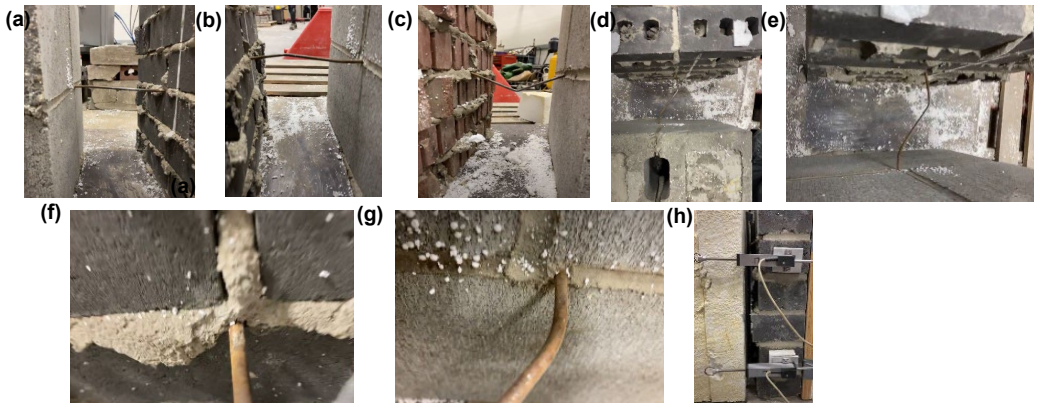

Figure C.31: C-Z.CN-2 after testing of (a) side view, (b) alternative side view, (c) alternative side view 2, (d) top view, (e) alternative top view, (f) connector brick veneer interface, (g) connector CMU interface, (h) specimen view during testing

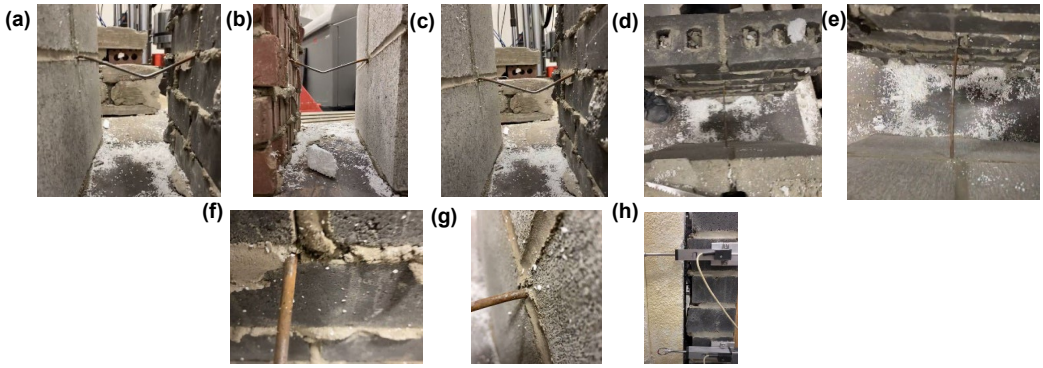

Figure C.32: C-Z.CN-3 after testing of (a) side view, (b) alternative side view, (c) alternative side view 2, (d) top view, (e) alternative top view, (f) connector brick veneer interface, (g) connector CMU interface, (h) specimen view during testing

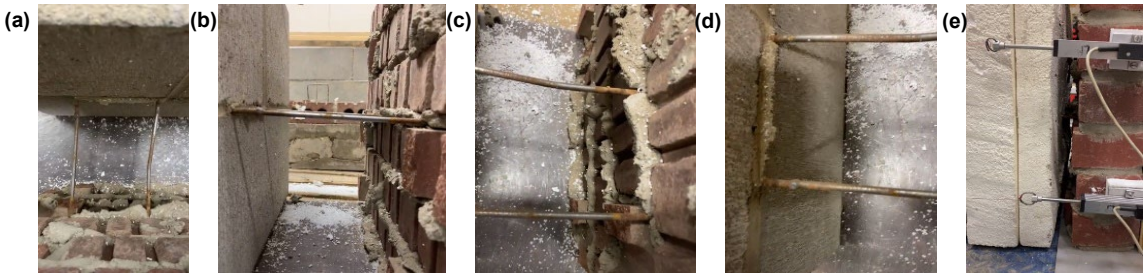

Figure C.33: C-R.CL-1 after testing of (a) top view, (b) side view, (c) connector brick veneer interface, (d) connector CMU interface, (e) specimen view during testing

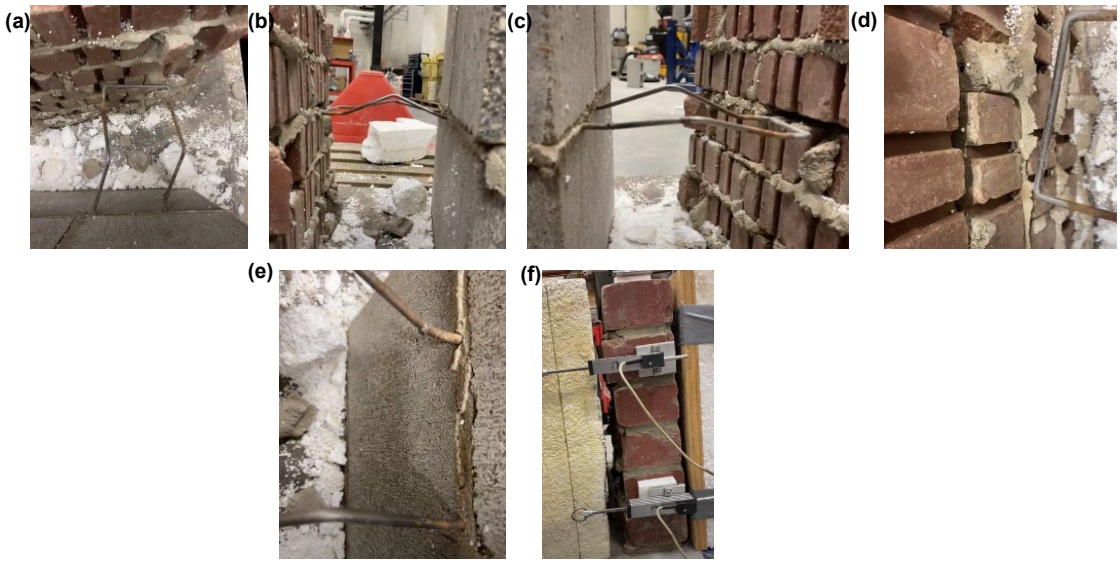

Figure C.34: C-R.CL-2 after testing, (a) top view, (b) side view, (c) alternative side view, (d) connector brick veneer interface, (e) connector CMU interface, (f) specimen view during testing

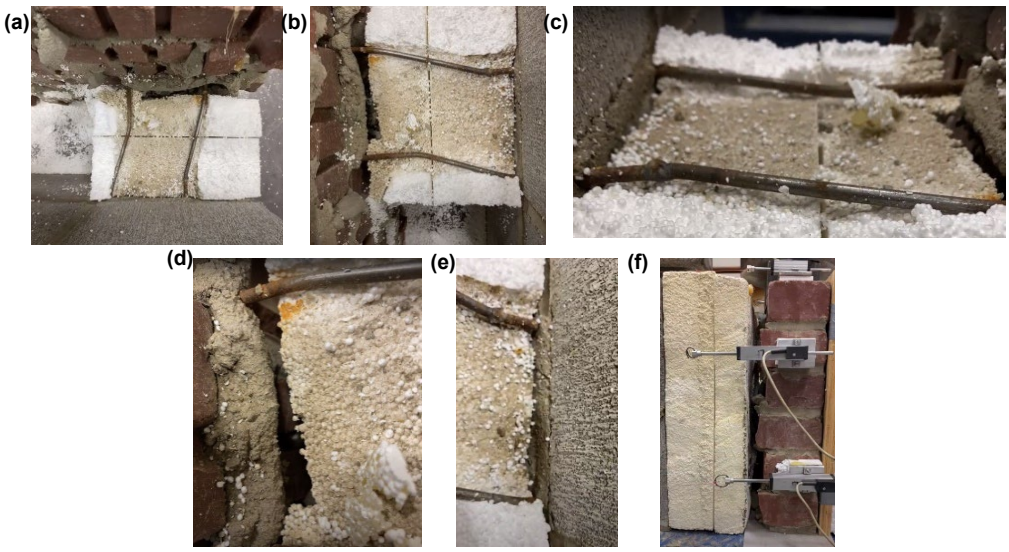

Figure C.35: C-R.CL-3 after testing of (a) top view, (b) alternative top view, (c) side view, (d) connector brick veneer interface, (e) connector CMU interface, (f) specimen view during testing

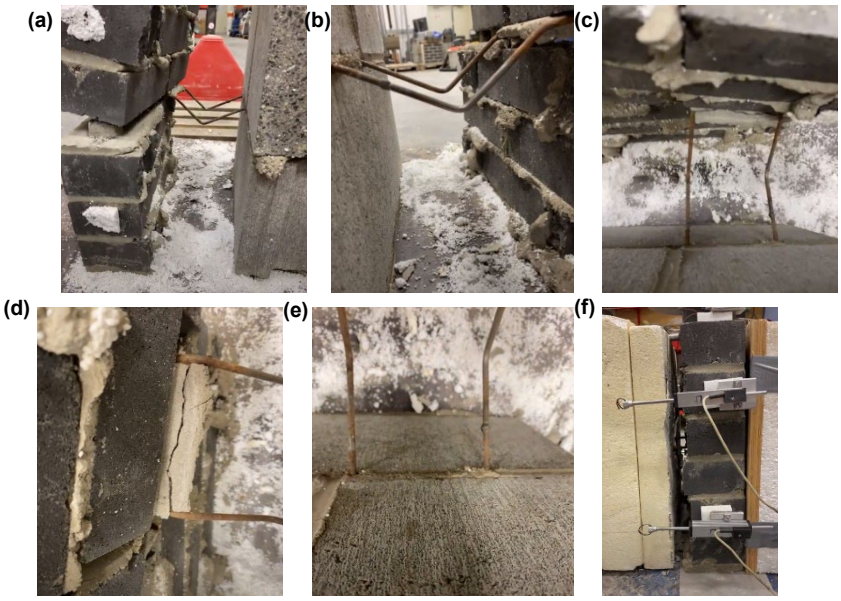

Figure C.36: C-R.CN-1 after testing of (a) side view with brick veneer manually lifted, (b) alternative side view, (c) top view, (d) connector brick interface, (e) connector CMU interface, (f) specimen view during testing

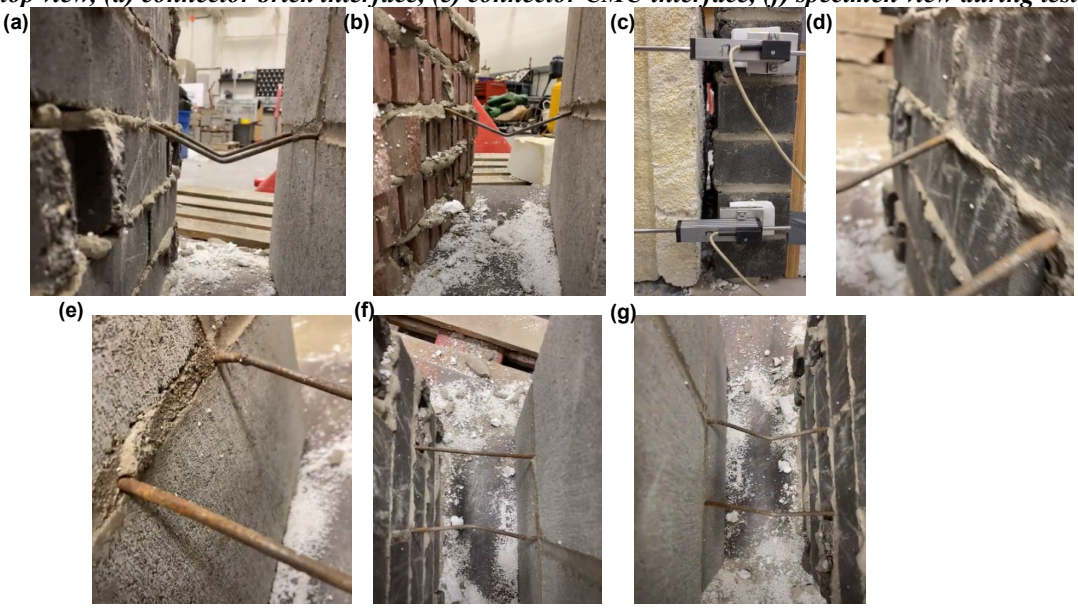

Figure C.37: C-R.CN-2 after testing of (a) side view, (b) alternative side view, (c) specimen view during testing, (d) connector brick interface, (e) connector CMU interface, (f) top view, (g) alternative top view

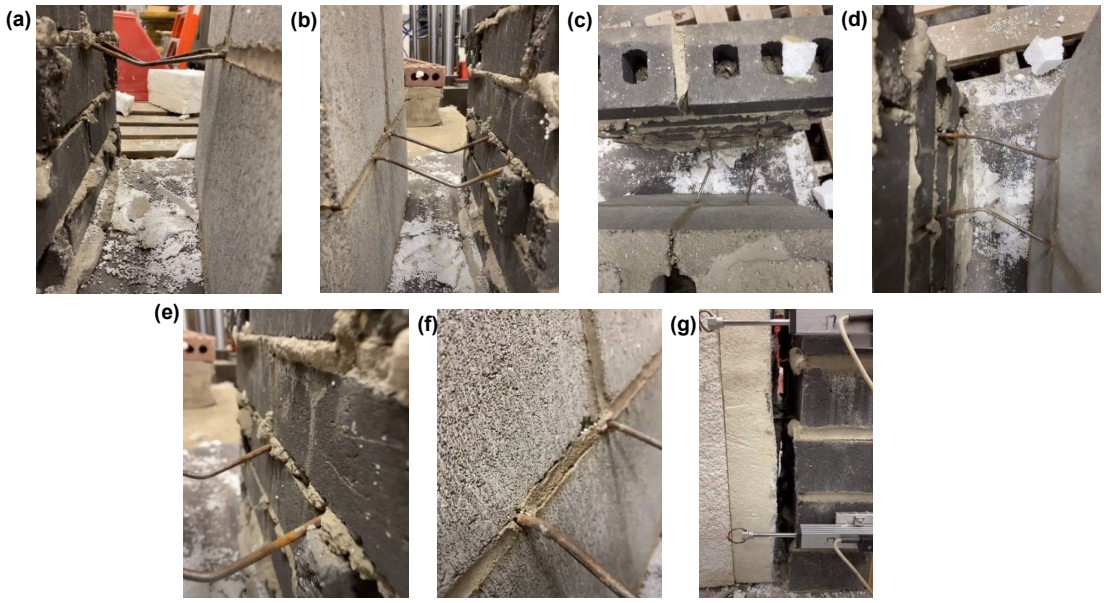

Figure C.38: C-R.CN-3 after testing of (a) side view, (b) alternative side view, (c) top view, (d) alternative top view, (e) connector brick interface, (f) connector CMU interface, (g) specimen view during testing

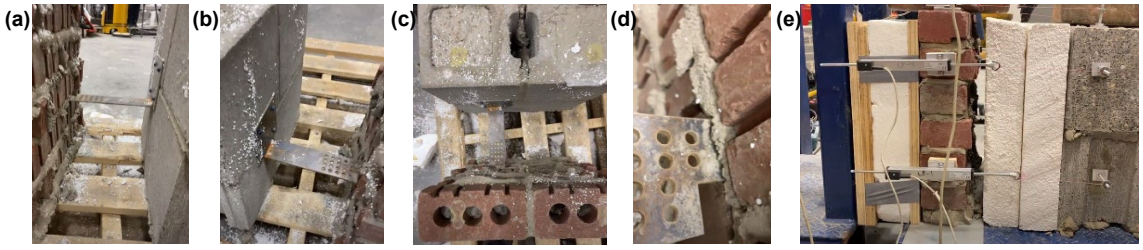

Figure C.39: C-PH.CL-1 after testing of (a) side view, (b) alternative side view, (c) top view, (d) clay brick veneer mortar joint condition, (e) specimen view during testing

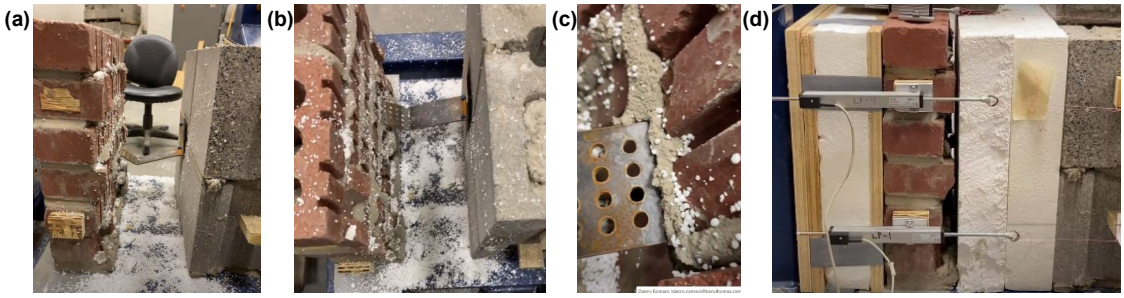

Figure C.40: C-PH.CL-2 after testing of (a) side view, (b) top view, (c) clay brick veneer mortar joint condition, (d) specimen view during testing

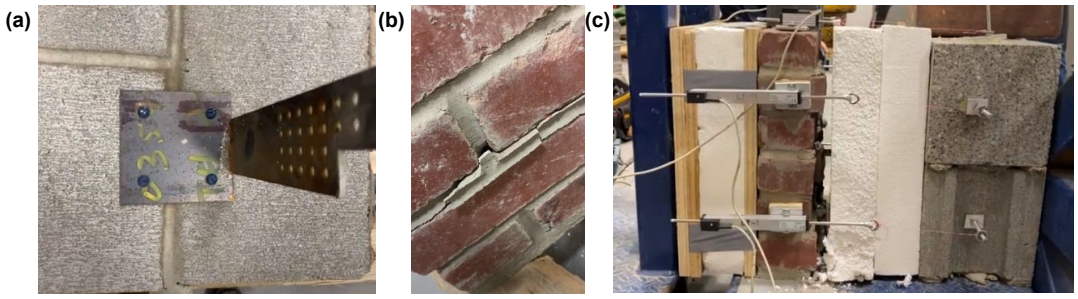

Figure C.41: C-PH.CL-3 after testing of (a) CMU connector interface condition, (b) horizontal mortar joint condition, (c) specimen view during testing

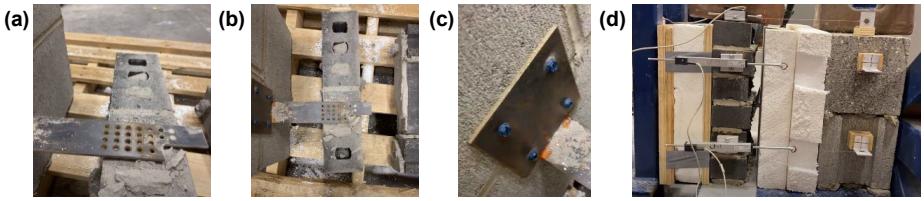

Figure C.42: C-PH.CN-1 after testing of (a) side view, (b) top view, (c) CMU connector interface, (d) specimen view during testing

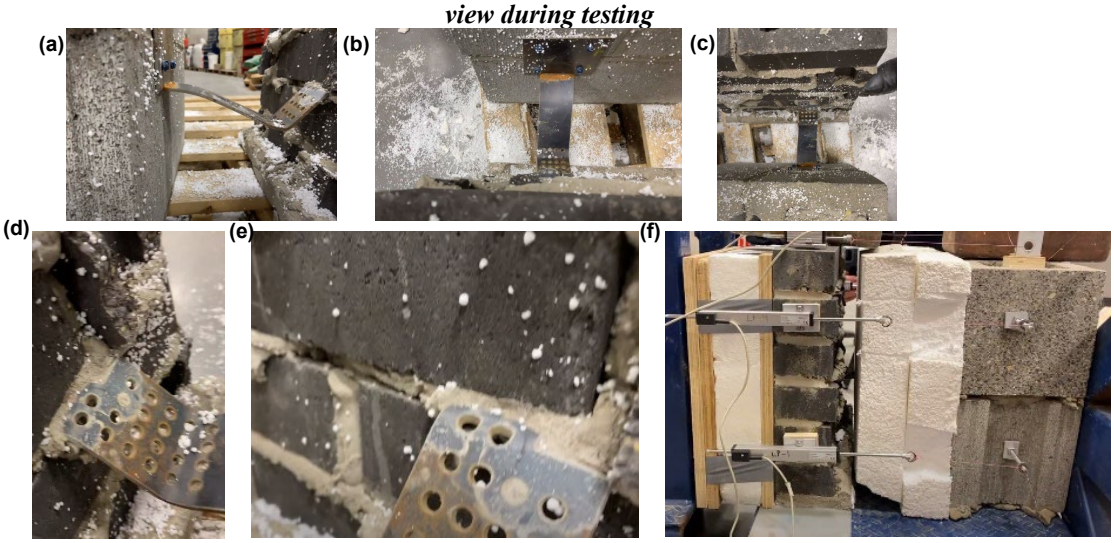

Figure C.43: C-PH.CN-2 after testing of (a) side view, (b) top view, (c) alternative top view, (d) clay brick veneer connector interface, (e) horizontal mortar joint condition, (f) specimen view during testing

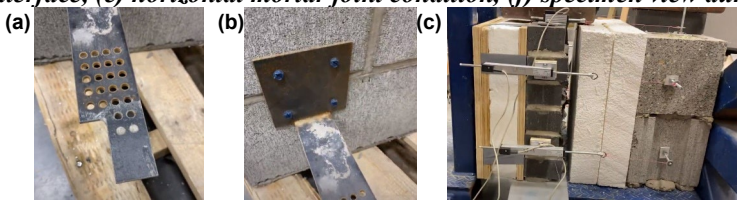

Figure C.44: C-PH.CN-3 after testing of (a) connector condition, (b) CMU connector interface, (c) specimen view during testing

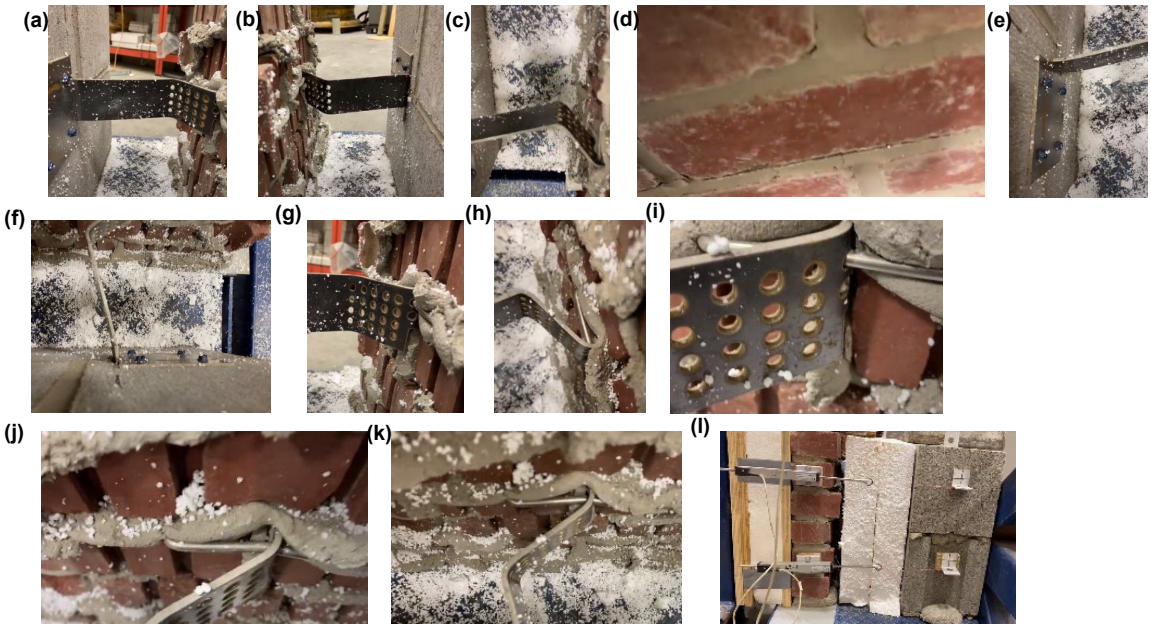

Figure C.45: C-PV.CL-1 after testing of (a) side view, (b) alternative side view, (c) top view, (d) brick veneer outside face condition, (e) CMU connector Tapcon fastener interface view, (f) CMU connector Tapcon fastener interface view 2, (g) veneer connector interface view, (h) veneer connector interface view 2, (i) mortar joint condition view 1, (j) mortar joint condition view 2, (k) mortar joint condition view 3, (l) specimen view during testing

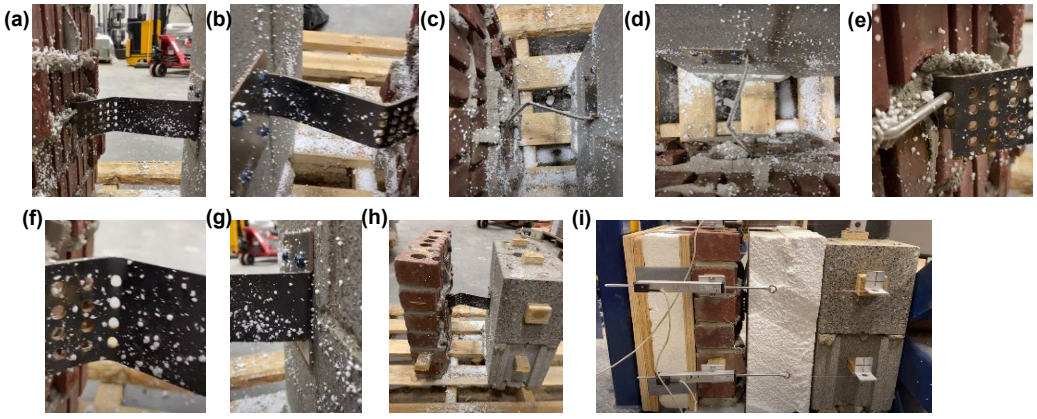

Figure C.46: C-PV.CL-2 after testing of (a) side view, (b) alternative side view, (c) top view, (d) alternative top view, (e) brick veneer connector interface, (f) connector condition, (g) CMU connector Tapcon fastener condition, (h) specimen view after frame removal, (i) specimen view during testing

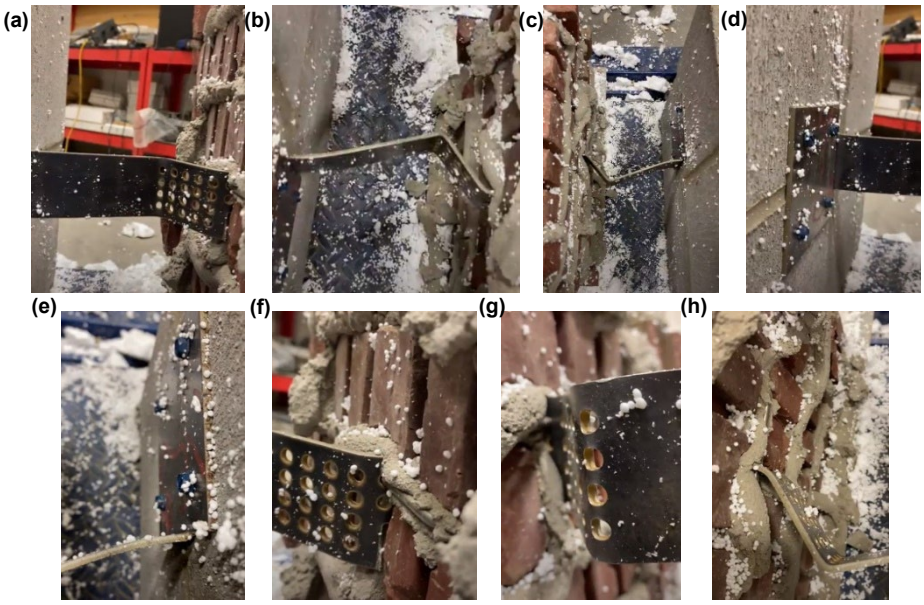

Figure C.47: C-PV.CL-3 after testing of (a) side view, (b) top view, (c) alternative top view, (d) CMU connector Tapcon fastener interface, (e) alternative view of CMU connector Tapcon fastener interface, (f) clay brick veneer connector interface, (g) brick veneer connector interface alternative view, (h) brick veneer connector interface alternative view 2

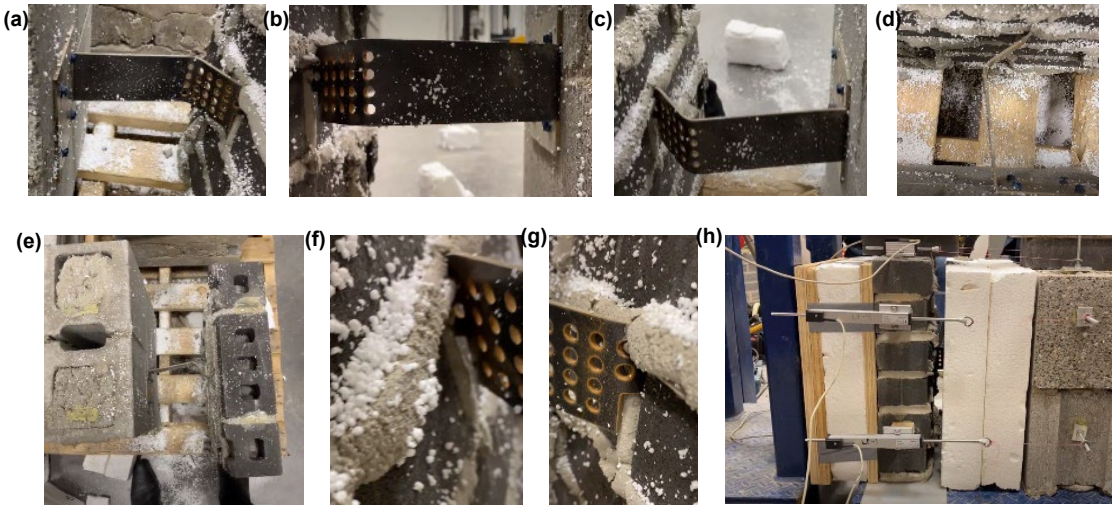

Figure C.48: C-PV.CN-1 after testing of (a) side view, (b) alternative side view, (c) alternative side view 2, (d) top view, (e) alternative top view, (f) concrete veneer connector interface, (g) concrete veneer connector interface view 2, (h) specimen during testing

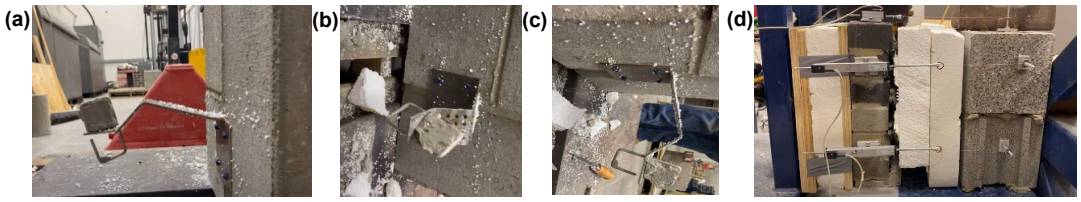

Figure C.49: C-PV.CN-2 after testing of (a) connector condition view, (b) connector condition alternative view 2, (c) connector condition alternative view 3, (d) specimen view during testing

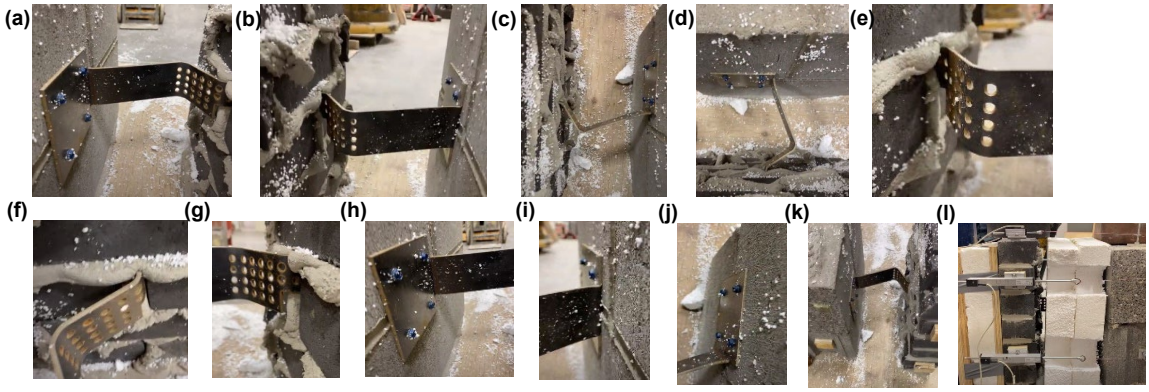

Figure C.50: C-PV.CN-3 after testing of (a) side view, (b) alternative side view, (c) top view, (d) alternative top view, (e) brick veneer connector interface, (f) brick veneer connector view 2, (g) brick veneer connector view 3, (h) CMU connector Tapcon fastener interface, (i) CMU connector view 2, (j) CMU connector view 3, (k) specimen after frame removal, (l) specimen view during testing

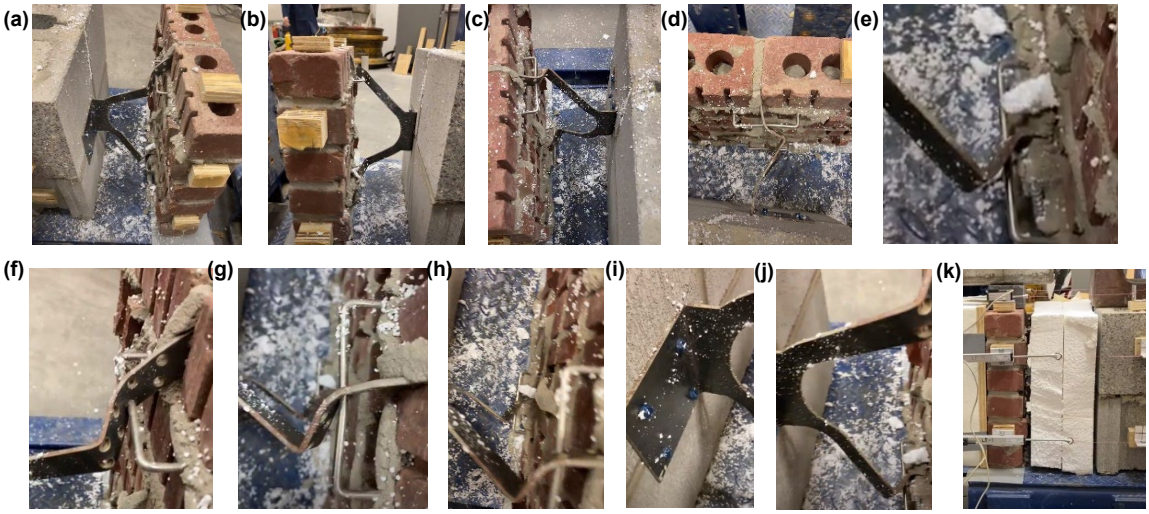

Figure C.51: C-INC.CL-1 after testing of (a) side view, (b) alternative side view, (c) elevated view, (d) top view, (e) bottom leg view, (f) top leg side view, (g) top leg top view, (h) both legs top view, (i) CMU connector Tapcon fastener interface, (j) connector mid location view, (k) specimen view during testing

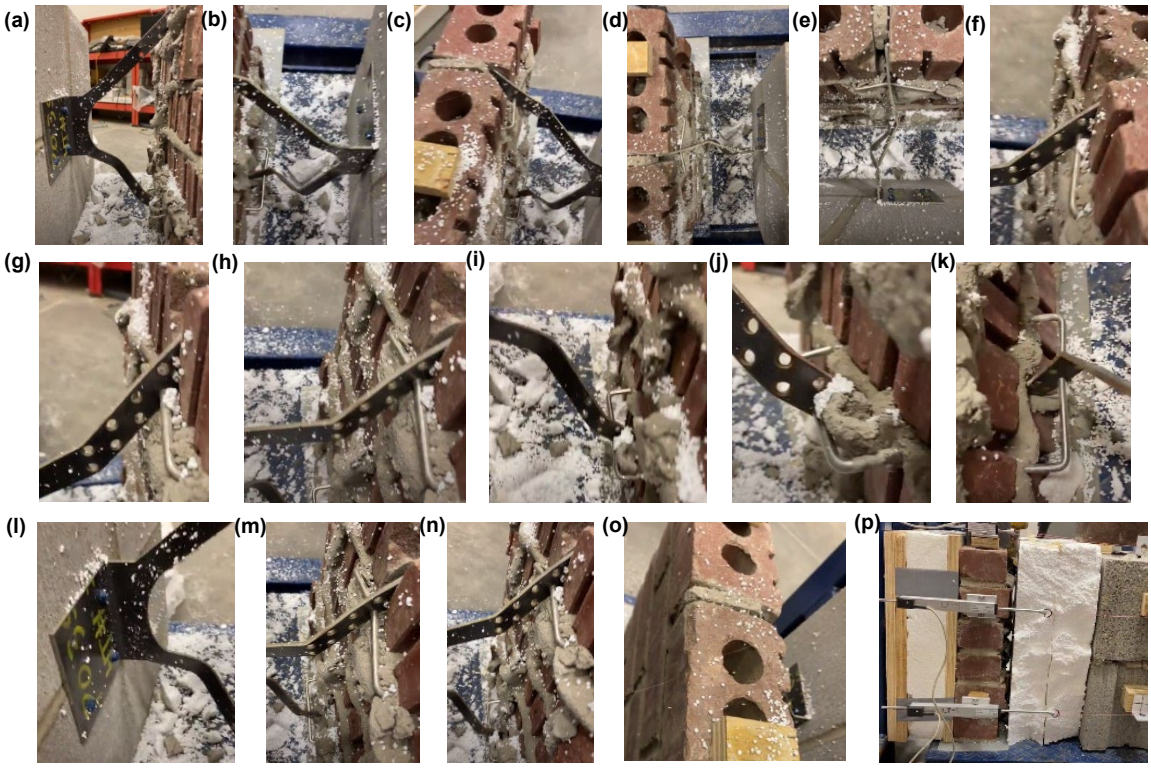

Figure C.52: C-INC.CL-2 after testing of (a) side view, (b) elevated side view, (c) alternative elevated side view, (d) top view, (e) alternative top view, (f) upper leg side view, (g) alternative upper leg side view, (h) upper connector side view, (i) lower leg side view, (j) alternative lower leg side view, (k) top view, (l) CMU connector interface view, (m) elevated connector view, (n) alternative elevated connector view, (o) upper vertical mortar joint condition, (p) specimen view during testing

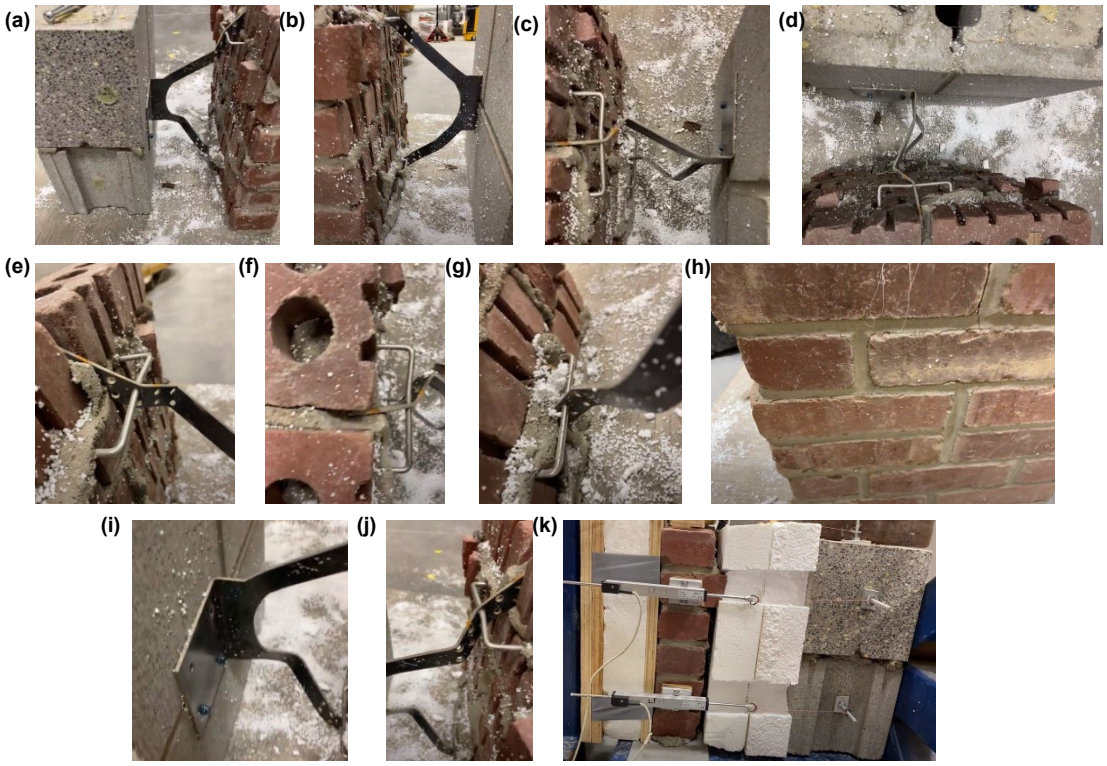

Figure C.53: C-INC.CL-3 after testing of (a) side view, (b) alternative side view, (c) top view, (d) alternative top view, (e) upper leg view, (f) upper leg top view, (g) bottom leg view, (h) mortar joint condition at brick veneer outside face, (i) CMU connector interface, (j) connector leg view, (k) specimen view during testing

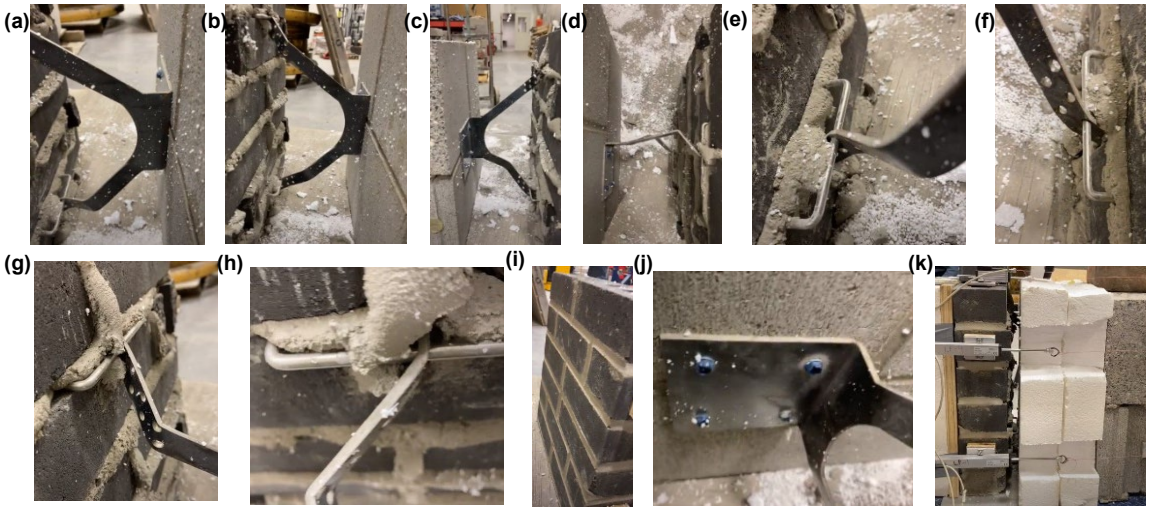

Figure C.54: C-IN.CN-1 after testing of (a) side view, (b) alternative side view, (c) alternative side view 2, (d) top view, (e) bottom leg view, (f) bottom leg view 2, (g) top leg view, (h) top leg view 2, (i) mortar joint condition at brick veneer outside face, (j) CMU connector Tapcon fastener interface, (k) specimen view during testing

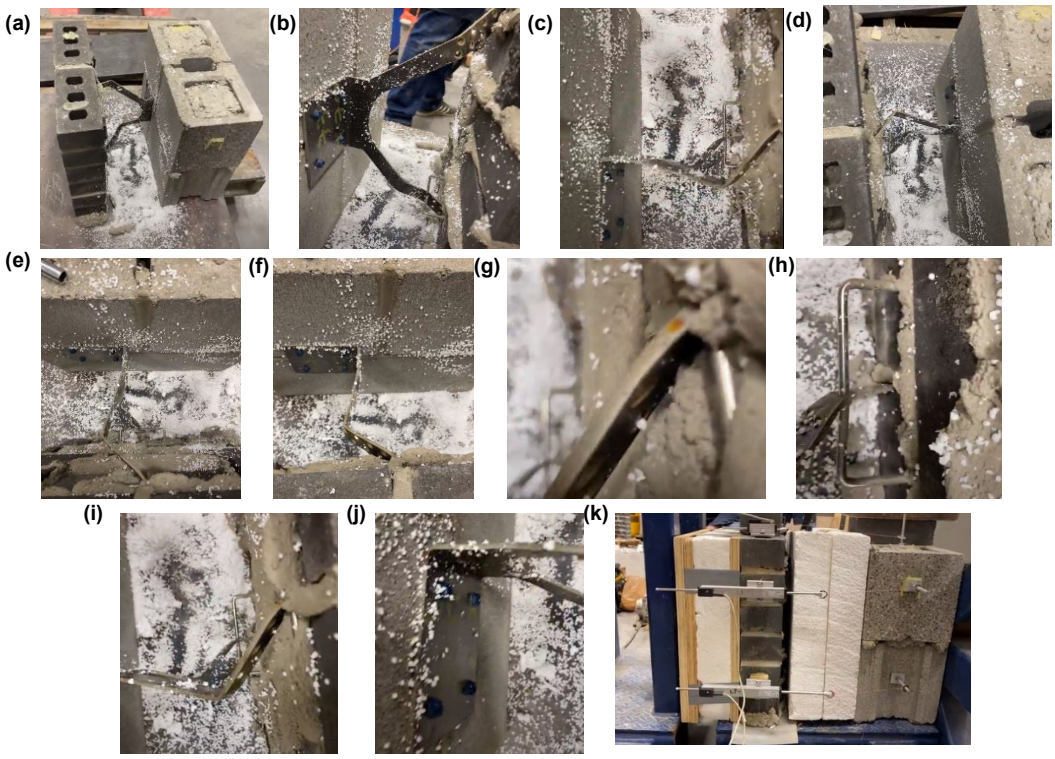

Figure C.55: C-IN.CN-2 after testing of (a) side view, (b) alternative side view, (c) top view, (d) top view 2, (e) top view 3, (f) top view 4, (g) top connector leg view, (h) bottom connector leg view, (i) top view with both legs, (j) CMU connector Tapcon fastener interface, (k) specimen view during testing

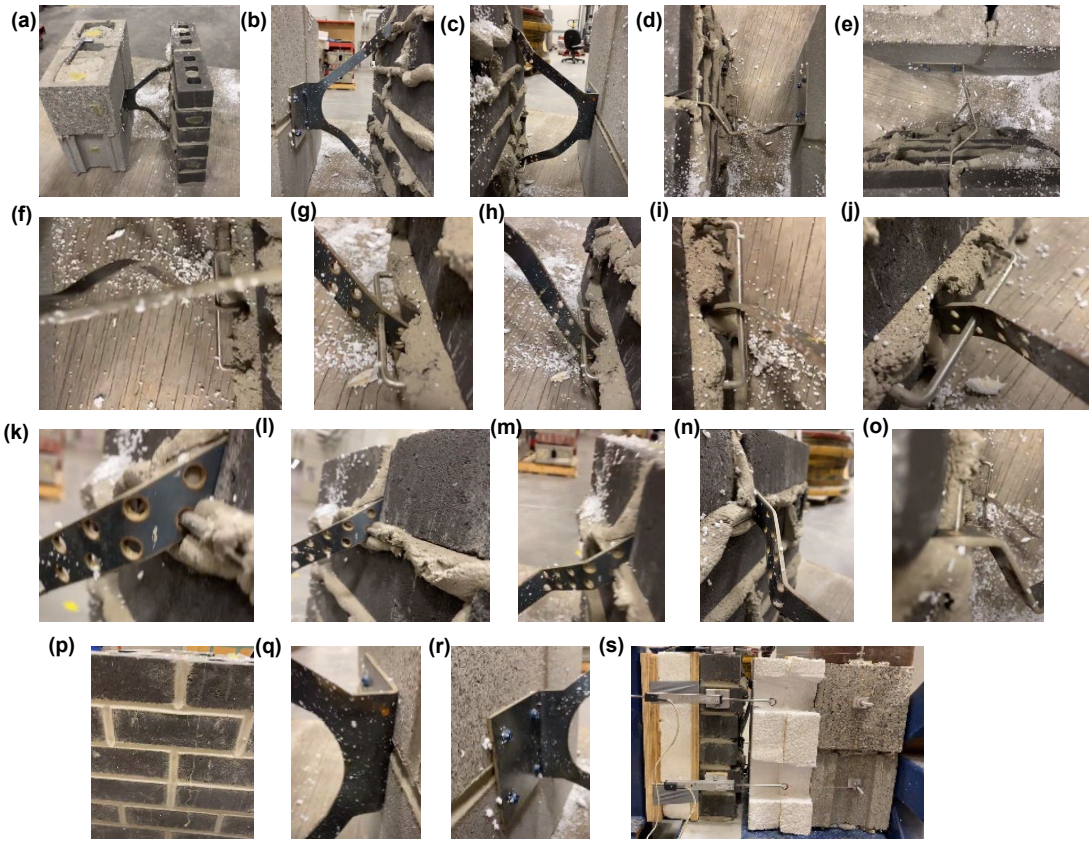

Figure C.56: C-IN.CN-3 after testing of (a) side view, (b) side view 2, (c) side view 3, (d) top view, (e) top view 2, (f) top view with bottom connector leg focus, (g) bottom connector leg side view, (h) bottom connector leg side view 2, (i) bottom connector leg top view, (j) bottom connector leg top view 2, (k) top connector leg side view, (l) top connector leg side view 2, (m) top connector leg side view 3, (n) top connector leg side view 4, (o) top connector leg top view, (p) outside face of brick veneer condition, (q) CMU connector interface view, (r) CMU connector Tapcon fastener interface view 2, (s) specimen view during testing

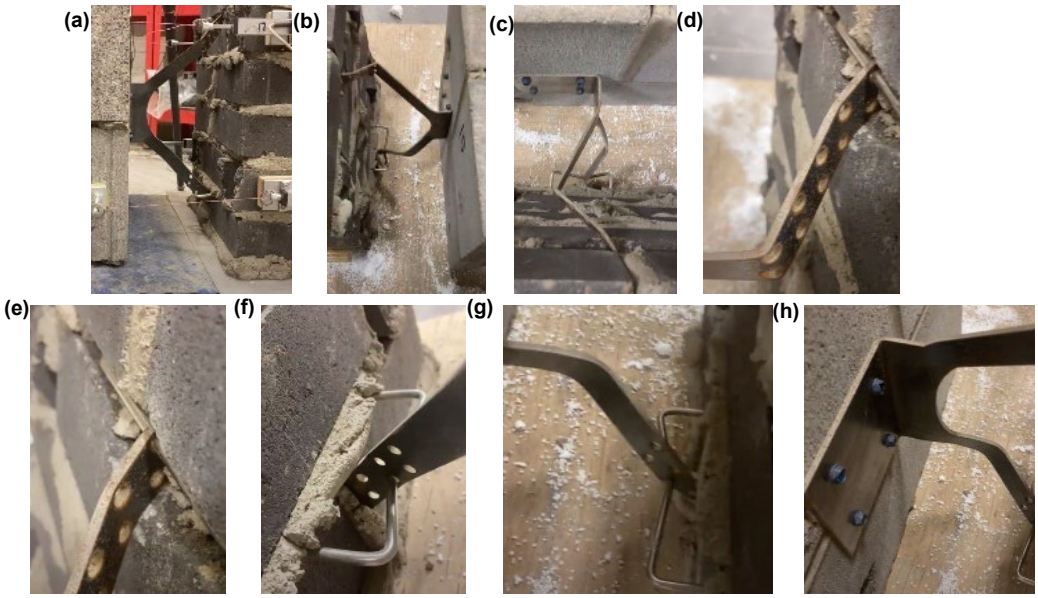

Figure C.57: C-IN.CN-4 after testing of (a) side view, (b) elevated side view, (c) top view, (d) top connector leg side view, (e) top connector leg side view 2, (f) bottom connector leg side view, (g) bottom connector leg side view 2, (h) CMU connector Tapcon fastener view